July 2016

Post-Wrinkling Behaviors in Layered Elastic Polymers

Anesia D. Auguste
University of Massachusetts Amherst

POST-WRINKLING BEHAVIORS IN LAYERED ELASTIC POLYMERS

A Dissertation Presented

by

ANESIA D. AUGUSTE

Submitted to the Graduate School of the

University of Massachusetts Amherst in partial fulfillment

of the requirements for the degree of

DOCTOR OF PHILOSOPHY

May 2016

Polymer Science and Engineering

POST-WRINKLING BEHAVIORS IN LAYERED ELASTIC POLYMERS

A Dissertation Presented

by

ANESIA D. AUGUSTE

Approved as to style and content by:

_____

Ryan C. Hayward, chair

_____

Alfred J. Crosby, member

_____

Christian Santangelo, member

_____

David A. Hoagland, Department Head

Polymer Science and Engineering

DEDICATION

To my loving husband, Orfely Auguste

ACKNOWLEDGMENTS

First, I would like to express my sincere gratitude to my advisor, Professor Ryan Hayward. I first fell in love with polymer research working in his lab as a summer undergraduate intern nine years ago. I am so grateful for all of his advice throughout my undergraduate and graduate career. I have become a better scientist because of him. I would also like to thank Professors Al Crosby and Chris Santangelo for being on my committee. I have learned so much from them through their thoughtful questions and constructive advice. I am very lucky to have three incredible committee members who are known for their work in surface instabilities and buckling mechanics to help guide my PhD thesis work.

I would like to express my great appreciation to Professor Zhigang Suo from Harvard University. Collaborating with him and his group (Lihua Jin and Jiawei Yang) has been a true joy. I regard Professor Suo as a second advisor. His knowledge of mechanics and his kind heart is something I truly admire. I especially want to thank Lihua Jin. We have worked very closely together over the past five and half years and she has conducted the majority of the simulations presented in this thesis. I admire her hard work ethic and I will miss our online chats about science and life. I would like to express my gratitude to Aude Duhamel whom I had the pleasure to work with over the past summer on the work in chapter 5.

I would like to acknowledge the funding agencies which supported the work presented in this thesis: The National GEM Consortium, Northeast Alliance for Graduate

Education and the Professoriate, and NSF Graduate Research Fellowship Program (NSF DGE-0907995) and NSF grant DMR-1309331.

I would like to thank the “surface instability” group which consisted of Dr. Chelsea Davis, Dr. Yuri Ebata, Dr. Dayong Chen, Dr. Bin Xu, Dr. Yu-Cheng Chen, Mike Imburgia and Tetsu Ouchi. I loved having people to talk to about my wrinkle and crease research. More specifically, I want to thank Chelsea for taking me under her wing when I was a summer intern and a 1st year graduate student; Yuri for teaching me about optical profilometry; Dayong for being a great friend and someone I could talk to about my new findings; Bin for being a good friend and someone I could bounce ideas off of; Mike for his positivity; and Tetsu for being an awesome friend, labmate and officemate. They all made learning about and exploring surface instabilities fun.

I absolutely loved being in the Hayward group. I feel so privilege to have known the first students (Dr. Jungwook Kim, Dr. Ian Henderson and Dr. Le Li) to the latest additions to the group (Alexa Kuenstler and Carolyn Zhao) and everyone inbetween (Dr. Felicia Bokel, Dr. Scott Christensen, Dr. Cheol Hee Lee, Dr. Dayong Chen, Dr. Jinhye Bae, Dr. Maria Chiappelli, Dr. Kyle Bryson, Rachel Letteri, Daniel Acevedo, Nakul Bende, Ying Zhou, Adam Hauser, Di Zeng, Tetsu Ouchi, Qi Lu, and Hyunki Kim). I would like to thank the group for being nice, helpful and dangerously smart. I especially want to thank my officemates (Rachel, Jinhye, Tetsu and Qi) for making our office a home.

The third floor was home away from home. From trick or treating on Halloween to just having lunch together, people from the Hayward, Crosby, Lesser and Grayson

groups just made working together so easy. The staff (Lisa Groth, Alyssa Kristek, Maria Farrigton, Alyssa Kristek, Lisa McNamara, Linda Chatfield, Greg Dabkowski and Dale-the former confocal manager) also made things easy and run smoothly. I could not graduate without them.

My time in Amherst was made better by being a part of the PSE softball, ASPIRE, Graduate Students for Diversity in Science and Engineering (GSDSE), Corning Mentoring program and the Northeast Alliance for Graduate Education and the Professoriate (NEAGEP). Being part of the executive board as well as a founding member of GSDSE with Jack Ly, Laura Lanier, Cristiam Santa, Daniel Acevedo, and Kara Martin has been amazing. It has been so great working with people who have the same passion for outreach. I am also so very thankful for NEAGEP and the NEAGEP staff but especially Vanessa Hill, Dr. Marlina Duncan and Prof. Sandy Peterson for all their support and their encouragement through the difficult and good times. It was through NEAGEP that I meet Greg Thomas and the Corning Mentoring program was started. Dr. Renee Duncan from Corning, inc was selected to be my mentor and she has been such a powerful role model. NEAGEP also gave me three wonderful mentees (Daniel Avecedo, Katherine Carrasquillo, and Sualyneth Galarza). I am so proud of them. Sualy, in particular, has been like a little sister to me. I will miss our times together.

Words cannot express how grateful I am for my close friends. I am so grateful for Dr. Polina Ware, Dr. Yuije Liu, Dr. Maria Chiapelli, Dr.Angela Cugini and Dr. Brittany deRonde for being awesome gym buddies and just being there when I needed to vent. I

also want to thank Rachel Letteri for being my work buddy and friend. We would spend many late nights working on papers, presentations or even writing our theses. I am also thankful to have a great friend and role model like Dr. Joelle Labastide and Dr. Ololade Fatunmbi. Especially my former roommate Ololade, who has been like a sister to me. She has been there through the tears and smiles since we first met back in 2009 at Georgia Tech. Even though my best friends (Dr. Suzana Vallejo-Heligon, Daniel Zambrano, Nicole Rodriguez, Elena Smith, Jeremy Magruder, JJ Revuelta and Christina Mills) from college live far away, I am so grateful for their support, love and encouragement. We have been through so much together in the past 11 years and they have always been there to celebrate my wins and to mourn my losses.

Family is important to me. I am grateful for my church family, MERCYHouse, and all of their support and prayers. In addition, words cannot describe the love that I have for my family (Eliana, Syliva, Mom and Dad), in-laws (Bildad, Franson, Offrand and Marie) and cousins (Emely, Abby, Luz, Rebecca, Bryan, Nadine, Marcos, and Anthony). I feel incredibly lucky to have them in my life. My Husband, Orfely, deserves a medal for being the best husband. I could not have completed my PhD if it were not for him.

Finally, I want to thank God. For through him, nothing is impossible.

ABSTRACT

POST-WRINKLING BEHAVIORS IN LAYERED ELASTIC POLYMERS

MAY 2016

ANESIA D. AUGUSTE, B.S., UNIVERSITY OF FLORIDA

M.S., UNIVERSITY OF MASSACHUSETTS AMHERST

Ph.D., UNIVERSITY OF MASSACHUSETTS AMHERST

Directed by: Professor Ryan C. Hayward

Surface instabilities include a variety of different modes such as wrinkles, folds, and creases. Such surface instabilities have been used in numerous contexts including changing the wetting, optical, and mechanical properties of different material surfaces for applications in flexible electronics, tissue engineering and biosensors. Interesting surface morphologies can arise due to differences in pre-strain, stiffness, and thickness between the film and substrate; however, the effects of these differences are not well understood. We have developed an experimental system, complemented by finite element simulations, to systematically vary the pre-stretch of the substrate, modulus contrast and thickness contrast to study the transitions of surface instabilities in compressed bi-layers as strain is increased. We find that for systems with large modulus contrast, but varying degrees of substrate pre-stretch, the pre-stretched substrates not only substantially shift the critical strain for post-wrinkling bifurcations, but also qualitatively change the post-wrinkling modes observed.

Understanding that pre-stretching the substrate affects post-wrinkling behaviors, the remaining experiments were conducted with no substrate pre-stretch. Examining the

effect of modulus contrast, we report that below a film to substrate elastic modulus ratio of approximately 2, the flat state transitions directly to the creased state. For slightly larger contrasts, wrinkling occurs first but there are two distinct types of post-wrinkling behaviors: (1) wrinkles that transition into creases without period-doubling; and (2) wrinkles to creases preceded by period doubling. Finally, considering the effect of thickness contrast between the film and substrate, we discover that the critical strain for post-wrinkling behavior increases as thickness contrast decreases leading to wrinkles with aspect ratios (defined as amplitude normalized by wavelength) as high as 0.6. Further increases in aspect ratio can be achieved by increasing the modulus contrast, leading first to the formation of localized ridges, and then uniform, high aspect ratio wrinkles. Understanding surface instabilities in such non-ideal bi-layer systems provides important insight into the behavior of natural and synthetic systems with varying substrate pre-strain and modulus and thickness contrast.

TABLE OF CONTENTS

LIST OF FIGURES

Figure Page

CHAPTER 1

BACKGROUND

1.1 Definition of surface mechanical instability

The application of a compressive load can lead to a variety of mechanical surface instabilities, including creasing, wrinkling, and folding. Many examples can be found in everyday life from the creases in a baby's arm to the wrinkling of human skin. Previously, research on surface mechanical instabilities treated these instabilities as failure mechanisms [1]; however, by controlling the onset and evolution of wrinkles and creases in a number of different material systems, researchers have demonstrated a wide range of applications. These include flexible electronic devices [2–5], surface patterning methods [6–9], and materials with tunable optical properties [10–13], as well as, tunable surface properties such as adhesion [14–16], and hydrophobicity [10,17,18].

1.1.1 Creases

Creasing occurs when a soft material is compressed beyond a critical point. The surface of the soft material becomes nonlinearly unstable and buckles to form sharp self-contacting regions with finite depth. It was predicted that an elastic body under plane strain compression would first form wrinkles [19], but it was then discovered that creasing lowers the elastic energy of the body and thereby creases occur first at lower strain [20].

Creases are localized features known to form by a nucleation and growth process, with crease nucleation usually occurring at defects [21,22]. After nucleation, creases grow and propagate across the surface [23,24]. For a uniaxially compressed thick substrate, creases propagate laterally to form a regularly-spaced array which grow across the surface. The equilibrium spacing of these creases is known to be a function of the substrate thickness and the degree of compression [25]. In Figure 1-1, w is the spacing between two creases in the deformed state, W is the spacing between two creases in the undeformed state, ε is the amount of compression, $w = W(1-\varepsilon)$, and H is the substrate thickness. The crease equilibrium spacing is determined to be $w/H \approx 3.5(1 - \varepsilon)$.

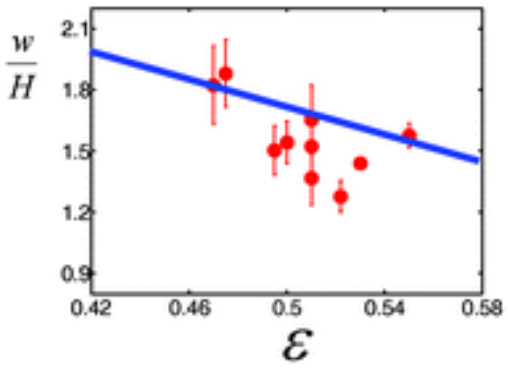

Figure 1-1. The equilibrium spacing of creases as a function of the compressive strain. The solid line is predicted by the calculation, and the symbols are experimental measurements, with error bars representing the standard deviation of average fold spacings (Reprinted with permission from ref. 25).

Recently, it has been proposed that creases may occur though either supercritical or subcritical instabilities, as summarized by the bifurcation diagrams in Figure 1-2 [26]. Figure 1-2, shows the bifurcation diagrams for supercritical and subcritical creases [26]. Supercritical creases transition from a flat state to a creased state where the creases have

an infinitesimal depth at a critical strain ε_c and grow as compression is added. With unloading, the crease unfolds itself and returns to the flat state since there is no hysteresis. A subcritical crease, on the other hand, will snap from a flat state to a crease with a finite crease depth beyond the snap forward strain, ε_f. When the compression is released, there is a hysteresis and the crease of a finite depth will return back to the flat state below the snap back strain ε_b.

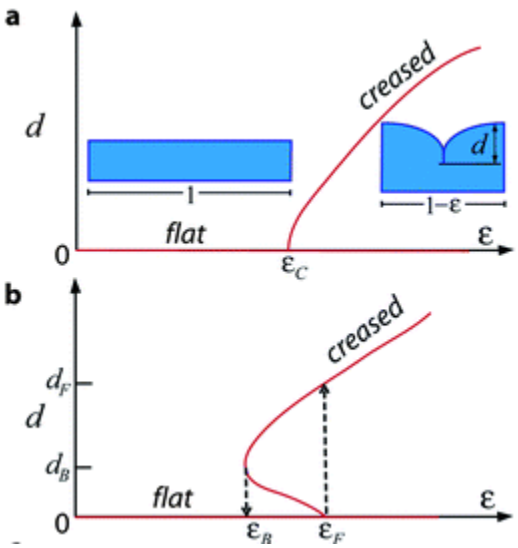

Figure 1-2. Bifurcation diagrams for (a) supercritical and (b) subcritical creases (Reprinted with permission from ref. 26).

1.1.2 Wrinkles

Wrinkles form in a bi-layer, consisting of a thin stiff film supported by a soft substrate, that is compressed beyond a critical strain [27–30] as shown in Figure 1-3. They are characterized by out-of-plane buckling features that forms smooth undulations. An unconstrained thin film has a preference for bending rather than stretching when compressed, since $U_{bend} \sim t^3 << U_{stretch} \sim t$ where U is the elastic energy and t is the film

thickness. On the other hand, a thick substrate prefers to stretch since $U_{bend} >> U_{stretch}$. When the thin film is attached to the thick substrate, wrinkles are formed to balance these two energies as the bending of the top film is restricted by the stretching of the soft substrate [19].

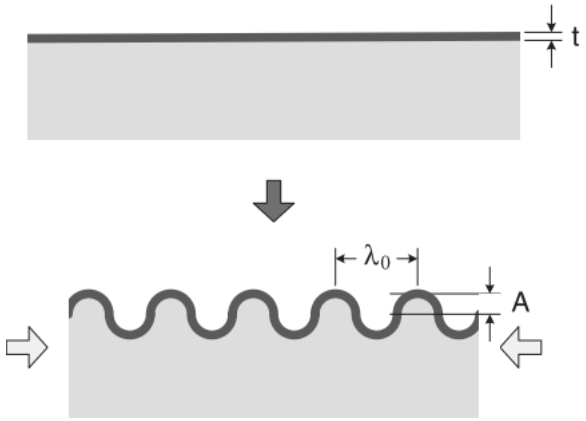

Figure 1-3. Schematic of the formation of wrinkles in a bi-layer with a stiff film on a soft substrate (Reprinted with permission from ref. 1)

Balancing the stretching energy of the substrate and bending energy of the thin film leads to an intermediate wavelength, **Equation 1,** where the wrinkle wavelength is dependent on the film thickness (*t*) and the plane strain modulus of the substrate ($\overline{E}_s = E_s/(1-\upsilon_s{}^2)$) and the film ($\overline{E}_f = E_f/(1-\upsilon_f{}^2)$) (i.e. the modulus E and Poisson's ratio v). The critical strain for the appearance of these wrinkles ε_c, **Equation 2**, is dependent on the modulus contrast between the film and substrate [28].

Equation 1

$$\lambda = 2\pi t \left(\frac{\overline{E}_f}{3\overline{E}_s}\right)^{1/3}$$

Equation 2

$$\varepsilon_c = \left(\frac{\overline{E}_f}{3\overline{E}_s}\right)^{-2/3}$$

The amplitude of the wrinkles will continue to increase, as the strain increases above the critical strain. Huang and co-workers[31] found that the amplitude of the wrinkles showed a square root dependence on the amount of compression past the critical strain for wrinkling and is shown in equation 3.

Equation 3

$$A = t\left(\frac{\varepsilon}{\varepsilon_c} - 1\right)^{1/2}$$

1.2 Numerical studies of post-wrinkling behaviors

As compression continues past the formation of wrinkles, one of a number of different post-wrinkling behaviors can be observed, depending on the strain state of the substrate and its adhesion to the thin film. A thin film on a liquid foundation first forms wrinkles but at higher strains transitions to folds [32,33]. For an elastomer attached to a stiff thin film, the thin film in this system can delaminate or fracture at higher compression depending on the adhesion and Poisson ratio of the two layers [34–36]. With good adhesion and similar Poisson ratio between layers, the wrinkles can transition to different post-

wrinkling modes: period doubling, period quadrupling and eventually folds [37,38]. In period doubling, the wrinkles undergo translational symmetry breaking, with the amplitude of every second wrinkle growing while its neighbor decreases, driven by the non-linear elastic response of the substrate [31,39]. Figure 1-4, shows the simulated values of critical strains for wrinkles, period doubling, and folds as a function of modulus contrast by Cao and co-workers, where μ_f and μ_s are the shear modulus of the film and substrate, respectively [37].

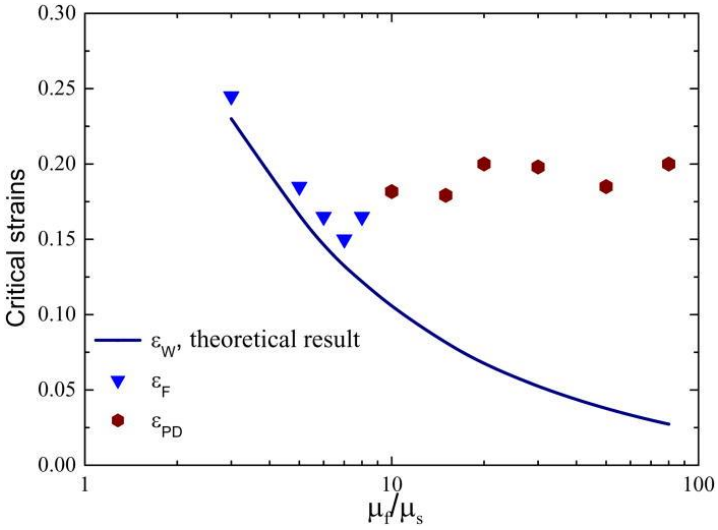

Figure 1-4. Critical strain for post-wrinkling bifurcations versus modulus contrast (Reprinted with permission from ref. 37).

Figure 1-4 shows that the critical strain for wrinkling is dependent on the modulus contrast, while the critical strain for period doubling becomes independent of modulus

contrast above a contrast of 10. This treatment ignores the possibility for pre-stretch of the substrate, which can have important effects. For large substrate pre-stretch, Hutchinson and co-workers have used numerical modeling to predict the emergence of localized ridges at higher critical strains as a different type of post-wrinkling bifurcation [36,37,39,40]. They found that the application of in-plane pre-tension causes a softening of the outward deflection of the substrate relative to the inward deflection, and hence promotes the formation of ridges. Conversely, the application of in plane pre-compression stiffens outward deflection of the substrate relative to inward, favoring the formation of folds.

Wang et al [36] identified different post-wrinkling bifurcations (period-doubling, creasing and delaminated buckling) through both simulations and experiments. The different behaviors were based on the adhesion strength, modulus contrast and strain mismatch between the film and the substrate. Zhao and co-workers studied the evolution of the surface instabilities using computational methods and constructed a phase diagram of different types of post-wrinkling bifurcation[41]: wrinkles that transition directly to creases; wrinkles that undergo period doubling and then give rise to creases; wrinkles form period doubling, period quadrupling and then folds. Still, understanding of these post-wrinkling behaviors is lacking.

1.3 Experimental status of post-wrinkling behaviors

Although a considerable amount of research is currently being carried out on wrinkling and creasing, experimental studies of post-wrinkling behaviors in elastomeric bi-layers have been more limited. One of the first experimental studies on post-wrinkling bifurcations was conducted by Brau and coworkers [38], who examined two types of systems. System 1 was a UV ozone surface treated PDMS substrate and system 2 was a thin stiff colored PDMS film on a thick soft PDMS substrate. System 1 was under pre-tension while system 2 was under no pre-stretch. The researchers created a bifurcation diagram, which is represented in Figure 1-5.

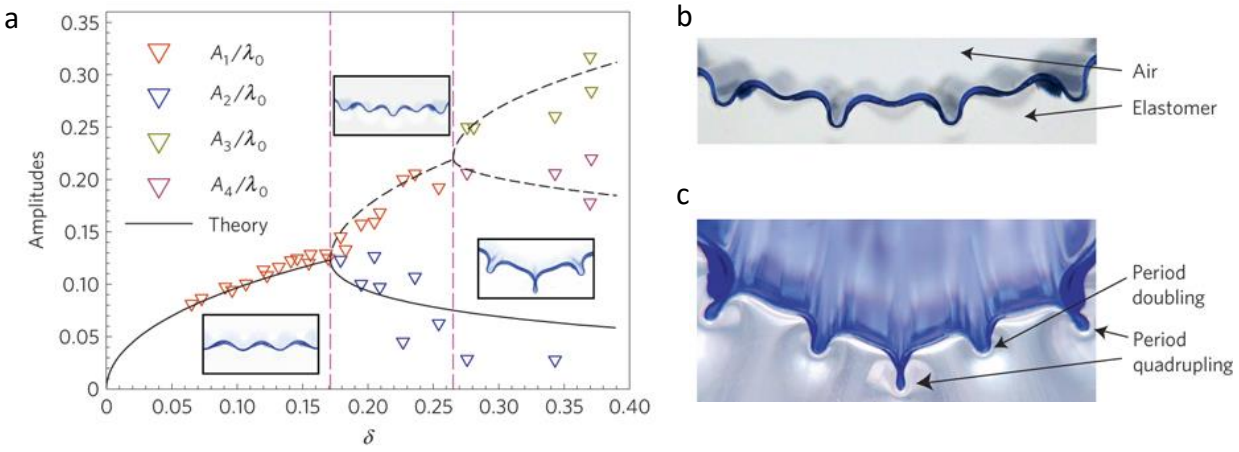

Figure 1-5. Evolution of amplitudes for large compressions showing the period-quadrupling bifurcation (a) Profile of a thin stiff PDMS membrane bound to a soft PDMS foundation for a relative compression of 0.23. (b) Wrinkled structure showing the period-quadrupling instability ($\delta \simeq 0.37$). (Reprinted with permission from ref. 38)

In Figure 1-5a, the amplitudes of a single wrinkle A_1 and its neighbor A_2 for system 2 are plotted as a function of compression δ. Wrinkles are first formed with A_1 and A_2

growing in unison as predicted in Equation 3 until a bifurcation occurred around a film strain of 0.18. At this point, the amplitudes at two times the wrinkle wavelength grow while the remaining amplitudes diminish, breaking the wrinkle symmetry and creating the cross sectional profile shown in Figure 1-5b. As compression continues to increase, the system undergoes a second bifurcation, called period quadrupling, which is shown in Figure 1-5c.

System 1 is reported to have a higher critical strain for period doubling (0.20) than system 2 (0.18), which is an effect from the pre-stretched substrate in system 1 [38]. There are only a few experimental studies on the effect of pre-stretch on the post-wrinkling modes, most of which focused on pre-tension in the substrate [35,42–44]. One of the first of these studies examined pre-tension by deflating a balloon which had a stiff film on top [44]. Figure 1-6 shows the images from this experiment, demonstrating the sample's transition from wrinkles to ridges when the thin film is placed under equi-biaxial compression.

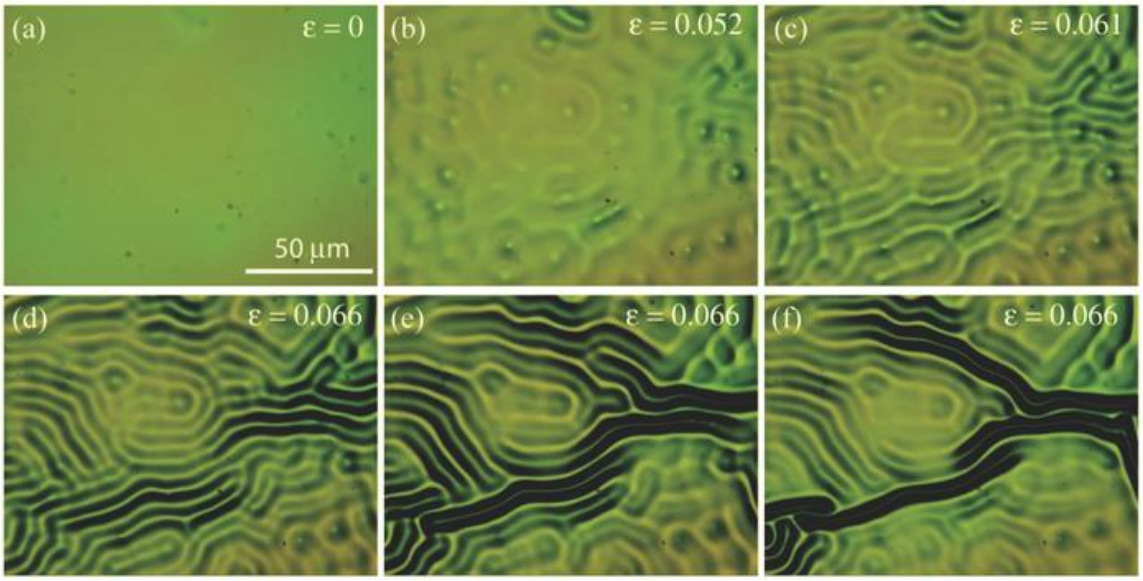

Figure 1-6. Wrinkle-to-ridge transition with increasing equi-biaxial compression (Reprinted with permission from ref. [44])

With increasing compressive strains, wrinkles form and grow in amplitude until a film strain of 0.66 is reached. At that point, ridges form, propagate and grow, leading to the relaxation of nearby wrinkles. When a thin film is attached to an uniaxial highly pre-strained substrate, the ridges can turn into regular high aspect ratio (amplitude/wavelength) wrinkles [42,43]. Creating surfaces with high aspect wrinkles are important since it can improve many applications with tunable surfaces. For example, high aspect ratio wrinkles increases the stretchability and the hydrophobicity of the surface [42,43].

Wang et al. [45] experimentally examined post-wrinkling behaviors as a function of adhesion, modulus contrast, and strain mismatch between the film and the substrate. The strain mismatch ε_M is determined by $(L_f-L_s)/L_s$, where L_f is the undeformed length of

the film, and L_s is the undeformed length of the pre-stretched substrate. They found several different types of post-wrinkling behaviors including wrinkles, creases, folds, period doubling, and ridges as shown in Figure 1-7. At high modulus contrast and high strain mismatch ridges will form, while the surface remains flat with no strain mismatch and low modulus contrast. Even though pre-stretch of the substrate was used to compile the phase diagram, the effects of pre-compression of the substrate was not considered.

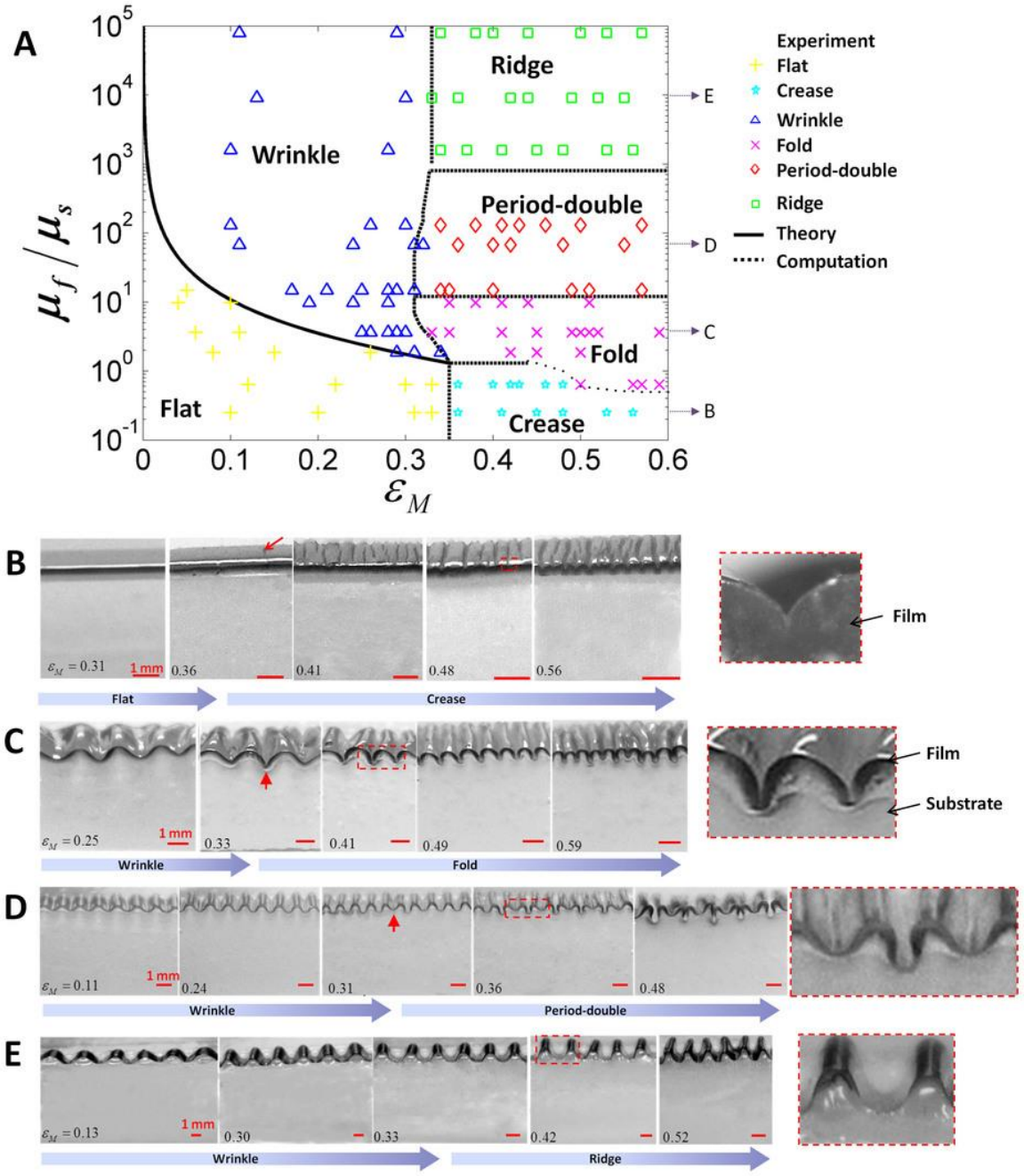

Figure 1-7. (A) Comparison between experimental data and the phase diagram of surface instability patterns. Experimental images of the formation of (B) the crease state, (C) the wrinkled and creased state, (D) wrinkled and period-doubled state, and (E) wrinkles and ridges in bi-layers with different modulus ratios and mismatched strains. The film-substrate modulus ratios are (B) 0.3, (C) 3.64, (D) 67.24 and (E) 9110, respectively. (Reprinted with permission from ref. 45)

1.4 Organization of the thesis

Although surface mechanical instabilities like wrinkles and creases have been extensively studied, research on the interplay between these different modes is limited. By examining modest modulus contrast and thickness contrast in a polymer bi-layer where wrinkles can transition to either creases or folds, we can bridge these two different types of surface instabilities together. This thesis explores the onset and evolution of post-wrinkling by alternating the substrate pre-stretch, thickness contrast and thickness contrast in layered elastic polymers.

Chapter 2 focuses on the effect of substrate pre-stretch on post-wrinkling behaviors. Substrate pre-stretch is a common method for studying wrinkling in an elastic polymer bi-layer, however the effects of pre-stretching the substrate is not well understood. In Chapter 2, we discover that pre-stretching the substrate can dramatically alter the appearance and evolution of post-wrinkling behaviors. Understanding that pre-stretch can affect post-wrinkling behavior, we create a method where the substrate is not pre-stretched to cleanly examine how different parameters, modulus and thickness contrast affect post-wrinkling behaviors. Chapter 3 examines the effects of modest modulus contrast between the film and substrate on post-wrinkling modes. We find that small modulus contrast dictates the onset and type of primary bifurcation while modest modulus contrast affects the wrinkle to fold transition leading to two different types of secondary bifurcations. Chapter 4 examines the effects of thickness contrast, which affects the onset of post-wrinkling behaviors and increases the aspect ratio of wrinkles.

In Chapter 5, we apply our understanding from the preceding three chapters to create high aspect ratio wrinkles. By investigating these parameters for an elastic polymer bi-layer system, we are able to further our understanding of different post-wrinkling behaviors. Understanding these post-wrinkling behaviors can provide insights relevant to many different fields with natural and synthetic materials including [46–48].

1.5 References

[1] S. Yang, K. Khare, P.-C. Lin, Harnessing Surface Wrinkle Patterns in Soft Matter, Adv. Funct. Mater. 20 (2010) 2550–2564. doi:10.1002/adfm.201000034.

[2] J.A. Rogers, T. Someya, Y. Huang, Materials and mechanics for stretchable electronics., Science. 327 (2010) 1603–7. doi:10.1126/science.1182383.

[3] D.-Y. Khang, H. Jiang, Y. Huang, J.A. Rogers, A stretchable form of single-crystal silicon for high-performance electronics on rubber substrates., Science. 311 (2006) 208–12. doi:10.1126/science.1121401.

[4] B. Xu, D. Chen, R.C. Hayward, Mechanically Gated Electrical Switches by Creasing of Patterned Metal/Elastomer Bilayer Films, Adv. Mater. 26 (2014) 4381–4385. doi:10.1002/adma.201400992.

[5] J.B. Kim, P. Kim, N.C. Pegard, S.J. Oh, C.R. Kagan, J.W. Fleischer, et al., Wrinkles and deep folds as photonic structures in photovoltaics, Nat. Photonics. 6 (2012) 327. doi:10.1038/NPHOTON.2012.70.

[6] J. Kim, J. Yoon, R.C. Hayward, Dynamic display of biomolecular patterns through an elastic creasing instability of stimuli-responsive hydrogels., Nat. Mater. 9 (2010) 159–64. doi:10.1038/nmat2606.

[7] M. Arifuzzaman, Z.L. Wu, R. Takahashi, T. Kurokawa, T. Nakajima, J.P. Gong, Geometric and edge effects on swelling-induced ordered structure formation in polyelectrolyte hydrogels, Macromolecules. 46 (2013) 9083–9090. doi:10.1021/ma401773w.

[8] A. Schweikart, A. Fery, Controlled wrinkling as a novel method for the fabrication of patterned surfaces, (2009) 249–263. doi:10.1007/s00604-009-0153-3.

[9] Q. Li, X. Han, J. Hou, J. Yin, S. Jiang, C. Lu, Patterning Poly(dimethylsiloxane) Microspheres via Combination of Oxygen Plasma Exposure and Solvent Treatment, J. Phys. Chem. B. 119 (2015) 13450–13461. doi:10.1021/acs.jpcb.5b07208.

[10] S.G. Lee, D.Y. Lee, H.S. Lim, D.H. Lee, S. Lee, K. Cho, Switchable transparency and wetting of elastomeric smart windows., Adv. Mater. 22 (2010) 5013–7. doi:10.1002/adma.201002320.

[11] P. Görrn, M. Lehnhardt, W. Kowalsky, T. Riedl, S. Wagner, Elastically tunable self-organized organic lasers., Adv. Mater. 23 (2011) 869–72. doi:10.1002/adma.201003108.

[12] C. Harrison, C.M. Stafford, W. Zhang, A. Karim, Sinusoidal phase grating created by a tunably buckled surface, Appl. Phys. Lett. 85 (2004) 4016. doi:10.1063/1.1809281.

[13] E. Lee, M. Zhang, Y. Cho, Y. Cui, J. Van der Spiegel, N. Engheta, et al., Tilted pillars on wrinkled elastomers as a reversibly tunable optical window., Adv. Mater. 26 (2014) 4127–33. doi:10.1002/adma.201400711.

[14] P.-C. Lin, S. Vajpayee, A. Jagota, C.-Y. Hui, S. Yang, Mechanically tunable dry adhesive from wrinkled elastomers, Soft Matter. 4 (2008) 1830. doi:10.1039/b802848f.

[15] E.P. Chan, E.J. Smith, R.C. Hayward, A.J. Crosby, Surface Wrinkles for Smart Adhesion, Adv. Mater. 20 (2008) 711–716. doi:10.1002/adma.200701530.

[16] E.P. Chan, J.M. Karp, R.S. Langer, A "self-pinning" adhesive based on responsive surface wrinkles, J. Polym. Sci. Part B Polym. Phys. 49 (2011) 40–44. doi:10.1002/polb.22165.

[17] J.Y. Chung, J.P. Youngblood, C.M. Stafford, Anisotropic wetting on tunable micro-wrinkled surfaces, Soft Matter. 3 (2007) 1163. doi:10.1039/b705112c.

[18] K. Khare, J. Zhou, S. Yang, Tunable open-channel microfluidics on soft poly(dimethylsiloxane) (PDMS) substrates with sinusoidal grooves., Langmuir. 25 (2009) 12794–9. doi:10.1021/la901736n.

[19] M.A. Biot, Surface instability of rubber in compression, Appl. Sci. Res. 12 (1963) 168–182.

[20] W. Hong, X. Zhao, Z. Suo, Formation of creases on the surfaces of elastomers and gels, Appl. Phys. Lett. 95 (2009) 111901. doi:10.1063/1.3211917.

[21] Y. Cao, J.W. Hutchinson, From wrinkles to creases in elastomers: the instability and imperfection-sensitivity of wrinkling, Proc. R. Soc. A Math. Phys. Eng. Sci. 468 (2011) 94–115. doi:10.1098/rspa.2011.0384.

[22] B. Li, Y.-P. Cao, X.-Q. Feng, H. Gao, Mechanics of morphological instabilities and surface wrinkling in soft materials: a review, Soft Matter. 8 (2012) 5728. doi:10.1039/c2sm00011c.

[23] V. Trujillo, J. Kim, R.C. Hayward, Creasing instability of surface-attached hydrogels, Soft Matter. 4 (2008) 564. doi:10.1039/b713263h.

[24] J. Yoon, J. Kim, R.C. Hayward, Nucleation, growth, and hysteresis of surface creases on swelled polymer gels, Soft Matter. 6 (2010) 5807. doi:10.1039/c0sm00372g.

[25] S. Cai, D. Chen, Z. Suo, R.C. Hayward, Creasing instability of elastomer films, Soft Matter. 8 (2012) 1301. doi:10.1039/c2sm06844c.

[26] D. Chen, L. Jin, Z. Suo, R.C. Hayward, Controlled formation and disappearance of creases, Mater. Horizons. (2014). doi:10.1039/c3mh00107e.

[27] E. Cerda, L. Mahadevan, Geometry and Physics of Wrinkling, Phys. Rev. Lett. 90

(2003) 074302. doi:10.1103/PhysRevLett.90.074302.

[28] J. Genzer, J. Groenewold, Soft matter with hard skin: From skin wrinkles to templating and material characterization, Soft Matter. 2 (2006) 310. doi:10.1039/b516741h.

[29] N. Bowden, W.T.S. Huck, K.E. Paul, G.M. Whitesides, The controlled formation of ordered, sinusoidal structures by plasma oxidation of an elastomeric polymer, Appl. Phys. Lett. 75 (1999) 2557. doi:10.1063/1.125076.

[30] D.-Y. Khang, J.A. Rogers, H.H. Lee, Mechanical Buckling: Mechanics, Metrology, and Stretchable Electronics, Adv. Funct. Mater. 19 (2009) 1526–1536. doi:10.1002/adfm.200801065.

[31] Z.Y. Huang, W. Hong, Z. Suo, Nonlinear analyses of wrinkles in a film bonded to a compliant substrate, J. Mech. Phys. Solids. 53 (2005) 2101–2118. doi:10.1016/j.jmps.2005.03.007.

[32] F. Brau, P. Damman, H. Diamant, T. a. Witten, Wrinkle to fold transition: influence of the substrate response, Soft Matter. 9 (2013) 8177. doi:10.1039/c3sm50655j.

[33] D. Holmes, A.J. Crosby, Draping Films: A Wrinkle to Fold Transition, Phys. Rev. Lett. 105 (2010) 1–4. doi:10.1103/PhysRevLett.105.038303.

[34] K. Srinivasan, G. Subbarayan, T. Siegmund, Wrinkling on irreversibly deforming foundations, Thin Solid Films. 520 (2012) 5671–5682. doi:10.1016/j.tsf.2012.04.071.

[35] Y. Ebata, A.B. Croll, A.J. Crosby, Wrinkling and strain localizations in polymer thin films, Soft Matter. 8 (2012) 9086. doi:10.1039/c2sm25859e.

[36] Q. Wang, X. Zhao, Phase Diagrams of Instabilities in Compressed Film-Substrate Systems, J. Appl. Mech. 81 (2013). doi:10.1115/1.4025828.

[37] Y. Cao, J.W. Hutchinson, Wrinkling Phenomena in Neo-Hookean Film/Substrate Bilayers, J. Appl. Mech. 79 (2012) 031019. doi:10.1115/1.4005960.

[38] F. Brau, H. Vandeparre, A. Sabbah, C. Poulard, A. Boudaoud, P. Damman, Multiple-length-scale elastic instability mimics parametric resonance of nonlinear oscillators, Nat. Phys. 7 (2010) 56–60. doi:10.1038/nphys1806.

[39] J.W. Hutchinson, The role of nonlinear substrate elasticity in the wrinkling of thin films, Philos. Trans. R. Soc. A Math. Phys. Eng. Sci. 371 (2013). http://rsta.royalsocietypublishing.org/content/371/1993/20120422.short (accessed November 26, 2013).

[40] J. Zang, X. Zhao, Y. Cao, J.W. Hutchinson, Localized ridge wrinkling of stiff films on compliant substrates, J. Mech. Phys. Solids. 60 (2012) 1265–1279. doi:10.1016/j.jmps.2012.03.009.

[41] R. Zhao, T. Zhang, M. Diab, H. Gao, K.-S. Kim, The primary bilayer ruga-phase diagram I: Localizations in ruga evolution, Extrem. Mech. Lett. (2015). doi:10.1016/j.eml.2015.04.006.

[42] Y.-C. Chen, A.J. Crosby, High Aspect Ratio Wrinkles via Substrate Prestretch, Adv. Mater. (2014) n/a–n/a. doi:10.1002/adma.201401444.

[43] C. Cao, H.F. Chan, J. Zang, K.W. Leong, X. Zhao, Harnessing Localized Ridges for High-Aspect-Ratio Hierarchical Patterns with Dynamic Tunability and Multifunctionality., Adv. Mater. (2013). doi:10.1002/adma.201304589.

[44] A. Takei, L. Jin, J.W. Hutchinson, H. Fujita, Ridge Localizations and Networks in Thin Films Compressed by the Incremental Release of a Large Equi-biaxial Pre-stretch in the Substrate., Adv. Mater. (2014) 1–7. doi:10.1002/adma.201306162.

[45] Q. Wang, X. Zhao, A three-dimensional phase diagram of growth-induced surface instabilities, Sci. Rep. 5 (2015) 8887. doi:10.1038/srep08887.

[46] J. Dervaux, M. Ben Amar, Morphogenesis of Growing Soft Tissues, Phys. Rev. Lett. 101 (2008) 068101. doi:10.1103/PhysRevLett.101.068101.

[47] C.T. McKee, J.A. Last, P. Russell, C.J. Murphy, Indentation versus Tensile Mesurements of Young ’s Modulus for Soft Biological Tissues, Tissue Eng. B. 17 (2011). doi:10.1089/ten.teb.2010.0520.

[48] J. Yin, X. Chen, I. Sheinman, Anisotropic buckling patterns in spheroidal film/substrate systems and their implications in some natural and biological systems, J. Mech. Phys. Solids. 57 (2009) 1470–1484. doi:10.1016/j.jmps.2009.06.002.

CHAPTER 2

PRE-STRETCH EFFECTS ON POST-WRINKLING MODES*

2.1 Introduction

When a bi-layer is compressed sufficiently far beyond the onset of wrinkling, new deformation modes may appear, with characteristics that depend sensitively on the details of the substrate response [1]. For a thin elastic film supported on a viscous substrate, wrinkles lose their periodicity and transition to localized folds once the total confinement of the thin film approaches one third of the initial wrinkling wavelength [2,3]. The transition to localized deformation may even lead to the fracture of the film [4]. For an elastomeric foundation, wrinkles lose their initial periodicity through the emergence of sub-harmonic modes due to nonlinear contributions to the elastic response of the substrate[5,6]. Typically, a progression from wrinkles to a period-doubled state is observed, followed by a period-quadrupled state, and finally the formation of self-contacting folds[1,6–8]. The emergence of sub-harmonic spatial modes in this context is analogous to appearance of temporal sub-harmonics for a non-linear oscillator[7].

In light of the key role played by the substrate in driving post-wrinkling bifurcations, it follows that this behavior should be highly sensitive to the state of the substrate, for example the presence of a compressive or tensile pre-stress. In spite of this expectation, however, only a limited number of studies along these lines have been

* A. Auguste, L. Jin, Z. Suo and R. C. Hayward, *Soft Matter*, 2014, **10**, 6520, **DOI:**10.1039/C4SM01038H - Reproduced by permission of The Royal Society of Chemistry

conducted while most wrinkling studies have substrates which are under tension prior to the attachment of the film or pre-stretched. While a few experiments have indicated the emergence of ridges[9–12] or other modes of strain localization[13] with pre-tension, the level of agreement with theory remains unclear. Further, there has been little work focused on the case of substrate pre-compression. Thus, there remains much to understand about how post-wrinkling behavior depends on substrate pre-stretch.

The aim of this study is to establish, through a combination of experiments and simulations, how substrate pre-stretch alters the onset and evolution of post-wrinkling modes as well as to understand the chaotic emergence of different sub-harmonic modes by adopting a general method to study the symmetry breaking from a periodic structure.

2.2 Method

2.2.1 Experimental

A trilayer system is used to independently vary the compression applied to the substrate and the silicate film. Our experiments rely on an elastic trilayer system modified from a recently described approach (Figure 2-1)[14]. A silica reinforced vinyl-terminated polydimethylsiloxane (PDMS) mounting layer (DMS-V31S15, Gelest Inc.) with a shear modulus 260 kPa and thickness 1 mm is uniaxially pre-stretched on a stretcher. A pre-cured substrate with thickness of approximately $400\ \mu\mathrm{m}$ and an initial length L_0 composed of a PDMS elastomer (Sylgard 184, Dow Corning) with a 50:1 weight ratio of base to crosslinker (shear modulus 12.5 kPa based on dynamic mechanical analysis). The

substrate is attached to the pre-stretched mounting layer using a thin (2-5 μm thick) layer of uncured PDMS with the same composition as the substrate. This bi-layer assembly is placed in an oven at 60 ºC for 4 h to bond the layers, and then allowed to cool to room temperature for over 30 minutes. This bi-layer is then partially released, or stretched further, to a new length L, placing the substrate under a pre-stretch $\lambda_0 = L/L_0$. The substrate was left at λ_0 for 30 min before being placed in a UV/O_3 cleaner for 25 min to convert the surface of the PDMS substrate into a stiffer oxide layer. This oxide film had an effective thickness of 3-8 μm and shear modulus of 620 kPa – 3.8 MPa as determined by fitting the dependence of the wrinkle amplitude and wavelength on film strain for samples with no substrate pre-stretch via the classical buckling equations as described by Stafford and others [15,16]. The variation in film modulus presumably reflects slight differences in sample position within the UV/O_3 cleaner, but as it is larger than the substrate modulus by a factor of 50 – 300, this variation should not play a significant role in the observed behavior. We consider the film to be stress free at this point, although we note the possibility for a slight residual stress due to mismatches in thermal expansion and/or oxidation-induced changes in volume. A subsequent partial release of the mounting layer to length l now places the bi-layer under compression, which we characterize in terms of the nominal strain applied to the film $\varepsilon_f = (L-l)/L$. The subsequent wrinkling and post-wrinkling behavior of the surface as a function of applied strain is then characterized by *in situ* optical profilometry. Using a defect in the wrinkling pattern as a point of reference, we track the same region while increasing the compressive strain in the film.

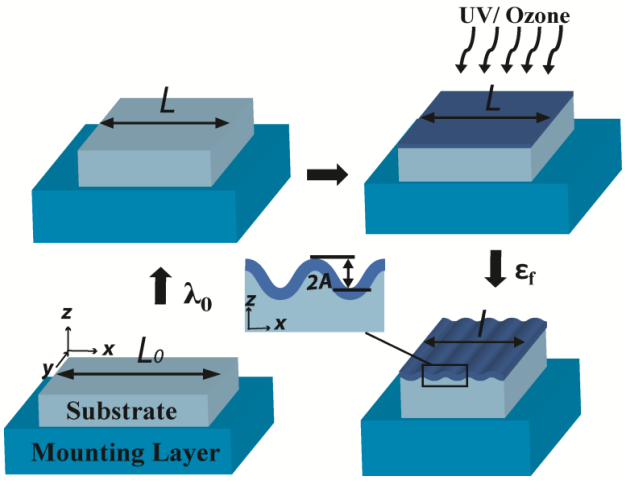

Figure 2-1. A schematic of the experimental procedure. An elastomeric substrate is attached to a pre-stretched mounting layer, deformed to λ_o, and exposed to UV/O_3 to form a stiff film layer. The stiff film is compressed with strain ε_f by partially releasing the mounting layer.

Optical profilometry (Zygo NewView 7300) is used for in-situ characterization of the height profiles of the sample surfaces using MetroPro 8.3.2 software. The 5x and 10x lenses are utilized as well as the stitch application to characterize a large area of the sample. At high film strains only the data points from the crest and trough could be imaged due to the steep angles of the surface; a spline is used to fill in the missing segments of the surface profiles in Figure 2-4. Laser scanning confocal fluorescence microscopy (Zeiss LSM 510 Meta) is used to characterize the shape of the wrinkles. Fluorescent labeling of the substrate is accomplished by adding 4.5 μg of fluorescein-o-acrylate in 1,4-dioxane per 1 g of PDMS prior to curing. During imaging, a refractive index matching fluid consisting of 72% glycerol and 28% water (weight percent) is used along with a 25x variable immersion lens. Several two-dimensional frames are taken and

manually stitched together by aligning peaks and troughs of the wrinkles to cover a larger area of the sample.

2.2.2 Simulations[†]

The commercial finite element software ABAQUS is used to computationally study the effect of pre-stretch on post-wrinkling bifurcations. The substrate is uniaxially pre-stretched and then the film-substrate bi-layer compressed under plane strain. Both the film and substrate are modeled as incompressible neo-Hookean materials, and the free energy of neo-Hookean material with a pre-stretch is implemented by a user-defined subroutine UMAT. For all the simulations except Figure. 2-2, the modulus ratio of the film to substrate is set to 50, and the thickness ratio of the bi-layer to the film was chosen as 50, both of which roughly match the experimental conditions. To break the symmetry of the surface during compression, the first and second eigenmodes obtained by a linear perturbation step are introduced as initial imperfections with very small amplitudes (roughly 1/2000 times the film thickness).

We call the wrinkle wavelength l_w. When we simulate the critical strain for period doubling (Figure 2-2 and 2-3), the simulation sample length is chosen as l_w. To understand chaotic period multiplication, we calculate the energy of different periodic states: wrinkling with the initial periodicity, period doubling, tripling and quadrupling. To realize these different periodicities, we simulate samples with lengths $l_w/2$, l_w, $3l_w/2$ and $2l_w$

[†] All finite element simulations were performed by Dr. Lihua Jin under the guidance of Professor Zhigang Suo at Harvard University

respectively. Symmetry condition is added on one boundary and uniform strain is applied on the other boundary. Static method is used for all the simulations.

2.3 Effects on the critical strain

We plot measured amplitudes for several different levels of pre-strain (λ_0 = 0.7 – 1.2) in Figure 2-2 (black triangles). The amplitude associated with a given feature on the surface is defined as half of the average out-of-plane displacement between a given 'trough' and its two neighboring 'crests'. For each sample, at least seven features are measured. The critical strain for wrinkling varied for different samples between 0.03-0.05, while the wrinkle wavelength was l_w = 100 – 160 μm. This degree of variability is apparently due to slight differences in the position of the sample relative to the UV light source during oxidation. Using the approach of Stafford and co-workers[17], the effective thicknesses of the silicate layers are estimated for samples with no substrate pre-stretch as h_f = 3 – 8 μm, with shear moduli of μ_f = 620 kPa – 3.8 MPa, corresponding to modulus mismatch values (μ_f/μ_s) of 50 – 300. As shown by Cao and Hutchinson [18], the modulus mismatch does not affect the critical strain for post-wrinkling bifurcations if the mismatch is above 10.

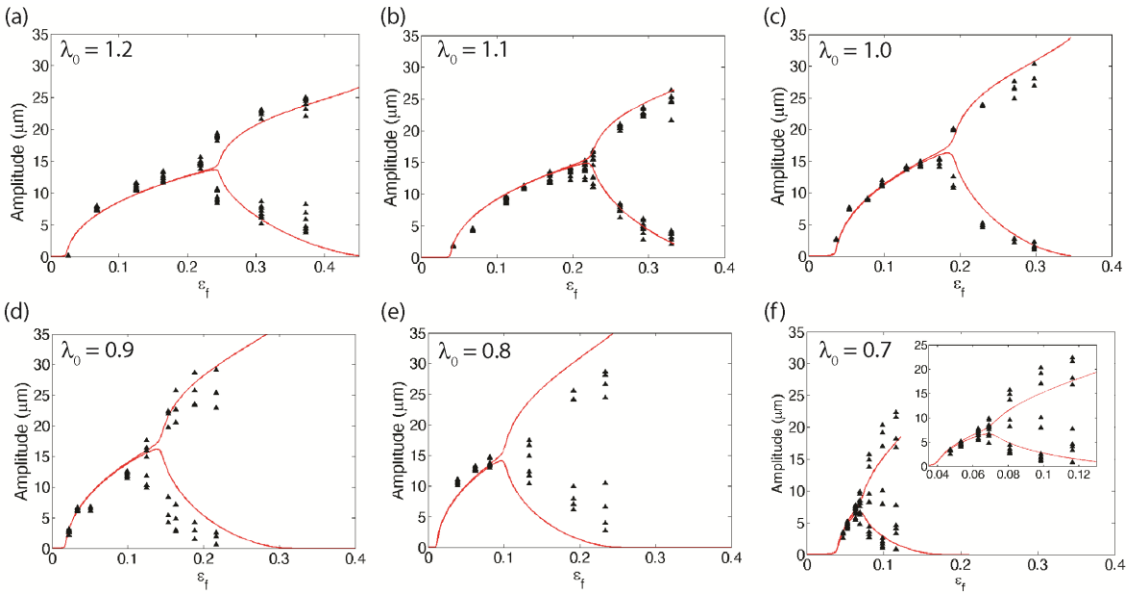

Figure 2-2. Bifurcation curves of the wrinkle amplitude as a function of film strain for substrates pre-stretched to λ_0 = (a) 1.2, (b) 1.1, (c) 1.0, (d) 0.9, (e) 0.8 and (f) 0.7. The experimental data (black triangles) reveal a gradual shift of the bifurcation point as well as an increase in distribution of amplitudes past ε_{pw} with a decrease in λ_0. Simulations (red lines) show good agreement with the experimental data.

In the wrinkle regime, the amplitudes are nearly homogeneous, as can be seen from the small amount of scatter in 2-2 (standard deviations in wrinkle amplitudes are typically less than 1 μm), and grow with increasing strain. However, at a sufficiently large value of ε_f, a post-wrinkling bifurcation is observed in which some wrinkles grow in amplitude while their neighbors shrink. As seen in Figure 2-2(a-c), pre-stretches from λ_0 = 1.0 – 1.2 show a clean bifurcation corresponding to a period doubled state, as first shown by Brau, et al [7] for the case of λ_0 = 1. We denote the strain at which this first

post-wrinkling bifurcation is observed as ε_{pw}, identified in practice as the point at which the standard deviation of wrinkle amplitudes show a dramatic increase.

For $\lambda_0 = 1$ (Figure 2-2c), we measure a value of $\varepsilon_{pw} = 0.18$, which is in good agreement with the values reported by Brau et al of 0.17 - 0.20[7]. When the substrate is under slight pre-tension, the period-doubled bifurcation shifts to higher strains but remains otherwise qualitatively similar; at $\lambda_0 = 1.2$ we measure $\varepsilon_{pw} = 0.23$ for the sample characterized in Figure 2-2(a) and at $\lambda_0 = 1.1$ we measure $\varepsilon_{pw} = 0.22$ for the sample in Figure 2-2(b). Under slight pre-compression the bifurcation occurs at lower film strain; at $\lambda_0 = 0.9$ and $\lambda_0 = 0.8$ (Figure 2-2d-e), we find $\varepsilon_{pw} = 0.11$ and $\varepsilon_{pw} = 0.10$, respectively. While a clear bifurcation into a bimodal collection of larger and smaller amplitudes can still be seen in this case, consistent with period doubling, the spread in amplitudes for each population is larger than for $\lambda_0 = 1$ and $\lambda_0 = 1.2$.

This non-uniformity becomes dramatically more pronounced for a film on a substrate with a larger pre-compression, $\lambda_0 = 0.7$ (Figure 2-2f). In this case, a clean bifurcation is lost, replaced instead by the emergence of a broad spread of amplitudes at a strain of $\varepsilon_{pw} = 0.06$, which is only slightly above the critical strain for wrinkling, $\varepsilon_w = 0.04$. The transition from regular wrinkles to irregular, or 'chaotic', structures occur over such a small range of strain that when plotted on the same scale as the other samples in Figure 2-2(a-e), the distinction between wrinkling and post-wrinkling is completely obscured; however, the inset to Figure 2-2(f) shows that indeed a narrow range of regular wrinkling can be discerned.

To better understand these effects, we model the system using the commercial finite element software ABAQUS. Both the film and substrate are taken to be incompressible neo-Hookean materials. For a ratio of the film to substrate modulus of only 50 – 300, as studied here, the maximum strain in the film can be as large as ~ 0.20 in our simulations. Thus, it is necessary to use a non-linear hyperelastic model for both the film and substrate. However, as the range of strains is still modest, the neo-Hookean model should provide a reasonable description of both materials. The substrate is uniaxially pre-stretched while the film/substrate bi-layer is subsequently compressed under plane strain, which is similar to the condition in the experiments. To simulate the period doubled state, we choose a unit cell of width l_w, the wrinkle wavelength. Symmetry is maintained across one boundary and uniform strain is applied on the other boundary. A small amplitude initial imperfection is introduced to break the translational symmetry of the surface. When compressive strain is incrementally applied, the surface initially remains flat and then forms wrinkles after a critical strain. With further increase in strain, the wrinkle amplitude grows but the nominal wavelength does not change. After a second critical strain, wrinkles lose their original periodicity through a supercritical period-doubling bifurcation. We record the second critical strain as ε_{pw}.

In Figure 2-2, we plot the simulation results for wrinkle amplitudes with different substrate pre-stretches as red lines. From the experimentally measured wrinkle wavelength, and the dependence of wrinkle amplitude on strain, we estimate the film thickness by fitting the classical buckling equations [17], as before. For the effective film modulus, however, we make use of the theoretical prediction that takes into account

substrate pre-stretch and assumes infinite substrate thickness [18]. The modulus ratios of the film to substrate estimated in this fashion are (a) 120, (b) 200, (c) 50, (d) 130, (e) 225 and (f) 35, while the film thickness are (a) 5.8 μm, (b) 6.0 μm, (c) 8.0 μm, (d) 6.6 μm, (e) 5.5 μm and (f) 7.8 μm. In the simulations, we choose a modulus ratio to match the experimental value for each plot, while the ratio of the total thickness to the film thickness is taken to be 50 in all cases. As seen in Figure 2-2, the simulations generally agree well with the experimental results, in terms of both the location of the post-wrinkling bifurcation and the subsequent evolution of amplitudes.

Figure 2-3 shows the dependence of ε_{pw} on λ_0, obtained from finite element simulations and experiments on at least 3 different samples at each λ_0. In this simulation and the remainder of the chapter, the ratio of the film modulus to substrate modulus is fixed as 50, and the ratio of the total thickness to the film thickness is also fixed as 50. When there is no pre-stretch in the substrate, ε_{pw} is calculated to be around 0.18, which matches the experimental value of 0.18 ± 0.02. A monotonic increase in ε_{pw} with λ_0 is seen: pre-compression in the substrate decreases ε_{pw}, while pre-tension increases ε_{pw}. Under pre-tension, e.g. $\lambda_0 = 1.2$, the finite element result of $\varepsilon_{pw} = 0.26$ agrees well with that from experiments (0.27 ± 0.07). Under pre-compression, e.g. at $\lambda_0 = 0.7$, the respective experimental and simulation results of $\varepsilon_{pw} = 0.05 \pm 0.02$ and 0.06 are again in agreement. Overall, the simulations in Figures 2-2 and 2-3 show almost quantitative agreement with experimental data, and the qualitative trend of ε_{pw} monotonically and strongly increasing with λ_0 over this range of substrate pre-stretch is clear in both cases.

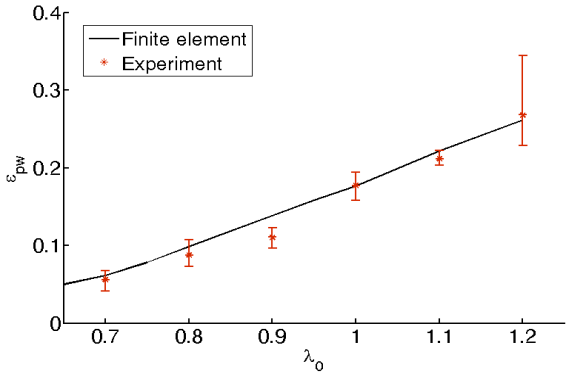

Figure 2-3. The critical film strain for post-wrinkling bifurcation ε_{pw} is plotted against the substrate pre-stretch λ_0. The solid lines represent finite element results and the solid symbol represents experimental results, with the error bars corresponding to minimum/maximum values for at least 3 samples. As pre-stretch increases, the film strain required for post-wrinkling bifurcation increases.

2.4 Emergence of chaotic behavior

We next consider the irregularity of amplitudes observed during post-wrinkling bifurcation for substrates under pre-compression. In Figure 2-4, we compare in detail the evolution of surface topography with increasing film strain for samples with λ_0 = 1.0 and 0.7. Color maps of the surface profiles are shown over large areas of the sample (Figure 2-4a-c, e-g), along with line profiles (Figure 2-4d,h) at the locations indicated. The profiles are taken at nearly the same position on each sample, and plotted with an x-axis normalized by (1- ε_f) to vertically align each crest and trough so that its evolution with film strain can be easily observed.

With no pre-stretch, the sample evolves from the wrinkled state (green trace in Figure 2-4d) at ε_f = 0.083 to a period-doubled state at ε_f = 0.16 (blue trace) and a period-

quadrupled state at ε_f = 0.23 (red trace). The amplitudes evolve in a fairly regular fashion across the entire sample, except in regions close to a defect in the wrinkling pattern (i.e., as seen to the lower left of Figures 2-4 (a-c) and correspondingly to the left side of the traces in Figure 2-4(d)).

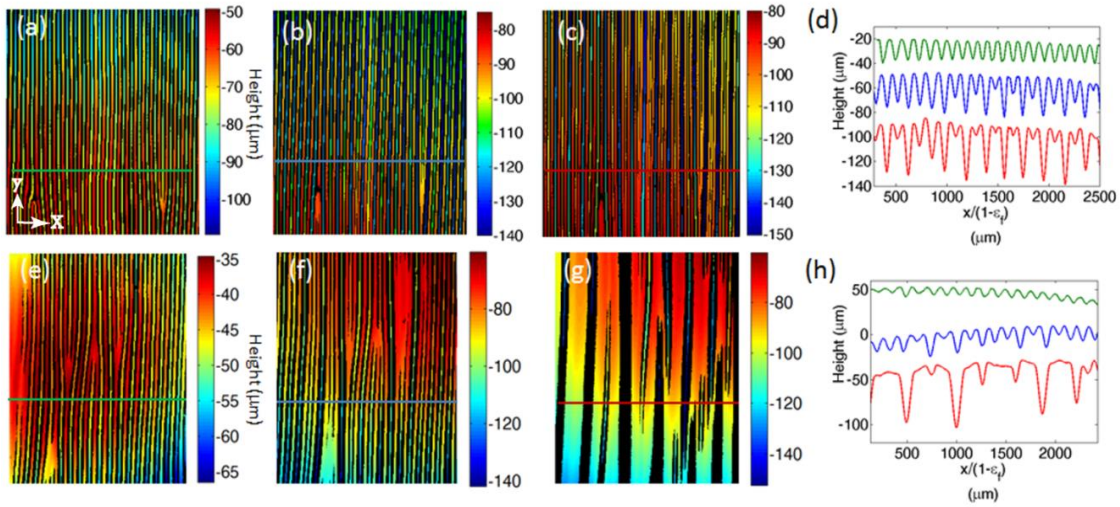

Figure 2-4. The surface profile of a sample with pre-stretch 1.0 at film strains of (a) 0.083, (b) 0.16, (c) 0.23. (d) One-dimensional profiles at the locations indicated by the solid lines in (a-c). The surface profile of a sample with pre-stretch 0.7 at film strains of (e) 0.045, (f) 0.063 and (g) 0.11. (h) One-dimensional profiles at the locations indicated by the solid lines in (e-g).

With a pre-compression of λ_0 = 0.7, however, dramatically different behavior is observed. A regular wrinkle pattern is first observed, as seen for ε_f = 0.045 (Figure. 2-5e, green trace in Figure 2-4h), but rapidly evolves into a set of deep features with irregular spacing by ε_f = 0.11 (Figure 2-4g, red trace in Figure 2-4h). Examination of the behavior at intermediate strains, e.g. at ε_f = 0.063 suggests that this pattern emerges through the competition between multiple different sub-harmonic modes with periodicities of 2, 3,

and 4 times the fundamental wrinkle mode. In other words, some regions show behavior locally characteristic of period doubling (two troughs that grow in depth separated by one that becomes more shallow), while others show characteristics of period tripling (deep troughs separated by two shallow troughs) and quadrupling (separation by three shallow troughs). Interestingly, this behavior shows variability across the transverse direction of the sample, as seen in Figure 2-4(g). We suspect this behavior arises because different regions of the sample spontaneously break the symmetry of the wrinkle pattern in different ways, leading to the presence of 'domain boundaries' where one set of deep features meets another, mismatched set.

The emergence of such chaotic behavior can be anticipated based on the analogy to the nonlinear oscillator [7,19,20], which is well-known to show chaotic behaviors in certain regimes. However, to provide a better understanding of the driving force in the current system, we use finite element methods to compare the energies of the different subharmonic modes. To realize these different periodicities, different symmetry conditions need to be prescribed. By simulating a sample with half the nominal wrinkle wavelength $l_w/2$, with symmetric conditions on the left boundary and applied strain on the right boundary, we enforce the initial wrinkle period to be conserved throughout the application of strain, and the corresponding energy per wavelength is called U_1. When we change the sample length to l_w, period doubling can occur at the critical strain ε_{pw}, and we call the energy per wavelength l_w of this configuration U_2. Similarly, when we simulate a sample with length $3l_w/2$, only period tripling, but not period doubling, can happen, and we call the corresponding energy per wavelength l_w as U_3. For a sample with length $2l_w$,

both period doubling and subsequently period quadrupling can occur, with the corresponding energy per wavelength l_w called U_4. Notably, for period tripling and quadrupling there can be more than one configuration. For example, period tripling can happen by one trough becoming deeper while the other two become shallower or alternatively by one becoming shallower while two becoming deeper. Here, we consider only the former case, which is the lower energy configuration.

In Figure 2-5 (a-c), we plot the normalized energy by which each of the configurations U_2, U_3, U_4 differ from the wrinkled state U_1, as a function of the applied strain ε_f. We normalize the energies by $\mu_s l_w h_f$, where h_f is the thickness of the film. When a given curve falls below 0, the corresponding type of period multiplication is energetically favorable, with the lowest energy curve representing the ground state. As seen in Figure 2-5(a) for no pre-stretch, the system remains in the wrinkled state and thus all of the curves stay at an energy of 0, until a strain of $\varepsilon_f = 0.19$. Beyond this point, the curves for U_2 and U_4 become negative, corresponding to period doubling. At a strain of $\varepsilon_f = 0.25$, the curve for U_4 becomes lower in energy compared to U_2, corresponding to period quadrupling. Over this range of strain, the energy U_3 remains above both U_2 and U_4 and thus period tripling is energetically disfavored. These findings are in excellent agreement with our experiments at $\lambda_0 = 1.0$, as well as previous work showing clean period doubling and period quadrupling bifurcations [1,6–8].

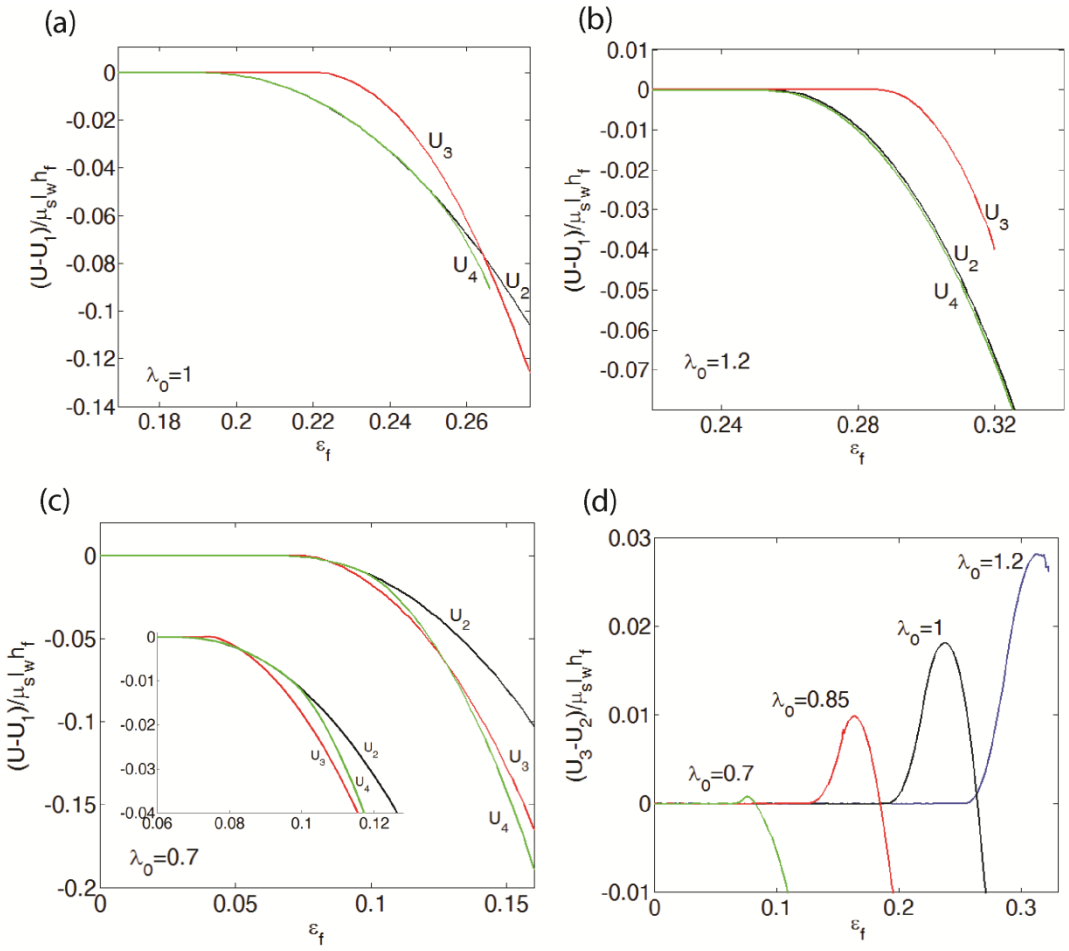

Figure 2-5. The energy of the period doubling U_2, tripling U_3, and quadrupling U_4 states relative to the energy of the single-period wrinkling state U_1. The pre-stretch in the substrate is (a) λ_0 = 1, (b) λ_0 = 1.2, and (c) λ_0 = 0.7 with an inset of ε_f between 0.06 and 0.13. (d) The difference in energy between period tripling state U_3 and period doubling state U_2.

The pre-tensioned substrate stabilizes both the wrinkled and period doubled states, as seen in Figure 2-5(b) for λ_0 = 1.2. Here, the onset of period doubling is delayed until ε_f = 0.25, while over the range of strain studied (up to ε_f = 0.32) period quadrupling is not observed at all, and U_3 remains well above U_2. The simulation results show excellent

agreement with our experimental findings that period doubling is shifted to higher strains when there is pre-tension in the substrate and no period quadrupling is observed over the range of ε_f studied.

In contrast, the pre-compressed substrate de-stabilizes both the wrinkled and period doubled states compared to the period tripled and quadrupled states. As seen in Figure 2-5(c), for λ_0= 0.7, the curves for U_2 and U_3 fall below zero at very similar strains (ε_f = 0.07 – 0.08). The period quadrupled state U_4 falls below U_2 at only slightly higher strain (ε_f = 0.10), and remains very close to U_3 for larger strains. Because period doubling, tripling and quadrupling all happen at strains close to the formation of wrinkles, wrinkles are still very shallow, and the energies of period doubling, tripling and quadrupling modes in the range of ε_f = 0.07 – 0.10 are very close to each other. The inset magnifies the energies in this region of strain. We further illustrate the effect of pre-stretch by plotting the difference between U_3 and U_2 for several values of λ_0 (Figure 2-5d). The pre-compressed substrate greatly reduces the energy difference between the period-tripling state and the period-doubling state. Presumably, this similarity in energy means that the presence of defects or even slight spatial variations in material properties would lead to local biases in favor of a given subharmonic mode, thus yielding a globally chaotic behavior. The prediction from the simulation is qualitatively in very good agreement with our experimental observations.

2.5 Conclusion

Our study reveals the strong effect of the pre-stretch in the substrate on post-wrinkling bifurcations. Pre-stretch shifts the critical strain for period doubling: modest amounts of pre-tension are found to stabilize wrinkles to higher strains, while modest pre-compression promotes the emergence of sub-harmonic modes at lower strains. For large substrate pre-compression, a new type of spatially chaotic behavior is found. The computational results reveal that energies of the different subharmonic modes become similar when the substrate is pre-compressed, thus eliminating the preference for a clean sequence of period doubling and quadrupling bifurcations. We anticipate that substrate pre-stretch will be an important parameter in future efforts to control the morphologies of wrinkled and post-wrinkled surfaces.

2.6 References

[1] F. Brau, P. Damman, H. Diamant, T. a. Witten, Wrinkle to fold transition: influence of the substrate response, Soft Matter. 9 (2013) 8177. doi:10.1039/c3sm50655j.

[2] L. Pocivavsek, R. Dellsy, A. Kern, S. Johnson, B. Lin, K.Y.C. Lee, et al., Stress and fold localization in thin elastic membranes., Science. 320 (2008) 912–6. doi:10.1126/science.1154069.

[3] D. Holmes, A.J. Crosby, Draping Films: A Wrinkle to Fold Transition, Phys. Rev. Lett. 105 (2010) 1–4. doi:10.1103/PhysRevLett.105.038303.

[4] R. Huang, H. Yin, J. Liang, J. Sturn, K. Hobart, Z. Suo, Mechanics of relaxing SiGe islands of a viscous glass, Acta Mech. Sin. 18 (2002) 441–456.

[5] B. Audoly, Localized buckling of a floating elastica, Phys. Rev. E. 84 (2011) 011605. doi:10.1103/PhysRevE.84.011605.

[6] S. Cai, D. Breid, A.J. Crosby, Z. Suo, J.W. Hutchinson, Periodic patterns and energy states of buckled films on compliant substrates, J. Mech. Phys. Solids. 59 (2011) 1094–1114. doi:10.1016/j.jmps.2011.02.001.

[7] F. Brau, H. Vandeparre, A. Sabbah, C. Poulard, A. Boudaoud, P. Damman, Multiple-length-scale elastic instability mimics parametric resonance of nonlinear oscillators, Nat. Phys. 7 (2010) 56–60. doi:10.1038/nphys1806.

[8] J.-Y. Sun, S. Xia, M.-W. Moon, K.H. Oh, K.-S. Kim, Folding wrinkles of a thin stiff layer on a soft substrate, Proc. R. Soc. A Math. Phys. Eng. Sci. 468 (2011) 932–953. doi:10.1098/rspa.2011.0567.

[9] Y. Ebata, A.B. Croll, A.J. Crosby, Wrinkling and strain localizations in polymer thin films, Soft Matter. 8 (2012) 9086. doi:10.1039/c2sm25859e.

[10] Q. Wang, X. Zhao, Phase Diagrams of Instabilities in Compressed Film-Substrate Systems, J. Appl. Mech. 81 (2013). doi:10.1115/1.4025828.

[11] C. Cao, H.F. Chan, J. Zang, K.W. Leong, X. Zhao, Harnessing Localized Ridges for High-Aspect-Ratio Hierarchical Patterns with Dynamic Tunability and Multifunctionality., Adv. Mater. (2013). doi:10.1002/adma.201304589.

[12] A. Takei, L. Jin, J.W. Hutchinson, H. Fujita, Ridge Localizations and Networks in Thin Films Compressed by the Incremental Release of a Large Equi-biaxial Pre-stretch in the Substrate., Adv. Mater. (2014) 1–7. doi:10.1002/adma.201306162.

[13] J. Zang, X. Zhao, Y. Cao, J.W. Hutchinson, Localized ridge wrinkling of stiff films on compliant substrates, J. Mech. Phys. Solids. 60 (2012) 1265–1279. doi:10.1016/j.jmps.2012.03.009.

[14] D. Chen, L. Jin, Z. Suo, R.C. Hayward, Controlled formation and disappearance of

creases, Mater. Horizons. (2014). doi:10.1039/c3mh00107e.

[15] C.M. Stafford, C. Harrison, K.L. Beers, A. Karim, E.J. Amis, M.R. VanLandingham, et al., A buckling-based metrology for measuring the elastic moduli of polymeric thin films., Nat. Mater. 3 (2004) 545–50. doi:10.1038/nmat1175.

[16] J.Y. Chung, A.J. Nolte, C.M. Stafford, Surface wrinkling: a versatile platform for measuring thin-film properties., Adv. Mater. 23 (2011) 349–68. doi:10.1002/adma.201001759.

[17] C.M. Stafford, C. Harrison, K.L. Beers, A. Karim, E.J. Amis, M.R. VanLandingham, et al., A buckling-based metrology for measuring the elastic moduli of polymeric thin films., Nat. Mater. 3 (2004) 545–50. doi:10.1038/nmat1175.

[18] Y. Cao, J.W. Hutchinson, Wrinkling Phenomena in Neo-Hookean Film/Substrate Bilayers, J. Appl. Mech. 79 (2012) 031019. doi:10.1115/1.4005960.

[19] R.M. May, Simple mathematical models with very complicated dynamics, Nature. 261 (1976) 459–467.

[20] J. Testa, J. Perez, C. Jeffries, Evidence for universal chaotic behavior of a driven nonlinear oscillator, Phys. Rev. Lett. 48 (1982) 714–717.

CHAPTER 3

MODULUS CONTRAST EFFECTS ON POST-WRINKLING MODES[‡§]

3.1 Introduction

In biological systems, many tissues and organs are composed of multi-layers with similar moduli, which may undergo a variety of buckling instabilities during growth or deformation.[1–6] Thus, understanding the buckling behaviors of elastic multi-layers with modest modulus contrast may provide insight into pattern formation in such systems. However, most studies have focused on bi-layers with a stiff thin film on top of a compliant thick substrate,[7–9] and so there remains a lack of understanding of surface instabilities when the ratio of the film to substrate modulus is modest, i.e., from ~ 2 to 10.

Wrinkling is the result of balancing the stretching energy of the substrate and the bending energy of the film. Above a critical compressive strain, wrinkles appear with an initial wavelength set by the film thickness and the modulus ratio of the film to the substrate. A stiffer and thinner film tends to form smooth wrinkles under small compressive strains, while when a more compliant and thicker film tends to form self-contacting creases under larger strains [10–13]. Upon further compression of a bi-layer with a large modulus contrast, different post-wrinkling behaviors occur. If the substrate

---

[‡] Jin, L., Auguste, A., Hayward, R. C., & Suo, Z. (2015). *J. of Applied Mech*. 82, 061008

[§] Auguste*, L. Jin*, Z. Suo, R.C. Hayward, (2016) *Extreme Mechanics Letters*. In preparation. (*equally contributed)

is not highly pre-stretched, period doubling is the first mode to appear [14–18]. In period doubling, the amplitude of every other wrinkle peak grows while its neighbors shrink. As more compression is added, period quadrupling and eventually folding occur in the bi-layer.

At the boundary between the wrinkle regime and the crease regime, there is a region rich with different post-wrinkling bifurcations. In this region, the modulus ratio between the film and the substrate is often modest. However, there are few studies on elastic bi-layers with modest modulus contrast [19–23]. Hutchinson and coworkers showed computationally that at low modulus contrast, wrinkles can transition into creases, at the initiation of which the simulations terminated [21]. Kim and coworkers [24] also showed wrinkles can transition to creases for graded samples with an elastic stiffness that decreases with distance from the free surface through the substrate depth. Later, they studied the evolution of the surface instabilities in bi-layers with low modulus contrast using computational methods and constructed a phase diagram of different types of post-wrinkling bifurcations [20]: wrinkles that transition directly to creases; wrinkles that undergo period doubling and then creases; wrinkles that form period doubling, period quadrupling and then folds. However, this study was solely computational. Wang et al[22] computationally identified different post-wrinkling bifurcations: period-doubling, creasing and delaminated buckling, and experimentally showed the existence of each of these different post-wrinkling modes. However, their simulations could not continue when creases set in and their experiments show these

post-wrinkling modes under the influence of substrate pre-stretch which is known to affect post-wrinkling modes from the previous chapter.

In this chapter, we combine experiments and simulations to track the evolution of surface instabilities in bi-layers with a modest modulus ratio between 1 and 10 and examine the spacing of these instability patterns. Particularly, we investigate the 3 dimensional behavior of surface instabilities, such as coexistence of, and channeling between, different modes of instability in samples with no substrate pre-stretch. In addition, we study primary bifurcations as well as build upon the work of Kim and coworkers[20] by examining two different types of secondary bifurcations that we call type 1 and type 2.

3.2 Method

3.2.1 Experimental

From Chapter 2, we understand that pre-stretch of the substrate impacts post-wrinkling behaviors, therefore in the current chapter we consider only substrates with no pre-stretch. Instead, uniform compression is applied to the bi-layer structures through an underlying pre-stretched mounting layer. The mounting layer needs to be stiff and thick enough so that it only functions to add a uniform compression to the bi-layer and does not buckle. A schematic of the experiment procedure is shown in Figure. 3-1. The silica reinforced polydimethylsiloxane (PDMS) mounting layer with shear modulus 260 kPa and thickness 1 mm is pre-stretched uniaxially on a stretcher. Then the substrate of the bi-layer, a fully pre-cured 30:1 (base to crosslinker weight ratio) PDMS layer (Sylgard 184,

Dow Corning) with thickness of approximately 550 μm is attached to the pre-stretched mounting layer using a thin layer (2-5 μm thick) of uncured PDMS with the same composition as an adhesive. The much thinner film is made by spin-coating uncured PDMS onto a trimethylchlorosiloxane treated glass slide and then is placed into a 120 ºC oven for 10 min. The partially cured PDMS coated glass slide is attached to the substrate and the bi-layer assembly is held at 40 ºC for 16 h to bond the layers and fully cure the film. This two-step curing process provides a strong bond between the film and substrate without the use of an adhesive. The crosslink density of Sylgard 184 is varied for the film and the substrate by using 5:1, 7.5:1, 10:1, 20:1, and 30:1 (weight ratio of base to cross-linker) compositions to access a range of moduli (2.6 ± 0.8 MPa, 2.1 ± 0.5 MPa, 1.6 ± 0.5 MPa, 0.75 ± 0.08 MPa and 0.4 ± 0.05 MPa, respectively)[25,26]. The spincoating speed for the film is altered from 1000 rpm to 4000 rpm to allow access to different thicknesses ranging from 5 – 50 μm. By relaxing the pre-stretch of the mounting layer, uniaxial compression ε is applied to the film-substrate bi-layer.

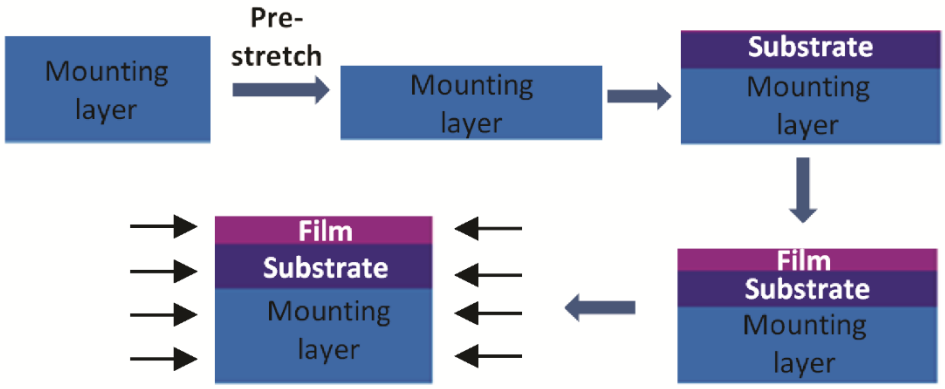

Figure 3-1. Experimental setup and the observations of three types of bifurcation behavior. (a) A pre-stretched elastomeric mounting layer is used to apply compression to a film-substrate bi-layer. Both the film and substrate are made of polydimethylsiloxane (PDMS).

3.2.2 Simulations**

We use 2-dimensional finite element simulations based on the commercial software ABAQUS to study the initiation and evolution of the surface instability, especially the secondary bifurcations, in elastic bi-layer structures with modest modulus contrast. Both the film and substrate are modeled as neo-Hookean materials, with perfect bonding between each other. We set the total thickness of the bi-layer to be 50 times the film thickness so that the substrate is effectively infinite. We first use a linear perturbation analysis to determine the wavelength of wrinkles in the bi-layers, L_w. Then we perform a second simulation to capture the quasi-static process of the wrinkle formation and the transition of several wrinkles to one crease. By varying the size of the simulation box, we can vary the spacing of creases L_c.

** All finite element simulations were performed by Dr. Lihua Jin under the guidance of Professor Zhigang Suo at Harvard University

To break the translational symmetry of the surface, we introduce the first eigenmode from the linear perturbation analysis times a small amplitude value (5 x 10^{-4} times the film thickness) into the second simulation as an initial imperfection of the system. Besides that, a geometric defect is also introduced on the surface of the film to set the location where a crease will form, and also ensure the formation of only one crease in the simulation box. The size of the geometric defect is 5 x 10^{-3} times the film thickness to otherwise minimize the effect of the defect. On the other hand, the mesh is refined around the geometric defect to resolve the field. We assume the crease to be symmetric and thus apply a mirror symmetry condition on one side of the simulation box, with the geometric defect located at the corner of that boundary and the top surface of the film. On the other side of the simulation box, homogeneous compression is applied. The Riks method is used to solve the boundary value problem so that not only the stable solutions, but also the unstable solutions, can be captured. An extremely compliant layer (0.01 times the film stiffness) is introduced on the top of the film to facilitate the convergence of the simulation when contact of the crease is involved in the boundary value problem solved by the Riks method, as we have used and tested in previous studies [13,27,28]. Moreover, to realize the uniaxial compression condition as used in the experiment, we simulate an axisymmetric ring under uniaxial compression in the direction of the symmetry axis, as employed in previous work [13]. The radius of the ring is set to be 10 times of the total thickness of the bi-layers so that the effect of the curvature of the ring is small. Element type CAX8H is used.

3.3 Results

3.3.1 Primary Bifurcation

It is tempting to expect that the boundary of the equal critical strain of wrinkles and creases demarcates regions in which wrinkles or creases form. However, we demonstrate remarkably rich bifurcation behavior when the ratios of moduli and thicknesses are slightly different. We simulate the bi-layer structures for different ratios of moduli and thicknesses leading to the formation of a phase diagram shown in Figure 3-2(a). First, we consider the region of the phase diagram below the solid black line, where creases represent the primary bifurcation from the flat state. We find that the creases can be subcritical or supercritical. Supercritical creases tend to form in a bi-layer with thicker and more compliant film, while subcritical creases tend to form in a bi-layer with thinner and stiffer film.

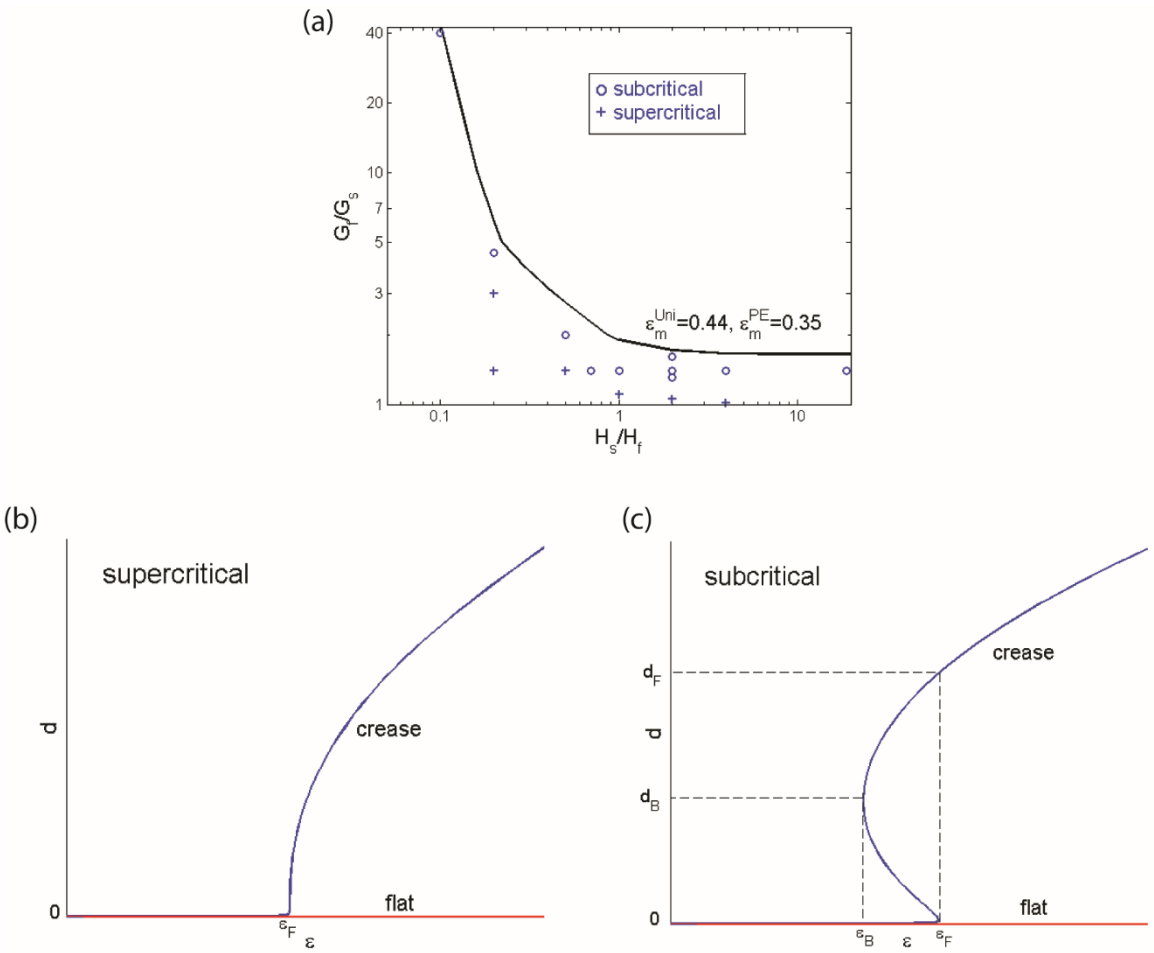

Figure 3-2. The formation of creases in bi-layers of various ratios of moduli and thicknesses. (a) Below the solid curve, the critical strain for the onset of wrinkles is larger than that of creases. Creases in a bi-layer can be subcritical or supercritical with the boundary drawn in dashed line. (b) Bifurcation diagram of a supercritical crease, where the applied strain represents the loading parameter, and the depth of the crease represents the state of the system. (c) Bifurcation diagram of a subcritical crease.

Figure 3-2(b) is a bifurcation diagram of a supercritical crease, where the applied strain represents the loading parameter, and the depth of the crease represents the state of the system. The flat state becomes unstable and creases initiate at a strain of 0.35 under plane strain condition and 0.44 under uniaxial condition. With further increase of strain, the crease gradually grows deeper.

Figure 3-2 (c) is a bifurcation diagram of a subcritical crease. When the strain is smaller than the snapping backward strain ε_B, the flat state with $d = 0$ is the only solution to the boundary value problem. When the strain is larger than the snapping forward strain ε_F, the crease state with a finite depth is the only solution to the boundary value problem. When the strain is in between the snapping forward and snapping backward strains $\varepsilon_B < \varepsilon < \varepsilon_F$, both the flat state and the deep crease state are the solutions to the boundary value problem, and can coexist.

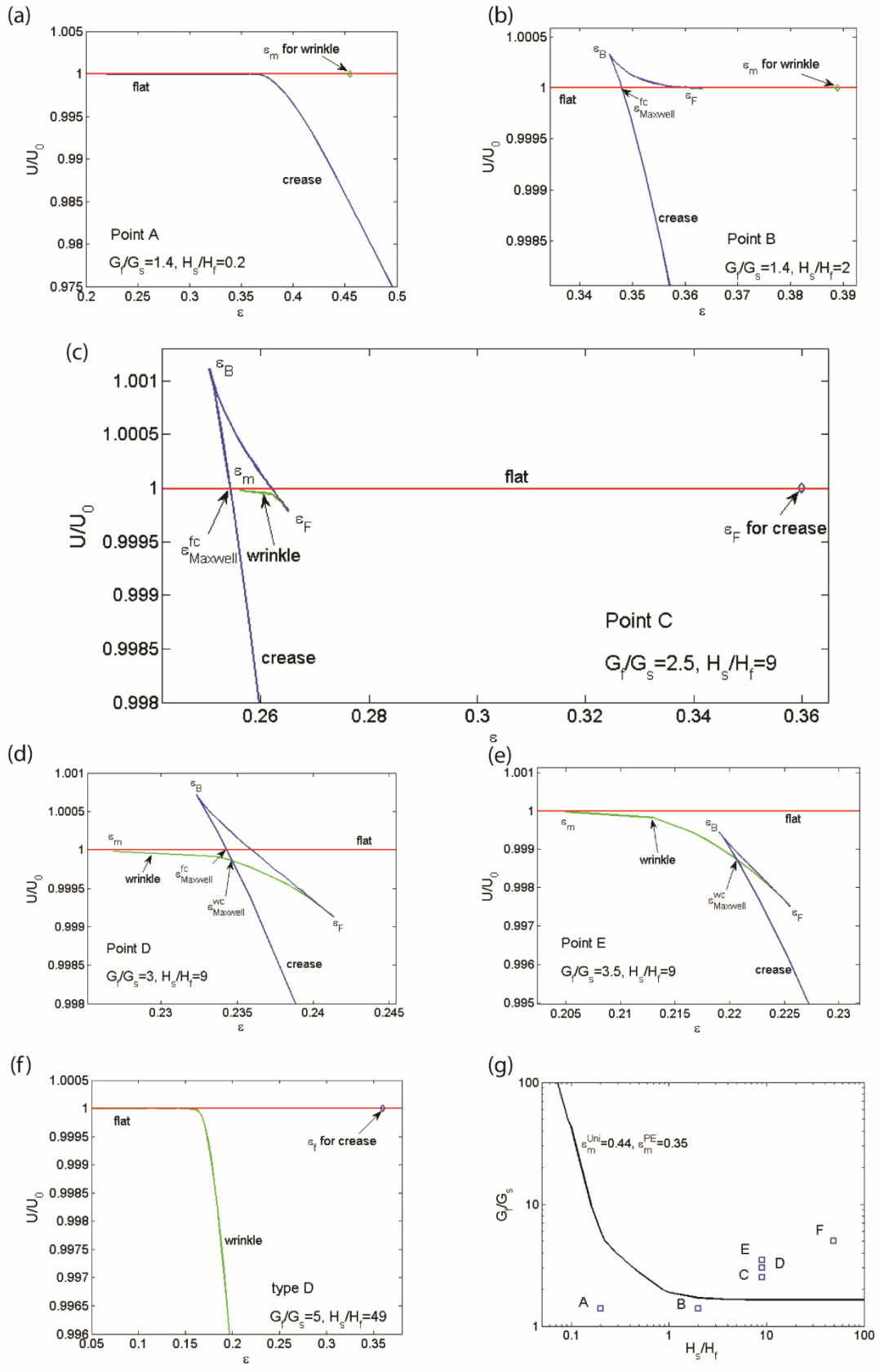
(a)
flat
ε_m for wrinkle
crease
Point A
G_f/G_s=1.4, H_s/H_f=0.2
U/U0
ε
(b)
ε_B
ε_m for wrinkle
flat
$\varepsilon_{Maxwell}^{fc}$
ε_F
crease
Point B
G_f/G_s=1.4, H_s/H_f=2
(c)
ε_B
ε_m
flat
ε_F
$\varepsilon_{Maxwell}^{fc}$
wrinkle
ε_F for crease
crease
Point C
G_f/G_s=2.5, H_s/H_f=9
(d)
ε_B
ε_m
flat
wrinkle
$\varepsilon_{Maxwell}^{fc}$
$\varepsilon_{Maxwell}^{wc}$
ε_F
Point D
G_f/G_s=3, H_s/H_f=9
crease
(e)
ε_m
flat
wrinkle
ε_B
$\varepsilon_{Maxwell}^{wc}$
ε_F
Point E
G_f/G_s=3.5, H_s/H_f=9
crease
(f)
flat
ε_f for crease
wrinkle
type D
G_f/G_s=5, H_s/H_f=49
(g)
ε_m^{Uni}=0.44, ε_m^{PE}=0.35
F
E
D
C
A
B
G_f/G_s
H_s/H_f

Figure 3-3. Bi-layers with various ratios of moduli and thicknesses exhibit various types of bifurcation. (a)-(b) The critical strain for the onset of creases is smaller than that for the onset of wrinkles. Point A: The creases are supercritical. Point B: The creases are subcritical, and can coexist with the flat state at a strain smaller than the critical strain for the onset of creases. Such a strain for the coexistence of two states is known as Maxwell strain. (c)-(f) The critical strain for the onset of wrinkles is smaller than that for the onset of creases. Point C: The flat state and creases coexist at a strain $\varepsilon_{Maxwell}^{fc}$ even smaller than the critical strain for the onset of wrinkles. Point D: The wrinkles form at a certain strain, and can coexist with the creases at a larger strain $\varepsilon_{Maxwell}^{wc}$. The creases can also coexist with the flat state at strain $\varepsilon_{Maxwell}^{fc}$. Point E: The wrinkles form at a certain strain, and can coexist with the creases at a larger strain $\varepsilon_{Maxwell}^{wc}$. Type F: The wrinkles form, and no creases are found in the range of the strain calculated. (g) The points for various bifurcation behaviors identified on the plane of the axes G_f / G_s and H_s / H_f.

Figure 3-3 (a) shows the computed bifurcation diagram for a supercritical crease with $G_f / G_s = 1.4$ and $H_s / H_f = 0.2$ (indicated as point A in Figure. 3-3g). In the bifurcation diagram, the applied strain ε represents the loading parameter, and the total elastic energy U normalized by the total elastic energy for the flat state U_0, U / U_0, represents the state of the system. The flat line $U / U_0 = 1$ represents the flat state. For a supercritical crease, U becomes smaller than U_0 after the formation of the crease. The minimal strain for the initiation of wrinkles ε_m (represented by the diamond in Figure 3-3a) is higher than the critical strain for the initiation of creases. Figure 3-3(b) shows the bifurcation diagram of a subcritical crease with $G_f / G_s = 1.4$ and $H_s / H_f = 2$ (indicated as point B in Figure. 3-3g). The crease can coexist with the flat state at a strain smaller than the critical strain for the onset of creases. The strain of the coexistence is called the Maxwell strain $\varepsilon_{Maxwell}^{fc}$, defined as the critical condition when the energy of the deep crease state is the

same as the flat state. The diamond represents the critical condition for the initiation of wrinkles ε_m, which is also higher than the snapping forward strain ε_F.

When the critical strain for the onset of wrinkles ε_m is smaller than that for the onset of creases, creases instead of wrinkles may still form first, or wrinkles may further transit to creases under a strain much smaller than the critical strain for the onset of creases in a homogeneous material. Figure 3-3(c) is an example of this for $G_f / G_s = 2.5$ and $H_s / H_f = 9$ (indicated as point C in Figure. 3-3g). The line $U / U_0 = 1$ represents the flat state. The crease solution can coexist with the flat state under the Maxwell strain $\varepsilon_{Maxwell}^{fc}$, which is smaller than the critical strain for the onset of wrinkles ε_m. When the defect in the sample is small enough, the flat surface cannot overcome the energy barrier to form creases under $\varepsilon_{Maxwell}^{fc}$, but needs to go to a strain larger than $\varepsilon_{Maxwell}^{fc}$. Therefore, wrinkles may initiate at strain ε_m first, and then snap to creases under a larger strain. When the defect in the sample is large enough, creases can initiate directly from the flat surface, and channel across the surface. This explains why in [23] the authors observed creases experimentally under higher G_f / G_s than the value predicted by their theory, which only considers supercritical creases. The diamond in Figure 3-3 (c) represents the critical strain for the initiation of creases on the flat surface. We notice the critical strain for the initiation of creases with the facilitation of wrinkles is much lower than the critical strain for the initiation of creases in a homogeneous material. Figure 3-3 (d) shows the energy bifurcation diagram for $G_f / G_s = 3$ and $H_s / H_f = 9$ (indicated as point D in Figure.

5g). The flat surface form wrinkles at strain ε_m, and the wrinkles can coexist with creases under a larger strain $\varepsilon_{Maxwell}^{wc}$, which is much smaller than the critical strain for the onset of creases in a homogeneous material (not indicated in the Figure). On the other hand, creases can also coexist with the flat state under strain $\varepsilon_{Maxwell}^{fc}$, which satisfies $\varepsilon_m < \varepsilon_{Maxwell}^{fc} < \varepsilon_{Maxwell}^{wc}$. Figure 3-3 (e) is the energy bifurcation diagram for $G_f / G_s = 3.5$ and $H_s / H_f = 9$ (indicated as point E in Figure. 3-3g). The crease solution no longer has an intersection with the flat state, but still has an intersection with the wrinkle solution. Wrinkles form on a flat surface at strain ε_m, and can coexist with creases at a larger strain $\varepsilon_{Maxwell}^{wc}$, which is also much smaller than the critical strain for the onset of creases in a homogeneous material (not indicated in the Figure). Figure 3-3 (f) shows the energy bifurcation diagram for $G_f / G_s = 5$ and $H_s / H_f = 49$ (indicated as point F in Figure. 3-3g). The elastic energy U for the wrinkle solution becomes smaller than U_0 when the strain is larger than the critical strain for the onset of wrinkles ε_m. No other bifurcation is observed soon after the formation of wrinkles. The critical strain for the initiation of creases on a flat surface, represented by a diamond, is higher.

The bifurcation behavior of supercritical creases, such as for point A in Figure 3-3(a), and wrinkles (Figure 3-3f, point F) is classical, whereas the other types of bifurcation diagrams are new. Here, experiments were conducted to realize these new behaviors, i.e., subcritical creases channeling from a flat surface (Figure. 3-4a, corresponding to point B in Figure. 3-3b) and creases coexisting with wrinkles (Figure. 3-4b, corresponding to

points C, D and E in Figure. 3-3c-e) in bi-layers. The classical wrinkles were also realized as a comparison (Figure. 3-4c). The confocal microscopy insets show the side views of each sample. Fluorescein o-acrylate is added to the films, as shown in green color. In the side view, wrinkles look quite smooth, while a crease forms a sharp tip and has a region of self-contact, highlighted by the brightness in color, which protrudes into the substrate.

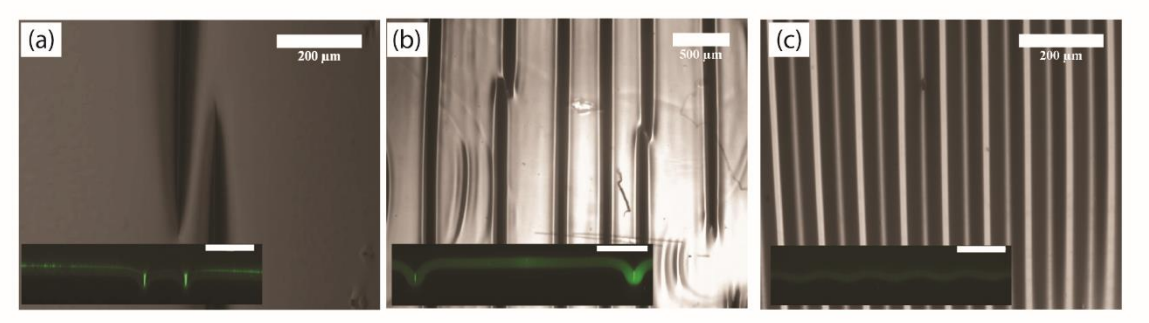

Figure 3-4. The optical micrographs display the top views, and the inset confocal micrographs show the side views (the scale bars in the insets are equal to 100 μm). The micrographs are taken at the applied compressive strains where the instabilities first appear. (a) Subcritical creases at the strain of 0.37. (b) Coexistence of creases and wrinkles at the strain of 0.29. (c) Wrinkles at the strain of 0.21.

In Figure 3-4 (b), the image shows the coexistence of wrinkles and creases. The sample begins to develop wrinkles similar to those in Figure 3-4 (c) over the range of strains from 0.22 – 0.28 (apparently reflecting some variability in conditions across the sample surface, as well as some viscoelastic relaxation in the bi-layer), but then at a strain of 0.28, creases form and channel across the surface, eventually causing the wrinkles to relax and disappear. This strain for the onset of creases is much less than that for

channeling of subcritical or supercritical creases, in good agreement with simulations (Figure. 3-3 c-e). This rich behavior will be discussed in more detailed in the next section.

3.3.2 Secondary Bifurcation

3.3.2.1 Type 1 bifurcation

Kim and co-workers have predicted that a modulus ratio between 1.74 and 5.86, wrinkles will transition into creases[20] similar to the transition observed in Figure 3-4 (b). We call this type of transition a type 1 bifurcation. To further elucidate the nature of the type 1 bifurcation, we simulate the initiation and evolution of the surface instability for a bi-layer in the large thickness contrast region, $(H_s+H_f)/H_f$ =50, with modulus ratio $G_f / G_s = 3$ under uniaxial compression with finite element method. In Figure 3-5(a), we plot the bifurcation diagram with the external strain ε as the loading parameter, and the energy normalized by the value of the flat state U / U_0 as the state of the field. When the strain is small, the flat state is the only solution. When the strain is large enough, the solutions of wrinkle and crease start to emerge. The insets of Figure 3-5(a) show the simulation results of the wrinkle state and the crease state. Wrinkles will first form on the flat surface at strain ε = 0.30. However, the energy of the crease solution will soon be lower than the wrinkle solution. At the Maxwell condition, the wrinkle state and the crease state have the same energy, after which the shallow wrinkles will channel to creases. The wrinkle state becomes unstable at strain ε = 0.309.

With the emergence of the crease solution, wrinkles lose their periodicity. When the crease spacing is set to $L_c = 3L_w$, we distinguish two different types of wrinkle troughs, one of which transitions to a crease and the other does not. Figure 3-5(b) shows the bifurcation diagram with the amplitude normalized by the film thickness H_f as the state of the field. The amplitude is defined as half of the vertical distance between one wrinkle trough and the neighboring wrinkle peak, as sketched in the inset of Figure 3-5(b). Especially, here we calculate the amplitudes of the two different troughs and the wrinkle peak between them; we mark the curves for the two different types of troughs as 'crease tip' and 'wrinkle trough' respectively in Figure 3-5(b). The amplitude remains zero until the initiation of wrinkles. After the emergence of the crease solution, the two curves start to bifurcate from each other. The crease tip grows deeper and therefore the amplitude gets larger, while the other amplitude gets smaller and reaches zero after certain strain.

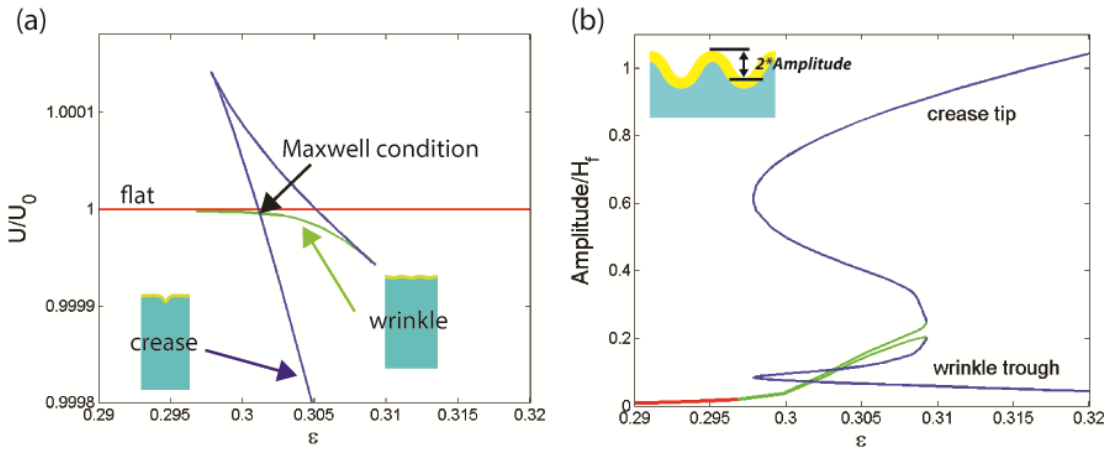

Figure 3-5. Bifurcation diagrams of the type 1 bifurcation for the bi-layer with modulus ratio $G_f / G_s = 3$. The uniaxial strain ε is set as the loading parameter. (a) The state of the field is chosen as the free energy of the block normalized by the flat state U / U_0. The insets show the simulation results of the wrinkle state and the crease state. (b) The amplitude between the wrinkle trough and peak normalized by the film thickness H_f is chosen as the state of the field.

Experiments demonstrate wrinkles transitioning directly to creases in an elastic bi-layer below a modulus contrast of 5, in agreement with the simulation. The sample in Figure 3-6 (a) has a modulus contrast of approximately 4 (1.6 ± 0.5 MPa film and 0.40 ± 0.050 MPa substrate) and shows a type 1 bifurcation, imaged in top view. Faint wrinkles first form at a film strain of 0.28 (Figure. 3-6a). As compression is increased to 0.29, creases nucleate in some of the troughs of the wrinkles. Once creases nucleate, they channel across the surface and relax the wrinkles to zero amplitude over a period of 10 min, leaving behind only the creases.

Confocal microscopy images show the cross-section of a sample with a modulus contrast of approximately 3.5 (750 ± 0.6 kPa substrate and 2.6 ± 0.080 MPa film) going through a type 1 secondary bifurcation during compressive loading and unloading (Figure

3-6b). Faint wrinkles appear at a film strain of 0.33. As the compression increases, the wrinkles snap to a localized crease with a finite depth and the neighboring region flattened. Further compression leads to the creases growing in depth. When the compression is slowly decreased, the crease depth decreases until the system snaps back to the flat state while bypassing the wrinkle state, clearly demonstrating the hysteretic nature of the subcritical type I wrinkle to crease transition.

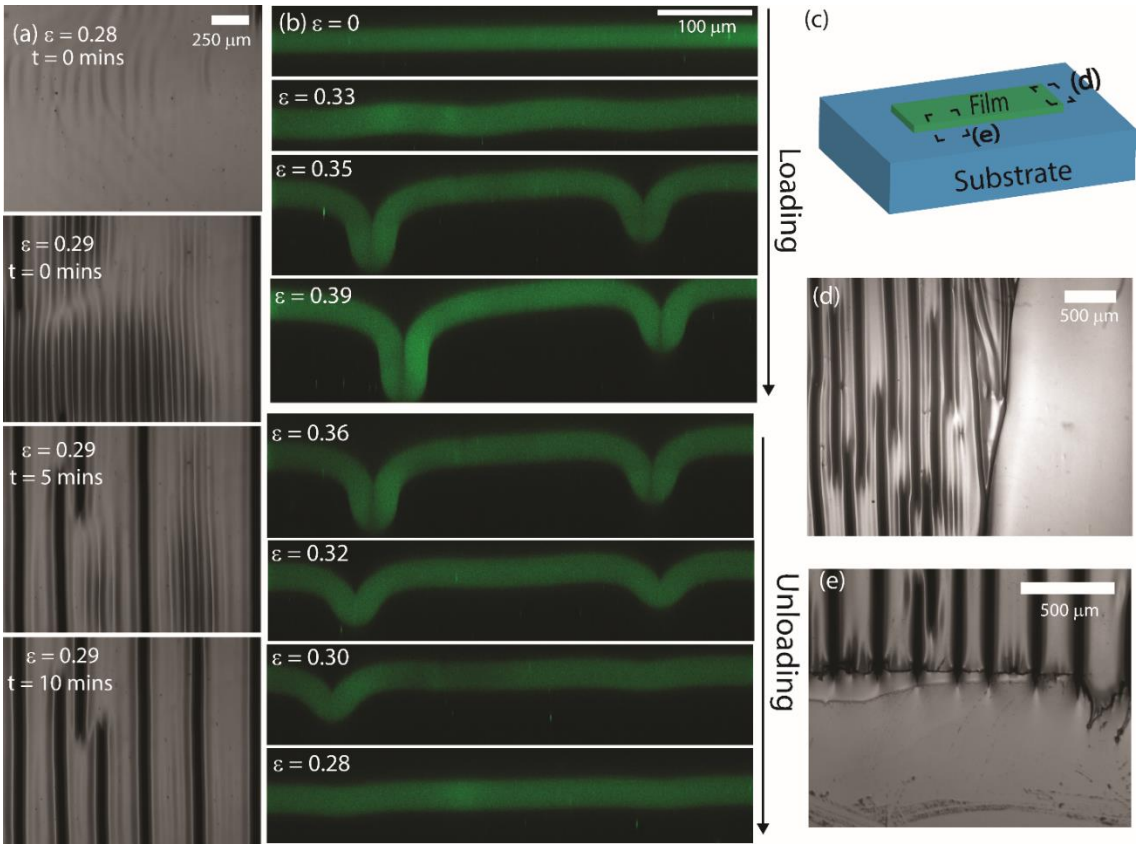

Figure 3-6. The type I bifurcation: (a) Optical micrographs showing the formation of type 1 bifurcation, with wrinkles first appearing and then creases channeling in the troughs of the wrinkles (b) Confocal image showing loading and unloading (c) Schematic of a strip of film partially covering the substrate, with indications of the location of images (d) and (e). (d) For a sample with a film strain of 0.33, the right half of the optical micrograph shows the bare substrate and the left half is the film attached to the substrate which shows the coexistence of wrinkles and creases. (e) Creases do not propagate onto the bare substrate below a film strain of 0.44.

In another experiment, a small strip of the film is used to cover a portion of the substrate, while the surrounding areas are left bare, as illustrated in Figure 3-6 (c). We then examine the edges of the film, as denoted by the two dotted boxes in Figure 3-6 (c) and shown in Figure 3-6 (d) and (e). The left part of the Figure 3-6 (d) image is the substrate covered by a film with a modulus contrast of 4 while the right part does not

have the film. Similarly, the top part of the image in Figure 3-6 (e) is covered with the film while bottom part is not and the bare substrate is exposed. These images demonstrate two important points. First, the presence of a slightly stiffer film significantly lowers the critical strain for creases compared to a homogeneous material like the bare substrate. This is evident in both Figure 3-6 (d) and (e), where creases are present in the bi-layer but the bare substrate remains flat at a strain of 0.33. Secondly, creases will remain on the bi-layer and will not channel into regions where the film is not present as shown in Figure 3-6 (e). Once the system is uniaxially compressed beyond the critical strain for creasing in a thick soft substrate, 0.44, creases are formed on the bare substrate.

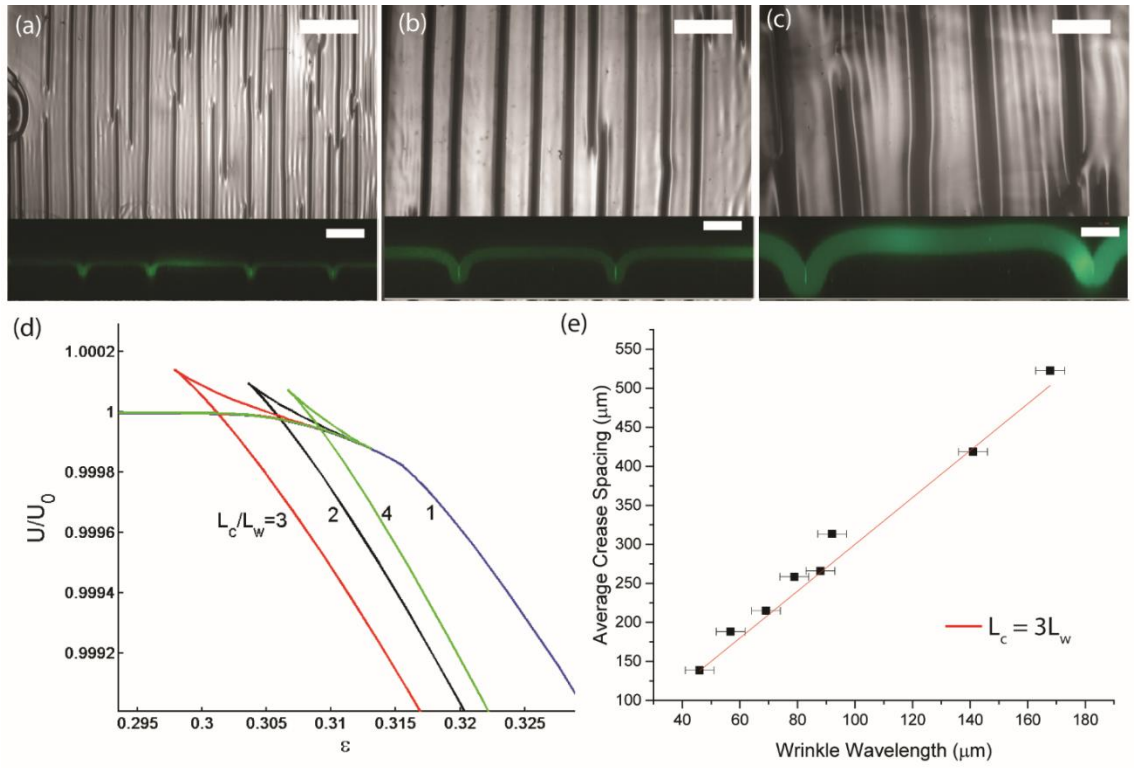

Figure 3-7. (a, b, c) Top view optical micrographs (top, 500 μm scale bar) and cross-sectional confocal images (bottom, 50 μm scale bar) for creases formed by type 1 bifurcation, where the film thickness increases from (a) 5 μm (at ε= 0.26), to (b) 18 μm (at ε= 0.30), and to (c) 26 μm (at ε= 0.29), while the thickness of the substrate remains the same (400 μm). The film thickness affects crease spacing; the crease spacing for (a) is 200 μm, for (b) is 290 μm, and for (c) is 550 μm. (d) Simulation results of the bifurcation diagram with strain ε as the loading parameter and the free energy as the state of the field for $G_f / G_s = 3$. Different curves are for different spacing of creases. In the strain range covered by the simulation $0 \le \varepsilon \le 0.47$, the spacing of creases as 3 times of wrinkle wavelength has the lowest energy. (e) Experimental result of the average crease spacing as a function of wrinkle wavelength.

As a further demonstration that creases formed by type I bifurcation differ from creases in the substrate alone, we characterize the effect of film thickness on crease spacing. Creases in a thick soft substrate are known to adopt a spacing of approximately $3.5(1-\varepsilon)H_s$ [13]; however, we find that in bi-layers the crease spacing in type 1 bifurcations is controlled by the film thickness and not substrate thickness (Figure 3-7). Example

optical micrographs (top views) of creases formed by type 1 bifurcation, along with corresponding confocal cross-sections (50 μm scale bar) are shown for film thicknesses of 5, 18, and 26 μm, at constant substrate thickness (400 μm). The average spacing between creases L_c can clearly be seen to increase with film thickness, with respective values of 200, 290, and 550 μm. Here, we measure L_c by drawing a line along the compression direction across each top view micrograph, and dividing the length of the line by the number of creases that cross the line.

To better understand the relationship between the crease spacing and the wrinkle wavelength, we performed finite element simulations with different box sizes, where we ensure that several wrinkles transition to one crease by prescribing only one geometric defect to initiate the crease. Therefore, we can vary the crease spacing by varying the size of the simulation box. Figure 3-7 (d) shows the free energy U/U_0 as a function of strain ε for $G_f/G_s = 3$ with different crease spacing L_c/L_w =1, 2, 3, 4. The free energy of the creased state for L_c/L_w =3 becomes lower than the wrinkled state earlier than for other spacings. Moreover, in the range of strain covered by our simulation $0 \le \varepsilon \le 0.47$, the mode L_c/L_w = 3 always has the lowest energy, which is different than the L_c/L_w = 4 predicted by Kim [20]. As shown in Figure 3-7 (e), our prediction is in excellent agreement with the experimental measurements (where the wrinkle wavelength L_w is measured at the strain where creases first appear).

3.3.2.2 Type 2 bifurcation

For a modulus ratio between 5.86 to 13, Kim and coworkers predicted that wrinkles will first undergo period doubling, followed by formation of creases [20]. We call this type of evolution type 2. We analyze the type 2 bifurcation through finite element simulations of an elastic bi-layer with modulus ratio $G_f / G_s = 8$ under uniaxial compression. Since we expect wrinkles to double in period prior to crease formation in the deeper troughs, we control the size of the simulation box to be one wrinkle wavelength, such that one crease forms for every two wrinkles due to the mirror symmetric boundary condition. Figure 3-8 (a) shows the simulation result of the bifurcation diagram with the strain ε as the loading parameter, and the energy normalized by that of the flat state U / U_0 as the state of the field. The flat state is the only solution before the critical strain for the initiation of wrinkles ε = 0.174. With the further increase of the strain, wrinkles form and the energy becomes lower than the homogeneous state. At ε = 0.202, the period doubled state occurs and further decreases the energy compared to the wrinkled state. Soon after that, creases form on the lower trough in the period doubled state. Figure 3-8 (b) is the bifurcation diagram with the amplitude normalized by the film thickness H_f as the state of the field. The curves for the two different types of troughs remain at zero in the flat state, become non-zero after the wrinkles form, and bifurcate from each other after period doubling. The amplitude for the crease tip increases with further increases of the strain, while the amplitude for the other type of wrinkle trough, where a crease does not form, decreases. This is different than the

prediction from Kim and coworkers where the crease form in every fourth wrinkle tough [20].

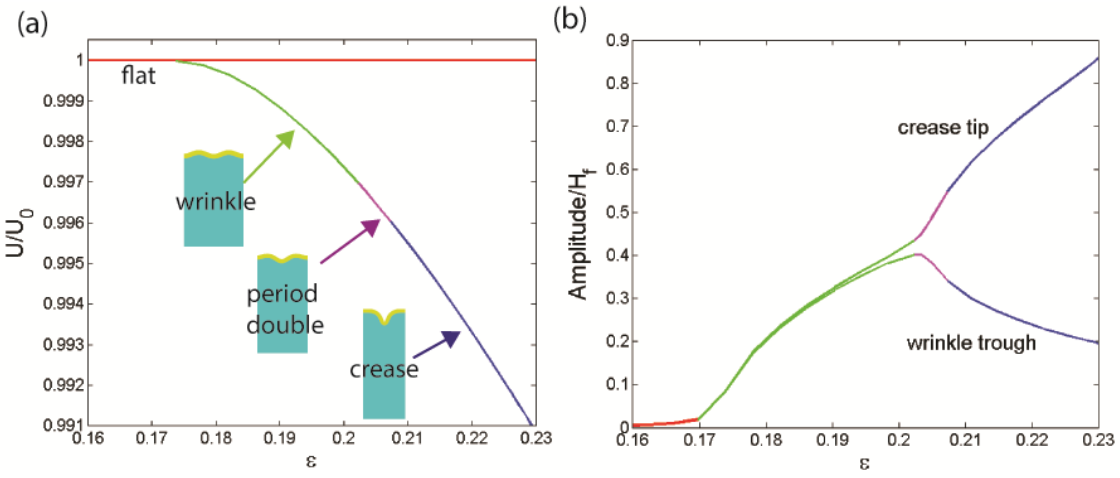

Figure 3-8. Bifurcation diagrams for type 2 bifurcation of a bi-layer with modulus ratio $G_f / G_s = 8$. The uniaxial strain is set as the loading parameter. (a) The state of the field is chosen as the free energy of the block normalized by the flat state U / U_0. The insets show the simulation results of the wrinkle, period doubling and the crease states. (b) The amplitude between the wrinkle trough and peak normalized by the film thickness H_f is chosen as the state of the field.

The experimental results of the type 2 bifurcation show an evolution of wrinkles to creases that closely matches that predicted in the simulations. The loading and unloading of a bi-layer with a modulus contrast of approximately 5 is shown in Figure 3-9 (a). The surface remains in the flat state until wrinkles form at a strain of about 0.15. Afterwards, wrinkles grow in amplitude with further increases in the strain. At a strain of 0.28, the wrinkles undergo period doubling. However, unlike the traditional period doubled state in bi-layers with high modulus contrast, creases form in the troughs of the deeper wrinkles, as can be seen from the shift from a smooth 'U' shape, to a 'V' shape in

every other trough. As compression increases, the amplitudes of the self-contacting creases increase, while the amplitudes of the neighboring wrinkle troughs continue to diminish. With unloading, the self-contacting depth of the crease decreases while the amplitude of the other type of wrinkle trough increases. At a film strain of 0.25, the shape of the crease tips return to a 'U' shape but the bi-layer still shows slight differences in amplitude between successive features (i.e., corresponding to the period doubled state). Upon further release of compression, the system returns to a wrinkled state and then eventually a flat state highlighting that the type 2 bifurcation is supercritical and has little to no hysteresis.

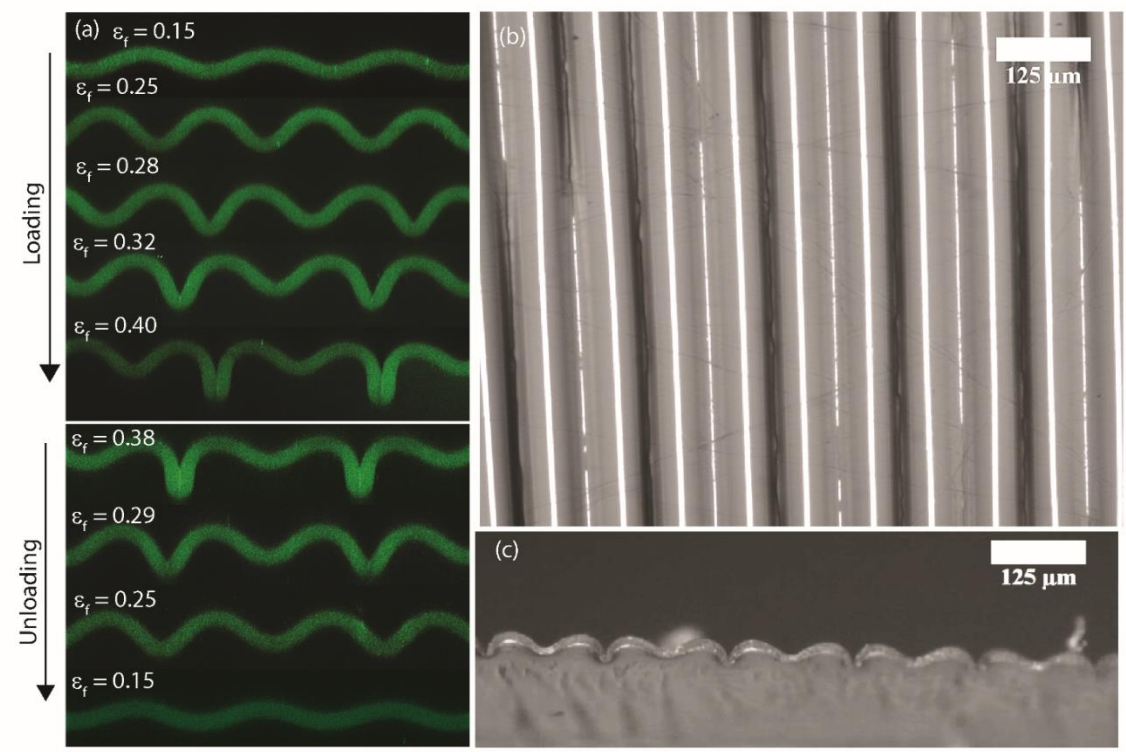

Figure 3-9. The type 2 bifurcation: (a) confocal image showing loading and unloading; optical micrographs showing (b) top and (c) side views of a bi-layer at $\varepsilon = 0.26$ in the period doubled state with creases in the deeper troughs.

The top view optical micrograph of a bi-layer having undergone type 2 bifurcation with a modulus contrast of approximately 5 in Figure 3-9(b) shows uniform creases, characterized by the dark lines, with a spacing equal to two times the wrinkle wavelength. The thick solid white lines are the peaks of the wrinkles while the thinner solid white lines are the shallow wrinkle troughs. The cross-sectional optical micrograph in Figure 3-9 (c) shows that creases form in every other wrinkle trough, and that these troughs have a qualitatively different shape than those without creases. Since the crease spacing is dictated by the location of the deeper trough in the period doubled state, creases adopt a highly uniform spacing of 2 times the wrinkle wavelength (ignoring the influence of

defects in the initial wrinkle pattern). Type 2 slightly deviates from the result of Kim and coworkers [20] where they predicted that a type 2 bifurcation would be observed at a modulus contrast of 5.84 and would lead to a crease spacing of 4 times the wrinkle wavelength. However, we find a smooth transition from a type 1 to a type 2 bifurcation as the modulus contrast increases which could account for the slight difference from their predicted modulus contrast. In addition, the difference in crease spacing is likely due to the difference in the construction of the simulation cells and perturbing the surface to first initiate the crease.

3.4 Conclusion

We have experimentally and computationally characterized the formation and evolution of primary and secondary bifurcation modes including two types of post-wrinkling bifurcations for elastic bi-layers with modulus ratio of the film to substrate between 1 and 10. Whether creases or wrinkles appear first is dependent on both the modulus contrast and the thickness contrast. Below a modulus contrast of 1.65, creases will form first, while above 1.65 wrinkles will form first in a defect-free sample. At the boundary between these two instability phases are rich post-wrinkling bifurcation behaviors. For secondary bifurcations in bi-layers with large thickness contrast, type 1 bifurcation corresponds to wrinkles transitioning into subcritical creases, without the appearance of period-doubling, while type 2 bifurcation corresponds to wrinkles that first undergo period doubling, followed by the supercritical formation of creases. For type 1 bifurcation, the crease spacing is dictated by the film thickness and is, on average, three

times the wrinkle wavelength, although creases do not form a regularly spaced array. For type 2 bifurcation, on the other hand, creases form in each of the deeper troughs in the period doubled state, thereby providing a regular pattern of creases with spacing equal to twice the wrinkle wavelength. We anticipate that the understanding gained of surface instabilities within elastic bi-layers of modest modulus contrast may have relevance for pattern formation in a variety of biological and man-made systems.

3.5 References

[1] J. Dervaux, M. Ben Amar, Morphogenesis of Growing Soft Tissues, Phys. Rev. Lett. 101 (2008) 068101. doi:10.1103/PhysRevLett.101.068101.

[2] C.T. McKee, J.A. Last, P. Russell, C.J. Murphy, Indentation versus Tensile Mesurements of Young ’s Modulus for Soft Biological Tissues, Tissue Eng. B. 17 (2011). doi:10.1089/ten.teb.2010.0520.

[3] J. Yin, X. Chen, I. Sheinman, Anisotropic buckling patterns in spheroidal film/substrate systems and their implications in some natural and biological systems, J. Mech. Phys. Solids. 57 (2009) 1470–1484. doi:10.1016/j.jmps.2009.06.002.

[4] T. Tallinen, J.Y. Chung, J.S. Biggins, L. Mahadevan, Gyrification from constrained cortical expansion., Proc. Natl. Acad. Sci. U. S. A. 111 (2014) 12667–72. doi:10.1073/pnas.1406015111.

[5] B.R. Wiggs, C. a Hrousis, J.M. Drazen, R.D. Kamm, On the mechanism of mucosal folding in normal and asthmatic airways., J. Appl. Physiol. 83 (1997) 1814–1821.

[6] W. Yang, T.C. Fung, K.S. Chian, C.K. Chong, Instability of the two-layered thick-walled esophageal model under the external pressure and circular outer boundary condition, J. Biomech. 40 (2007) 481–490. doi:10.1016/j.jbiomech.2006.02.020.

[7] J.-Y. Sun, S. Xia, M.-W. Moon, K.H. Oh, K.-S. Kim, Folding wrinkles of a thin stiff layer on a soft substrate, Proc. R. Soc. A Math. Phys. Eng. Sci. 468 (2011) 932–953. doi:10.1098/rspa.2011.0567.

[8] J. Genzer, J. Groenewold, Soft matter with hard skin: From skin wrinkles to templating and material characterization, Soft Matter. 2 (2006) 310. doi:10.1039/b516741h.

[9] Z.Y. Huang, W. Hong, Z. Suo, Nonlinear analyses of wrinkles in a film bonded to a compliant substrate, J. Mech. Phys. Solids. 53 (2005) 2101–2118. doi:10.1016/j.jmps.2005.03.007.

[10] J. Yoon, J. Kim, R.C. Hayward, Nucleation, growth, and hysteresis of surface creases on swelled polymer gels, Soft Matter. 6 (2010) 5807. doi:10.1039/c0sm00372g.

[11] W. Hong, X. Zhao, Z. Suo, Formation of creases on the surfaces of elastomers and gels, Appl. Phys. Lett. 95 (2009) 111901. doi:10.1063/1.3211917.

[12] E. Hohlfeld, L. Mahadevan, Unfolding the Sulcus, Phys. Rev. Lett. 106 (2011) 105702. doi:10.1103/PhysRevLett.106.105702.

[13] S. Cai, D. Chen, Z. Suo, R.C. Hayward, Creasing instability of elastomer films, Soft

Matter. 8 (2012) 1301. doi:10.1039/c2sm06844c.

[14] F. Brau, P. Damman, H. Diamant, T. a. Witten, Wrinkle to fold transition: influence of the substrate response, Soft Matter. 9 (2013) 8177. doi:10.1039/c3sm50655j.

[15] F. Brau, H. Vandeparre, A. Sabbah, C. Poulard, A. Boudaoud, P. Damman, Multiple-length-scale elastic instability mimics parametric resonance of nonlinear oscillators, Nat. Phys. 7 (2010) 56–60. doi:10.1038/nphys1806.

[16] L. Pocivavsek, R. Dellsy, A. Kern, S. Johnson, B. Lin, K.Y.C. Lee, et al., Stress and fold localization in thin elastic membranes., Science. 320 (2008) 912–6. doi:10.1126/science.1154069.

[17] J.W. Hutchinson, The role of nonlinear substrate elasticity in the wrinkling of thin films, Philos. Trans. R. Soc. A Math. Phys. Eng. Sci. 371 (2013). http://rsta.royalsocietypublishing.org/content/371/1993/20120422.short (accessed November 26, 2013).

[18] A. Auguste, L. Jin, Z. Suo, R.C. Hayward, The role of substrate pre-stretch in post-wrinkling bifurcations., Soft Matter. 10 (2014) 6520–9. doi:10.1039/c4sm01038h.

[19] Y.B. Fu, P. Ciarletta, Buckling of a coated elastic half-space when the coating and substrate have similar material properties, (2015).

[20] R. Zhao, T. Zhang, M. Diab, H. Gao, K.-S. Kim, The primary bilayer ruga-phase diagram I: Localizations in ruga evolution, Extrem. Mech. Lett. (2015). doi:10.1016/j.eml.2015.04.006.

[21] Y. Cao, J.W. Hutchinson, Wrinkling Phenomena in Neo-Hookean Film/Substrate Bilayers, J. Appl. Mech. 79 (2012) 031019. doi:10.1115/1.4005960.

[22] Q. Wang, X. Zhao, A three-dimensional phase diagram of growth-induced surface instabilities, Sci. Rep. 5 (2015) 8887. doi:10.1038/srep08887.

[23] Q. Wang, X. Zhao, Phase Diagrams of Instabilities in Compressed Film-Substrate Systems, J. Appl. Mech. 81 (2013). doi:10.1115/1.4025828.

[24] M. Diab, T. Zhang, R. Zhao, H. Gao, K. Kim, P.R.S. A, Ruga mechanics of creasing : from instantaneous to setback creases Ruga mechanics of creasing : from instantaneous to setback creases, (2013).

[25] G. Miquelard-Garnier, A.B. Croll, C.S. Davis, A.J. Crosby, Contact-line mechanics for pattern control, Soft Matter. 6 (2010) 5789. doi:10.1039/c0sm00165a.

[26] S. Park, Y.S. Huh, H.G. Craighead, D. Erickson, A method for nanofluidic device prototyping using elastomeric collapse., Proc. Natl. Acad. Sci. U. S. A. 106 (2009) 15549–15554. doi:10.1073/pnas.0904004106.

[27] J. Yin, Z. Cao, C. Li, I. Sheinman, X. Chen, Stress-driven buckling patterns in spheroidal core/shell structures., Proc. Natl. Acad. Sci. U. S. A. 105 (2008) 19132–

5. doi:10.1073/pnas.0810443105.

[28] Q. Wang, L. Zhang, X. Zhao, Creasing to Cratering Instability in Polymers under Ultrahigh Electric Fields, Phys. Rev. Lett. 106 (2011) 1–4. doi:10.1103/PhysRevLett.106.118301.

CHAPTER 4

THICKNESS CONTRAST EFFECTS ON POST-WRINKLING MODES[††]

4.1 Introduction

Wrinkles result from placing a thin stiff film bonded to a thick soft substrate under compression. A thin sheet prefers to bend to accommodate the compression, while a thick sheet prefers to stretch. It is the balance between bending and stretching energies that causes wrinkles to form. In prior studies on the formation and evolution of wrinkles, it has generally been assumed that the thickness of the film is much less than the thickness of the substrate[1–5]. This assumption underlies the classical wrinkling equations, for example, which predict the wrinkle wavelength and amplitude to be dependent on the film thickness and independent of the substrate thickness[6,7]; however, the properties of the substrate affect post-wrinkling modes. Previous work has shown that thin films on a liquid foundation will form wrinkles that transition into folds[8–10], while thin stiff films on a thick soft substrate will exhibit a sequence of post-wrinkling bifurcations (period doubling and quadrupling), due to non-linearity in the elastic energy of the substrate[10–13]. The modulus of the substrate compared to the film will dictate the formation of creases, wrinkles, or wrinkles that transition into creases[14,15]. Given the importance of the substrate, there is surprisingly little research on how the substrate

[††] A. Auguste, J. Yang, L. Jin, D. Chen, Z. Suo, R.C. Hayward, (2016). In preparation.

thickness affects these post-wrinkling behaviors as it approaches the thickness of the film, even though this situation has relevance in contexts such as flexible electronics and biological tissues which are composed of multiple layers with small thickness contrast[16–18].

In Chapter 3, we briefly discussed how thickness contrast affects primary bifurcations, while in this chapter we will focus on post-wrinkling behaviors. We show that by decreasing the thickness ratio in a bi-layer system, post-wrinkling bifurcations are delayed, allowing the amplitudes of the wrinkles to continue to grow prior to period doubling. As a result, high aspect ratio wrinkles can be achieved simply by changing the thickness contrast between the substrate and film. The ability to form high aspect ratio wrinkles may improve performance of flexible electronic devices and enable tuning of material properties including adhesion, friction, and wetting over wider ranges.

4.2 Method

4.2.1 Experimental

The experimental procedure is similar to the procedure in Chapter 3. Uniform uniaxial compression is applied to the bi-layer structures through a pre-stretched mounting layer underneath the bi-layers. A silica reinforced vinyl-terminated polydimethylsiloxane (PDMS) mounting layer (Elastosil M4600, Wacker Chemical Company) is uniaxially pre-stretched on a stretcher. The thin film is created by using

uncured 5:1 PDMS (Sylgard 184, Dow Corning) that is spin coated onto a trimethylchlorosiloxane treated glass slide and then placed in the oven at 120 ºC for 120 min (modulus of 2.6 ± 0.8 GPa) [19,20]. Changing the spin speed of the spin-coater provides access to a wide range of thicknesses for the substrate and thin film. Uncured 40:1 PDMS is coated on top of the 5:1 PDMS coated glass slide, placed in a 120 °C oven for 10 min, and then attached to the mounting layer and placed in an oven at 40 °C for 16 h to bond and cure the PDMS layers. The resulting bi-layer had a modulus contrast of ~50. Laser scanning confocal fluorescence microscopy (Zeiss LSM 510 Meta), optical microscopy (Zeiss Axiotech vario), and optical profilometry (Zygo NewView 7300) are used to characterize the evolution of wrinkled surface profiles.

4.2.2 **FEM Simulations**[‡‡]

To gain insight on how the thickness contrast affects post-wrinkling behaviors, we conducted finite element simulations using commercial software Abaqus 6.12/standard, under uniaxial compression. Since the modulus of mounting layer (~1000 kPa) used in the experiments is much larger than the modulus of substrate (~1 kPa), the mounting layer does not deform substantially. Hence, we only simulate the film and substrate bi-layers, and represent the mounting layer through the boundary conditions on the substrate, as described below. Linear perturbation analysis is performed to determine the wavelength of the bi-layer system [21]. For simplicity, we choose the computational cell (unit cell) to

[‡‡] All finite element model simulations were performed by Jiawei Yang under the guidance of Professor Zhigang Suo at Harvard University

be the bi-layer system with one wavelength λ. In the simulations, we take both the film and the substrate to be incompressible, neo-Hookean materials with shear moduli, G_f and G_s, and model them with element type CAX4RH. The right boundary of the unit cell is subject to displacement u_o ($0 < u_o < \lambda$), so that the applied strain is u_o/λ; the left boundary of the unit cell corresponds to the line of symmetry; on the bottom boundary of the unit cell, we constrain the vertical displacement of each point to be the same and also prescribe a linearly distributed horizontal displacement $u_o x/\lambda$. Here, *x* is the horizontal coordinate along the bottom boundary with the origin at the line of symmetry. Next, the wrinkle wavelength λ is calculated based on film thickness and modulus contrast. We perturb the top surface of the unit cell into a sinusoidal shape, with λ and small amplitude 0.001*H*. To trigger the period doubling, a linear displacement in the range $0 < x < \lambda/10$ is superimposed onto the sinusoidal shape with amplitude 0.0001*H* at the left boundary of the free surface and amplitude 0 at $x = \lambda/10$.

4.3 Results and discussion

4.3.1 Morphology

To investigate the effects of modest thickness contrast between the substrate and film on post-wrinkling behaviors, we first characterize the cross-sectional profile of experimental samples using confocal and optical microscopy. We analyze samples with a thickness contrast between 0.7 – 10. When the thickness contrast is below 2, the surface transitions from the flat state to the wrinkled state. As compression increases, creases

are formed as shown in Figure 4-1(a and c). Figure 4-1(a) shows that the film can grow in amplitude until it reaches the boundary of the mounting layer. At this point, the wrinkle amplitude can no longer grow and therefore creases are formed in every trough, which is evident by the bright spots in the wrinkle troughs in Figure 4-1(c). However, at the appearance of creases, we find that the mounting layer begins to show significant out-of-plane deformation, and thus the sample can no longer be adequately treated as a bi-layer, as shown in Figure 4-1(b). For simplicity, we therefore focus solely on samples with a thickness contrast above 2 where the boundary between the mounting layer and the substrate remains planar under high compression (0.6).

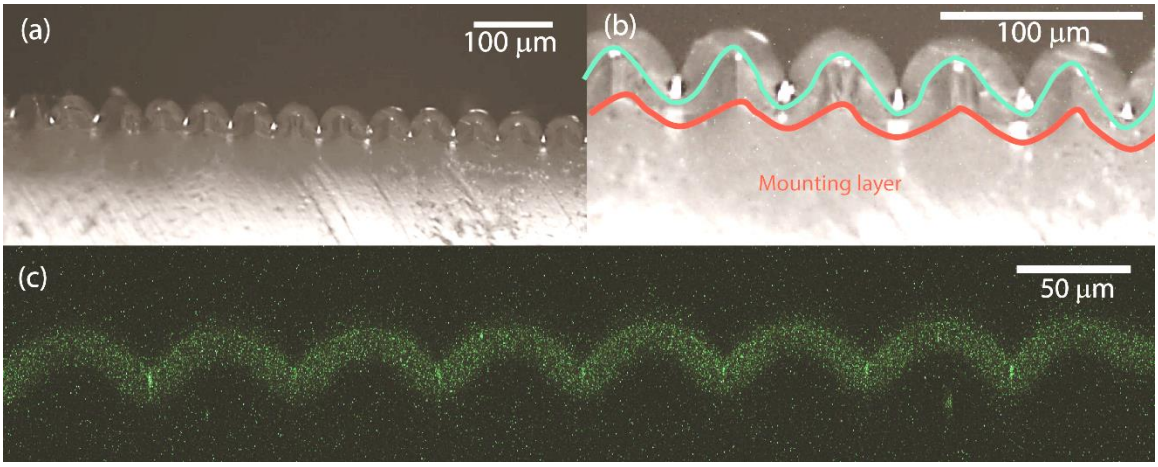

Figure 4-1. (a) An optical side view image of a sample with hf = 24 μm, hs=15 μm at a film strain of 0.38; (b) a zoomed in image of (a) showing the three different layers where the red line denotes the boundary between the mounting layer and the substrate and the blue line outlines the boundary between the substrate and the film; (c) confocal image shows that the sample exhibits creases at every wrinkle trough for a film strain of 0.39.

Above a thickness contrast of 2, wrinkles transition into the period doubled state as shown in Figure 4-2. At a thickness contrast of 3, the bi-layer forms wrinkles which

grow in amplitude and decrease in wavelength as compression is increased. As the compression is increased, the curvature of the peaks and troughs increase while the angle between each trough and its neighboring peaks decrease. This leads to a morphology of uniform large amplitude waves with a small wavelength, as shown in Figure 4-2 (a) for a strain of 0.44. Eventually, localization occurs and the wrinkles transition to the period doubled state at a film strain of 0.52.

The morphology from experiments matches closely the morphology found in simulations. Figure4-2 (c and d) show a sequence of simulation snap shots of the evolution of wrinkles with applied strain. The modulus contrast is fixed at 50 and thickness contrast is 3 and 9 respectively. When the thickness contrast is 3, the wrinkles form and keep developing until strain reaches 0.44. At 0.44, period doubling sets in and breaks the symmetry of the wrinkle patterns. The simulations are fairly consistent to experimental observation. The small thickness contrast delayed both the formation of wrinkles and period doubling compared to samples with thickness contrast greater than 10.

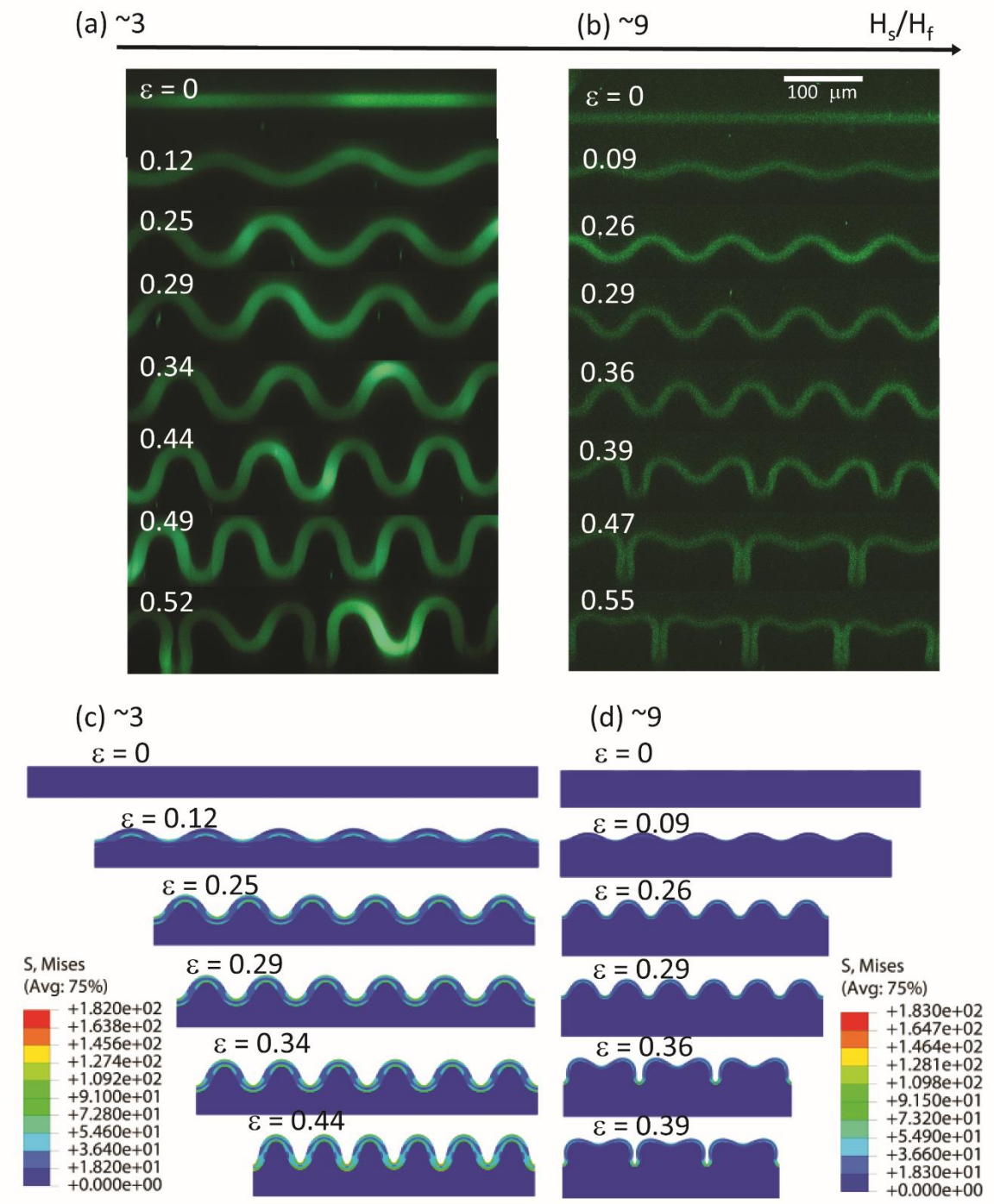

Figure 4-2. Confocal (a and b) and computational (c and d) cross-sectional view of the morphological change with changing strain and thickness contrast at (a and c) 3 and (b and d) 9.

Increasing the thickness contrast changes the morphology, as shown in Figure 4-2(b). At the thickness ratio of 9, the wrinkles grow in amplitude with increasing compression; however, since period doubling occurs at a strain of 0.39 instead of 0.52, the wrinkles never achieve such uniform high amplitude wrinkles as in Figure 4-2(a). The simulation, in Figure 4-2(d), also shows that period doubling occurs earlier at a strain of 0.315 for a thickness contrast of 9 compared to 3, which prevents the formation of high amplitude wrinkles. By decreasing the thickness contrast between the film and substrate, the onset of a post-wrinkling mode is delayed.

4.3.2 Critical Strain

As shown in the previous section, modest thickness contrast between the film and substrate affects the critical strain for wrinkling and post-wrinkling modes. Figure 4-3 plots the critical strain for wrinkling and period doubling versus thickness contrast. The critical strain for wrinkling is determined by taking the average between the strains at which the flat surface is last observed and the wrinkled surface is first detected. These strains also represent the lower and upper bounds of the error bars. The critical strain for period doubling is determined by plotting standard deviation of the amplitudes versus strain and is the point at which the standard deviation shows a dramatic increase.

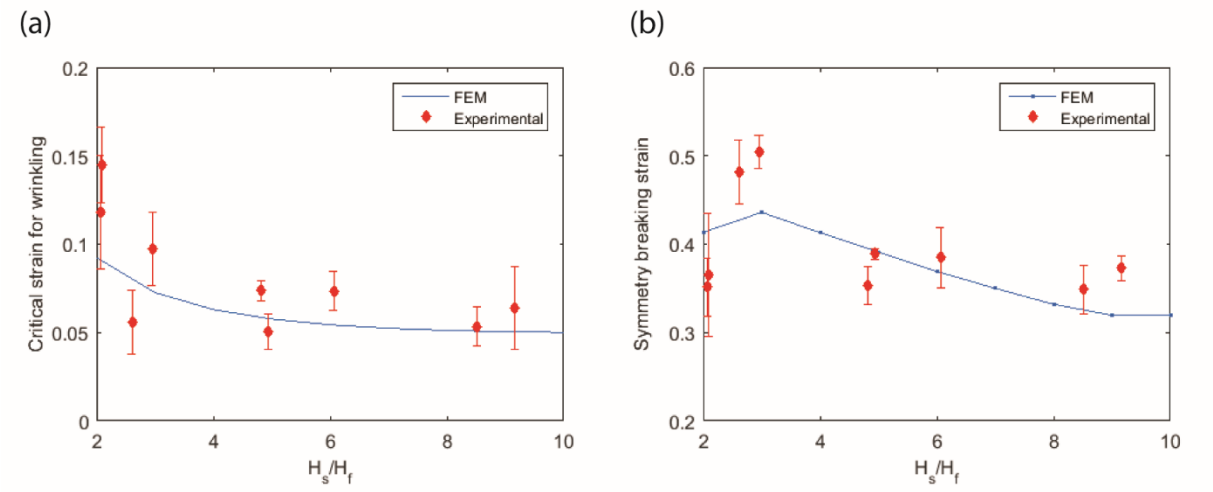

Figure 4-3. Effect on critical strain. (a) the critical strain for the onset of wrinkles as function of thickness contrast. (b) The symmetry breaking strain as function of thickness contrast. The modulus contrast is fixed at 50 for (a) and (b).

We see in Figure 4-3 (a) that the critical strain for wrinkling remains almost constant as the thickness contrast increases from 3 to 10. The largest difference in the critical strain for wrinkles is found for thickness contrasts below 3. As the thickness contrast decreases, the thin and compliant substrate has negligible constraint to the film, and the bi-layer approaches the limit of a free standing homogeneous material on a stiff mounting layer [22], causing a dramatic increase in the critical strain. Figure 4-3(a) shows good agreement of the FEM simulation with the experimental result.

Figure 4-3(b) shows the effect of modest thickness contrast on the critical strain of post-wrinkling behaviors. Again, the experiments are reasonably consistent with the simulation results. There is a maximum in the critical strain at a thickness contrast of 3. At a thickness contrast of 3, FEM simulation predicts a critical strain for the post-wrinkling

modes of 0.44 while a critical strain of 0.50 ± 0.02 is observed in experiment. Above a thickness contrast of 3, the critical strain decreases with increases in the thickness contrast. At a thickness contrast of 9, the critical strain decreases to 0.32 in simulations and 0.37 ± 0.01 in experiments. At higher thickness contrast, studies [12,23,24] have shown that the critical strain for period doubling plateaus around 0.18-0.20. Below a thickness contrast of 3, the critical stain decreases with decreasing thickness contrast as the bi-layer approaches the limit for creasing.

The delay in the appearance of post-wrinkling behaviors is due to the thin substrate suppressing localizations. This behavior is analogous to pre-stretching the substrate. Pre-stretch softens outward deflection compared to inward deflection. The preference for outward deflection favors ridge formation [25]. The thin substrate penalizes large localized inward deflections, thereby delaying the onset of period doubling. At large modulus ratios, but small thickness contrasts, the system prefers outward deflection and ridges are formed, which will be further discussed in Chapter 5.

4.3.3 Aspect Ratio

We characterized the aspect ratio of wrinkles as the amplitude (i.e., the vertical distance from wrinkle peak to trough) divided by the wavelength. When analyzing the samples, an average aspect ratio is determined by measurements on at least 4 waves. The aspect ratio of wrinkles is dependent on the compressive strain applied. As shown in Figure 4-4 (a), when the aspect ratio is plotted versus the compressive strain, the aspect ratio increases as strain increases. This is due to the wrinkle amplitude increasing while

the wrinkle wavelength decreases with increasing strain. The graph in Figure 4-4 compares both FEM and experimental results of a sample with a thickness ratio of 3 and a modulus contrast of 50. The simulation and experiments are in good agreement; however, experimentally, we are able to get a maximum aspect ratio slightly over 0.6, while the simulations end at 0.6 due to the formation of period doubling.

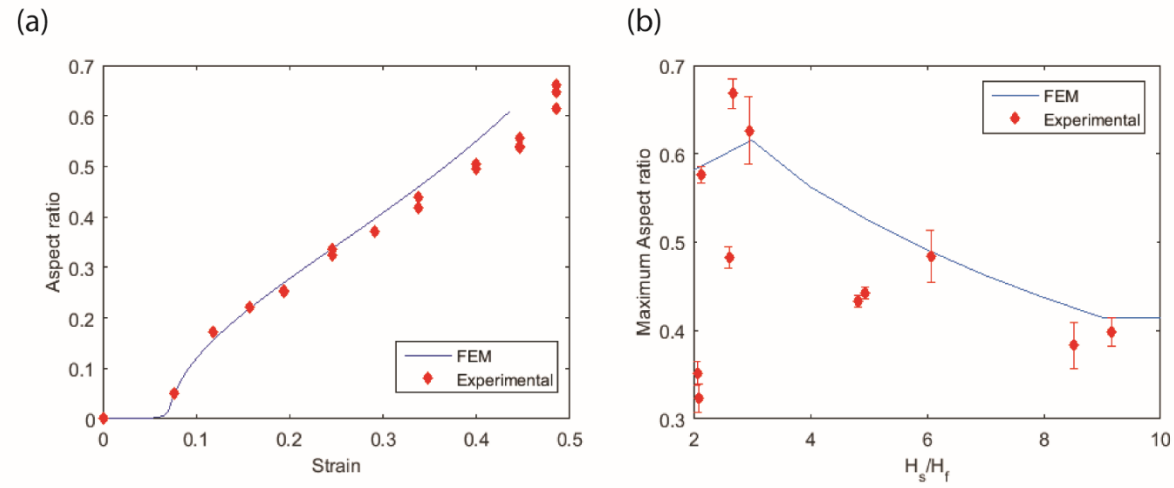

Figure 4-4. Effect on aspect ratio. (a) The increase of aspect ratio with applied strain. Thickness contrast is fixed at 3 and modulus contrast is 50. (b) Maximum aspect ratio as function of thickness contrast.

The maximum aspect ratio for each thickness contrast is plotted in Figure 4-4(b). In simulations, the strain is applied in small increments, and thus the maximum aspect ratio achieved prior to period doubling can be determined with good certainty. In experiments, the strain is applied in increments as large as 0.05 – 0.07, meaning that the highest aspect ratio achieved prior to the first strain at which period doubling was found may significantly underestimate the true maximum aspect ratio. Hence, the measured

maximum aspect ratio is usually lower than the predicted maximum aspect ratio by FEM simulations. The error bars in the y-direction represents the standard deviation of the aspect ratio for a minimum of 4 waves. As shown in Figure 4-4(b), samples with a thickness contrast of 3 have the highest maximum aspect ratio. FEM simulations predict that the maximum aspect ratio is 0.62 while the highest observed aspect ratio in experiments is 0.67 ± 0.02. As the thickness contrast increases from 3, the maximum aspect ratio decreases. The decrease in the aspect ratio corresponds to the decrease in critical strain of post-wrinkling behaviors observed in Figure 4-3(b). Decreasing the critical strain limits the range where the wrinkle amplitude increases as the wrinkle wavelength decreases prior to localization.

4.4 Conclusion

Thickness contrast impacts the morphology, critical strain, and maximum achievable aspect ratio of wrinkles formed by a compressed bi-layer. When the thickness contrast is below 2, wrinkles transition into creases. Above a thickness contrast of 2, the secondary bifurcation is period doubling but the period doubling behavior is delayed. As the thickness contrast increases above 3, the critical strain for period doubling decreases. The decrease in the critical strain of the post-wrinkling mode leads to earlier strain localization which decreases the maximum aspect ratio. Using both FEM simulations and experiments, we fixed the modulus contrast at 50 and varied the thickness contrast from 1.5 to 10. We found the optimal condition where period doubling is delayed to the highest strain at a thickness contrast to be 3 where the wrinkles reach the highest aspect ratio of

approximately 0.65. In summary, we are able to show how thickness contrast affects post-wrinkling behavior. Understanding the effects on layered systems with small thickness contrast has implications in the development and knowledge of natural and synthetic multi-layered materials that have small thickness contrast such as flexible electronics and biological tissues[16–18].

4.5 References

[1] Z.Y. Huang, W. Hong, Z. Suo, Nonlinear analyses of wrinkles in a film bonded to a compliant substrate, J. Mech. Phys. Solids. 53 (2005) 2101–2118. doi:10.1016/j.jmps.2005.03.007.

[2] A. Schweikart, A. Horn, A. Böker, A. Fery, Controlled Wrinkling as a Novel Method for the Fabrication of Patterned Surfaces, (2010) 75–99. doi:10.1007/12.

[3] C.-C. Lin, F. Yang, S. Lee, Surface wrinkling of an elastic film: effect of residual surface stress., Langmuir. 24 (2008) 13627–31. doi:10.1021/la802517b.

[4] R. Zhao, T. Zhang, M. Diab, H. Gao, K.-S. Kim, The primary bilayer ruga-phase diagram I: Localizations in ruga evolution, Extrem. Mech. Lett. (2015). doi:10.1016/j.eml.2015.04.006.

[5] D. Chen, J. Yoon, D. Chandra, A.J. Crosby, R.C. Hayward, Stimuli-responsive buckling mechanics of polymer films, J. Polym. Sci. Part B Polym. Phys. 52 (2014) 1441–1461. doi:10.1002/polb.23590.

[6] C.M. Stafford, C. Harrison, K.L. Beers, A. Karim, E.J. Amis, M.R. VanLandingham, et al., A buckling-based metrology for measuring the elastic moduli of polymeric thin films., Nat. Mater. 3 (2004) 545–50. doi:10.1038/nmat1175.

[7] E. Cerda, L. Mahadevan, Geometry and Physics of Wrinkling, Phys. Rev. Lett. 90 (2003) 074302. doi:10.1103/PhysRevLett.90.074302.

[8] L. Pocivavsek, R. Dellsy, A. Kern, S. Johnson, B. Lin, K.Y.C. Lee, et al., Stress and fold localization in thin elastic membranes., Science. 320 (2008) 912–6. doi:10.1126/science.1154069.

[9] D. Holmes, A.J. Crosby, Draping Films: A Wrinkle to Fold Transition, Phys. Rev. Lett. 105 (2010) 1–4. doi:10.1103/PhysRevLett.105.038303.

[10] F. Brau, P. Damman, H. Diamant, T. a. Witten, Wrinkle to fold transition: influence of the substrate response, Soft Matter. 9 (2013) 8177. doi:10.1039/c3sm50655j.

[11] S. Cai, D. Breid, A.J. Crosby, Z. Suo, J.W. Hutchinson, Periodic patterns and energy states of buckled films on compliant substrates, J. Mech. Phys. Solids. 59 (2011) 1094–1114. doi:10.1016/j.jmps.2011.02.001.

[12] F. Brau, H. Vandeparre, A. Sabbah, C. Poulard, A. Boudaoud, P. Damman, Multiple-length-scale elastic instability mimics parametric resonance of nonlinear oscillators, Nat. Phys. 7 (2010) 56–60. doi:10.1038/nphys1806.

[13] J.-Y. Sun, S. Xia, M.-W. Moon, K.H. Oh, K.-S. Kim, Folding wrinkles of a thin stiff layer on a soft substrate, Proc. R. Soc. A Math. Phys. Eng. Sci. 468 (2011) 932–953. doi:10.1098/rspa.2011.0567.

[14] Q. Wang, X. Zhao, Phase Diagrams of Instabilities in Compressed Film-Substrate

Systems, J. Appl. Mech. 81 (2013). doi:10.1115/1.4025828.

[15] Y. Cao, J.W. Hutchinson, From wrinkles to creases in elastomers: the instability and imperfection-sensitivity of wrinkling, Proc. R. Soc. A Math. Phys. Eng. Sci. 468 (2011) 94–115. doi:10.1098/rspa.2011.0384.

[16] M.S. White, M. Kaltenbrunner, E.D. Głowacki, K. Gutnichenko, G. Kettlgruber, I. Graz, et al., Ultrathin, highly flexible and stretchable PLEDs, Nat. Photonics. 7 (2013) 811–816. doi:10.1038/nphoton.2013.188.

[17] D.-Y. Khang, J.A. Rogers, H.H. Lee, Mechanical Buckling: Mechanics, Metrology, and Stretchable Electronics, Adv. Funct. Mater. 19 (2009) 1526–1536. doi:10.1002/adfm.200801065.

[18] D.-Y. Khang, H. Jiang, Y. Huang, J.A. Rogers, A stretchable form of single-crystal silicon for high-performance electronics on rubber substrates., Science. 311 (2006) 208–12. doi:10.1126/science.1121401.

[19] S. Park, Y.S. Huh, H.G. Craighead, D. Erickson, A method for nanofluidic device prototyping using elastomeric collapse., Proc. Natl. Acad. Sci. U. S. A. 106 (2009) 15549–15554. doi:10.1073/pnas.0904004106.

[20] E. a. Wilder, S. Guo, S. Lin-Gibson, M.J. Fasolka, C.M. Stafford, Measuring the Modulus of Soft Polymer Networks via a Buckling-Based Metrology. Volume 39, Number 12, June 13, 2006, pp 4138−4143., Macromolecules. 39 (2006) 5956–5956. doi:10.1021/ma0615607.

[21] L. Jin, A. Auguste, R.C. Hayward, Z. Suo, Bifurcation diagrams for the formation of wrinkles or creases in soft bilayers, J. Appl. Mech. 82 (2015) 1–11. doi:10.1115/1.4030384.

[22] E. Hohlfeld, L. Mahadevan, Scale and nature of sulcification patterns, Phys. Rev. Lett. 109 (2012) 1–5. doi:10.1103/PhysRevLett.109.025701.

[23] Y. Cao, J.W. Hutchinson, Wrinkling Phenomena in Neo-Hookean Film/Substrate Bilayers, J. Appl. Mech. 79 (2012) 031019. doi:10.1115/1.4005960.

[24] A. Auguste, L. Jin, Z. Suo, R.C. Hayward, The role of substrate pre-stretch in post-wrinkling bifurcations., Soft Matter. 10 (2014) 6520–9. doi:10.1039/c4sm01038h.

[25] J. Zang, X. Zhao, Y. Cao, J.W. Hutchinson, Localized ridge wrinkling of stiff films on compliant substrates, J. Mech. Phys. Solids. 60 (2012) 1265–1279. doi:10.1016/j.jmps.2012.03.009.

CHAPTER 5

ACHIEVING HIGH ASPECT RATIO WRINKLES[§§][***]

5.1 Introduction

Wrinkles are formed with an initial amplitude and wavelength. As compressive strains are applied, the amplitude increases while the wavelength decreases, leading to an increase in the aspect ratio (defined as the amplitude, i.e., the vertical distance from peak to trough in a wrinkle, divided by the wrinkle wavelength). Recently, there has been a growing interest in high aspect ratio wrinkles as a route to dynamically tune surface morphology [1–4]. High aspect ratio wrinkles are beneficial to achieve large changes in surface properties such as optical and wetting characteristics [5–8], and also improve the strecthability that can be achieved in flexible electronics[9–11]. For example, by increasing the aspect ratio from 0.3 to 0.6, the stretchability of flexible electronic devices could improve from 20% to 40% [3].

Despite these advantages of high aspect ratio wrinkles, the aspect ratio in most studies have been limited to approximately 0.35 or below. This limitation is set by the transition to different post-wrinkling modes such as creasing, period doubling, or folding. Chen et al. [3] summarize the aspect ratios Ω reported in 38 prior publications, with values all below 0.35, as reproduced in Figure 5-1. Additionally, they report achieving an aspect ratio of 0.6 by highly pre-stretching the substrate, indicated by the star in Figure

[§§] A. Auguste, J. Yang, L. Jin, D. Chen, Z. Suo, R.C. Hayward, (2016). In preparation.
[***] In collaboration with Aude Duhamel

5-1. Cao et al. [2] was able to achieve an even higher aspect ratio (1.45); however, the substrate had to be pre-stretched to λ_0 = (deformed length/undeformed length) = 3.5 which eliminates the use of certain materials that do not have high elongation values. For example, Sylgard 184 polydimethylsiloxane (PDMS), a commonly used commercially available elastomer in the fabrication of flexible electronics [11,12], only can be stretched to λ_0 = 2.4. Thus, it is necessary to develop a method, where aspect ratios greater than 0.6 can be created without the use of a highly pre-stretched substrate.

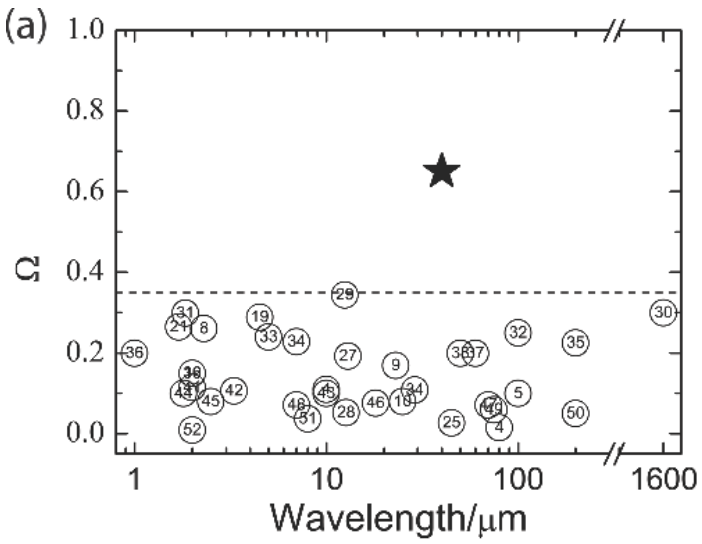

Figure 5-1. Summary of reported wrinkle aspect ratios in 38 published research articles. The star represents the work by Chen et al. Reprinted with permission from ref [3].

The goal of this chapter is to apply the understanding gained in the previous three chapters on substrate pre-stretch, modulus contrast, and thickness contrast to achieve high aspect ratio wrinkles. We are able to develop two strategies to create these surfaces with high aspect ratios. The first strategy is based on work in Chapters 2 and 4. We

observed that pre-stretching the substrate to 1.4 and decreasing the thickness contrast will delay period-doubling; hence, to achieve high aspect ratio wrinkles, we combine both parameters and examine the evolution of the wrinkle pattern and the onset of the secondary bifurcation. In Chapter 3, we saw that modulus contrast effects post-wrinkling behaviors; therefore, the second approach is to vary the modulus contrast while keeping the thickness contrast constant at 3 and investigate the effects on obtaining high aspect ratio wrinkles.

5.2 Experimental Method

5.2.1 Substrate pre-stretch with low thickness contrast

The experimental procedure is similar to the procedure in Chapter 2. A pink-colored mounting layer (Elastosil M4601, Wacker Chemical Company) with a thickness of 1 mm is uniaxially pre-stretched on a stretcher. To vary the thickness of the substrate below 100 μm, uncured 50:1 (base : crosslinker) PDMS (Sylgard 184, Dow Corning) is spin coated onto a trimethylchlorosiloxane treated glass slide and then placed in an oven at 120°C for 10 min. The substrate (shear modulus 12.5 kPa) is attached to the pre-stretched mounting layer and the two layers are cured at 40 °C for 16 h. To vary the thickness of the substrate above 100 μm, uncured PDMS 50:1 is poured into a Petri dish and pre-cured at 40 °C for 16 h. The pre-cured substrate is attached to the pre-stretched mounting layer with a thin layer of uncured PDMS 30:1. The substrate is attached to the mounting layer is then placed in an oven at 40 °C for 16 h to bond the layers and then allowed to cool to

room temperature for over 30 min. The bi-layer is then stretched to a new length L, placing the substrate under a pre-stretch $\lambda_0=L/L_0$. The substrate is placed in a UV/O_3 cleaner for 25 minutes to convert the surface of the PDMS substrate into a stiffer oxide layer. The film has an effective thickness of 3-8 μm and a shear modulus of 620 kPa – 3.8 MPa based on a thick substrate with no pre-stretch.

5.2.2 High modulus contrast and low thickness contrast

The experimental procedure is similar to the procedure in Chapter 3 and 4. Uniform uniaxial compression is applied to the bi-layer structures through a pre-stretched mounting layer underneath the bi-layers. A transparent silica reinforced vinyl-terminated polydimethylsiloxane (PDMS) mounting layer (Elastosil M4600, Wacker Chemical Company) is uniaxially pre-stretched on a stretcher. The thin film is created by using uncured 5:1, 10:1 or 20:1 PDMS that is spin coated onto a trimethylchlorosiloxane treated glass slide and then placed in the oven at 120 °C for 120 min resulting in a modulus of 2.6 ± 0.8 MPa, 1.6 ± 0.5 MPa, or 0.75 ± 0.08 MPa, respectively . Changing the spin speed of the spin-coater provides access to a wide range of thicknesses for the substrate and thin film. Uncured 40:1 PDMS is coated on the PDMS coated glass slide, attached to the mounting layer and placed in an oven at 70 °C for 1 h to bond and cure the PDMS layers (shear modulus of 1 kPa)[3].

5.3 Substrate pre-stretch with low thickness contrast

Both pre-tension in the substrate and modest thickness contrast are ways to delay period doubling. Thus, we undertook a fundamental study of the combined effects of pre-stretch and thickness contrast as a tactic to achieve high aspect ratio wrinkles. In order to calculate the aspect ratio, optical profilometry was used to measure the amplitude and wavelength of the UV/ozone treated PDMS surface. Controlling the film thickness and modulus with films made by UV/ozone is difficult [13], however, we were able to calculate the effective thickness and modulus by using the wrinkling equations (Equations 1.1 and 1.3). Unfortunately, the film thickness and modulus mismatch cannot be calculated when the thickness contrast is too low or when the substrate thickness is lower than 200 μm, since the equations are not valid for sample with low thickness contrast. Thus, we cannot unambiguously determine the thickness ratio. Instead, we plot our results as a function of substrate thickness, assuming that the film thickness is nearly constant between the different samples. For this series of samples, the substrate thickness varies between 16 μm and 600 μm. Figure 5-2 (a) and (b) demonstrate clean period doubling, while Figure 5-2 (c) and (d) show chaotic behavior. A pure period doubling behavior is defined as having a profile with a regular pattern of a deep trough followed by a shallow one. A 'chaotic' behavior does not have a regular pattern in an area. Defects can affect the pattern of wrinkles and the post-wrinkling patterns. To mitigate the effect of defects on the surface, the line profiles were taken far from any visible defects, and after increasing compression, the same position on the surface was characterized. As can be seen in Figure 5-2, the substrate thickness changes the surface morphology. In the thinner substrate,

86 μm, we see pure period doubling occurring at a strain of 0.217 while in the thicker substrate, 418 μm, the 'chaotic' morphology appears at a strain of 0.267.

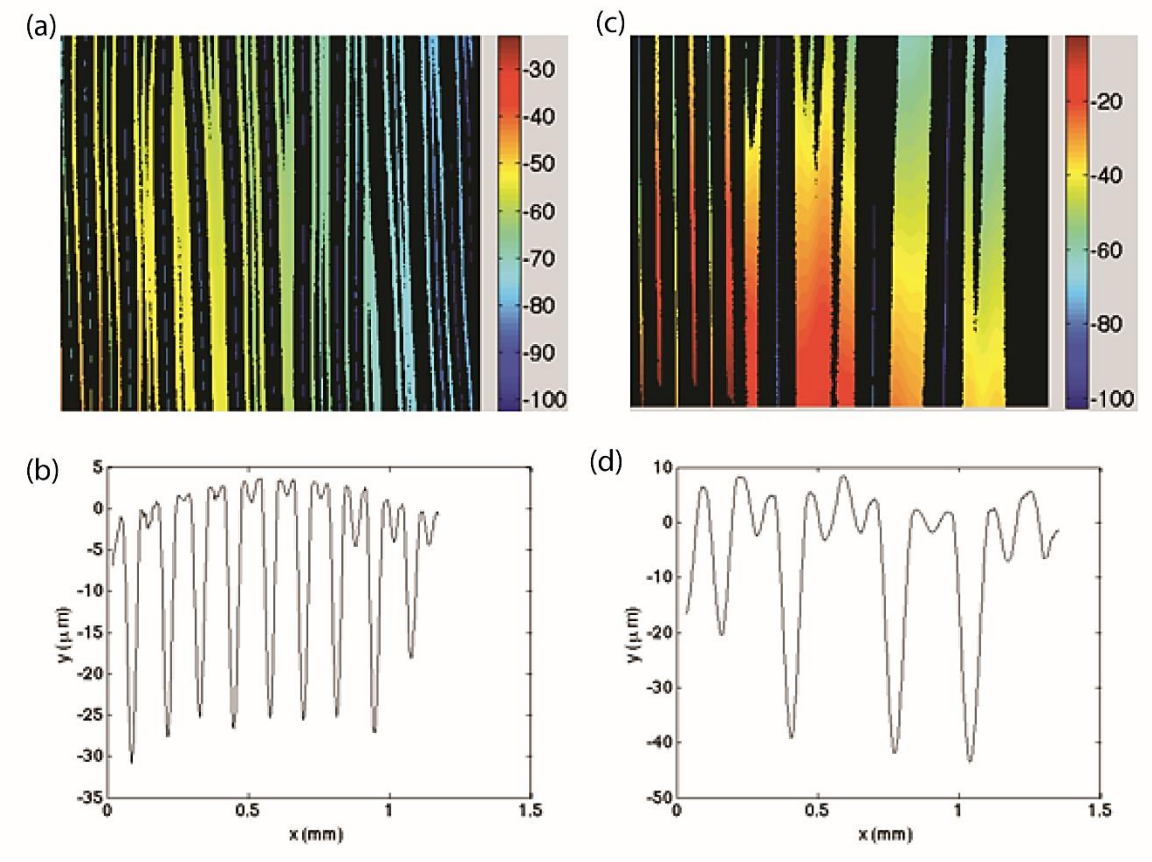

Figure 5-2. Surface profiles and corresponding one-dimensional profiles for samples pre-compressed at 0.7 and with (a and b) substrate thickness of 86 μm and film strain 0.217 and (c and d) with substrate thickness of 418 μm and film strain 0.267

For different substrate thicknesses, we have determined the value of the post-wrinkling bifurcation strain and the post-wrinkling behavior. Figure 5-3 (a) shows the critical strain of post-wrinkling as a function of substrate thickness. Reducing the substrate thickness delays the post-wrinkling bifurcation strain and diminishes the effects

of pre-compressing the substrate. Moreover, samples with substrate thickness below 100 μm do not exhibit any 'chaotic' behavior whereas samples with substrate thickness above 100 μm exhibit 'chaotic' behavior.

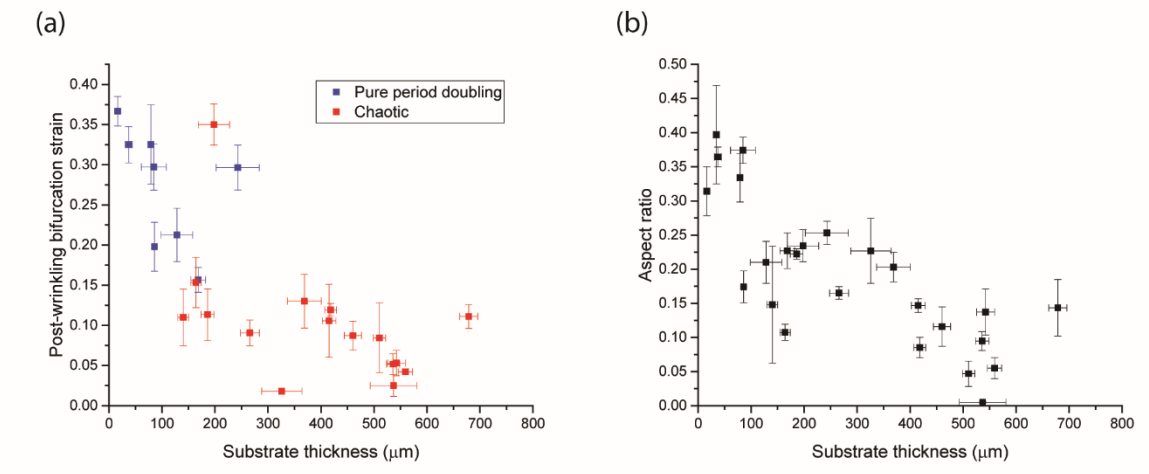

Figure 5-3. The effect of pre-compression ($\lambda_0 = 0.7$) in the substrate on (a) the post-wrinkling bifurcation strain and (b) aspect ratio as a function of substrate thickness

As has been shown in Chapter 4, decreasing substrate thickness delays the post-wrinkling bifurcation which allows wrinkles to grow. Thus, the aspect ratio is expected to increase as the thickness is decreasing. Figure 5-3 (b) shows the dependence of the aspect ratio on the substrate thickness. The aspect ratio increases as the substrate thickness is increases, especially for thin samples. By decreasing the substrate thickness from 500 μm to 50 μm, the aspect ratio increases from 0.10 ± 0.05 to 0.40 ± 0.05.

In Chapter 2, we have computed the energies of the subharmonics modes in bi-layers pre-stretched to different extents. For highly pre-tensioned substrates, no 'chaotic' behavior is expected to be observed as the period-doubled state is energetically preferred

compared to period tripling at λ= 1.4, while the energy difference between the two modes is minimal for pre-compressed bi-layers at 0.7.

To study the influence of substrate thickness on the post-wrinkling critical strain under pre-tension, samples with substrate thickness between 200 μm and 1100 μm are pre-stretched to λ=1.4. The post-wrinkling bifurcation strain seems to be independent of the substrate thickness in this range as shown in Figure 5-4 (a). As expected, 'chaotic' behavior was not observed for any of the samples. Without the large shift in critical strains, the aspect ratio remains nearly constant for the pre-tensed samples as plotted in Figure 5-4(b).

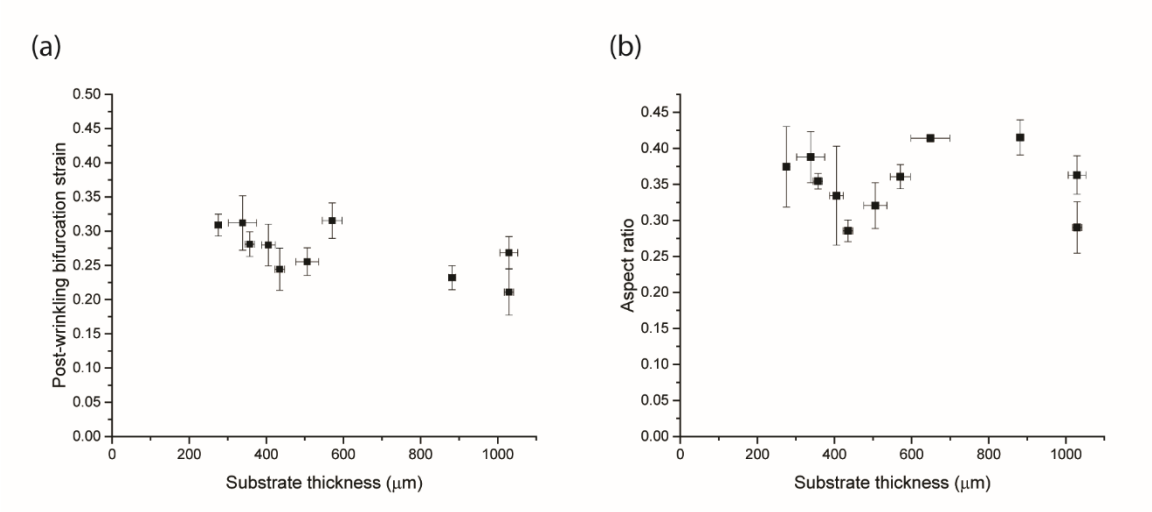

Figure 5-4. The effect of pre-tension (λ_0 = 1.4) in the substrate on (a) the post-wrinkling bifurcation strain and (b) aspect ratio as a function of substrate thickness

Figure 5-5 summarizes the effect of substrate thickness on the post-wrinkling critical strain of pre-stretched samples. A thin substrate suppresses localizations and

behaves as a highly pre-stretched sample. A thick highly pre-tensioned substrate has a post-wrinkling critical strain around 0.25 while a thin pre-compressed substrate has an even higher critical strain of about 0.37. Therefore, for pre-compressed thin substrates, the influence of pre-stretching is reduced while the effects of substrate thickness dominate.

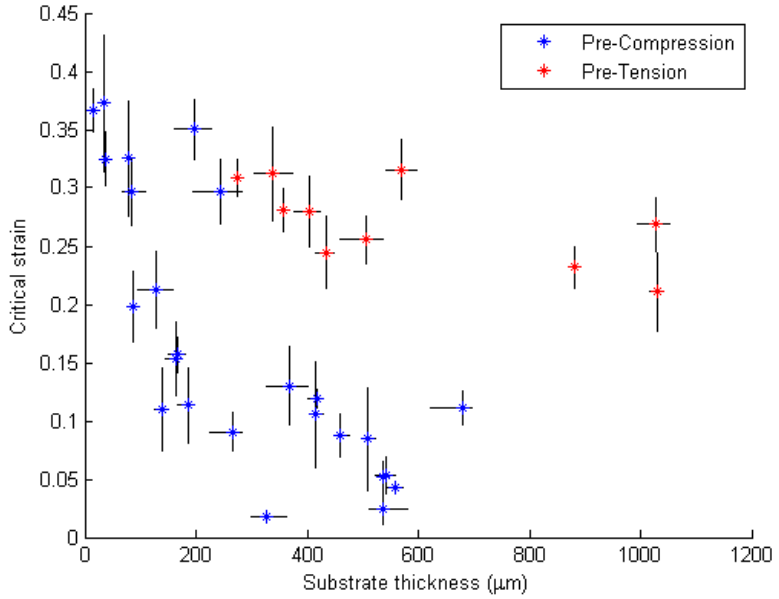

Figure 5-5. The post-wrinkling bifurcation strain dependence on substrate thickness for pre-compressed and pre-tensed bi-layers

5.4 High modulus contrast and low thickness contrast

The previous section demonstrated that decreasing the substrate thickness in a pre-stretched substrate can increase the aspect ratio of the sample to around 0.45 by delaying the post-wrinkling behavior. As an alternative strategy, the use of a bi-layer with a large variance in modulus contrast, to induce wrinkling at low strains, coupled with a

small thickness contrast, to delay the onset of post-wrinkling modes, may provide a more effective route to high aspect ratio wrinkles.

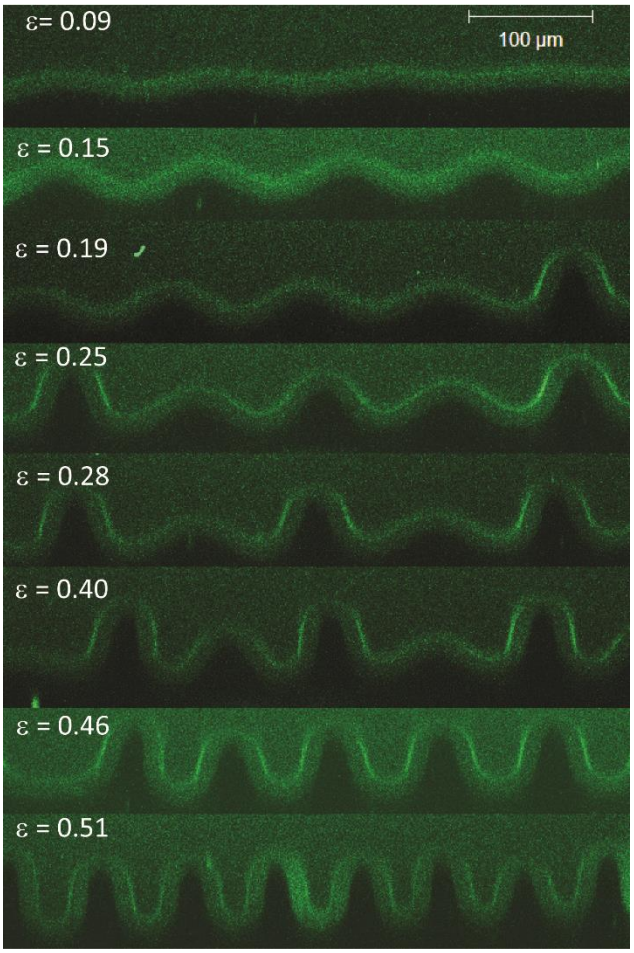

Figure 5-6. Confocal cross-sectional view of the morphological change of a high modulus contrast sample (G_f/G_s = ~870) with a small thickness contrast (~2.5)

Figure 5-6 shows the evolution of the wrinkle pattern for a sample with a modulus contrast of 870 and a thickness contrast of 2.5. Wrinkles undergo several transitions. First, the wrinkles grow in amplitude until a ridge is formed at a strain of 0.19. At a strain of 0.25, more ridges appear with a spacing of two times the wrinkle wavelength. As compression increases, the wrinkles between the ridges first relax as the ridge grows, but

then eventually grow in amplitude again, ultimately yielding uniform wrinkles with a high aspect ratio of 0.81 ± 0.05 at a strain of 0.51. Due to the limited travel of the stretching stage, we were unable to characterize the surface profile for samples compressed to strains above 0.51, but we expect that the aspect ratio will likely be increased above 0.81 with further compression.

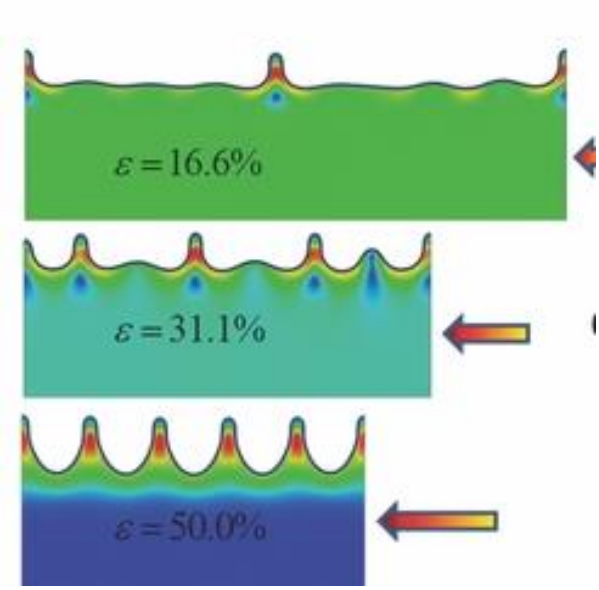

Figure 5-7. Finite element analysis of the evolution of localized ridges with the relaxation of uniaxially pre-strained substrate with a modulus ratio of 1000 and pre-strain ε_{pre1} = 100%. Reprinted from Ref. [2].

The same behavior displayed in Figure 5-6 has also been reported for samples with substrate pre-stretch [2,14], as shown in Figure 5-7. Cao and co-workers [2] conducted finite-element analysis on a bi-layer with modulus contrast =1000 and substrate pre-stretch of λ= 2.0. The colors in the figure represent the maximum in-plane strain. They observed the formation of ridges, at a strain of 0.166, followed by the “period doubling”

of ridges which ultimately led to uniform structures with high aspect ratios. For this system, they predicted an aspect ratio of 0.7.

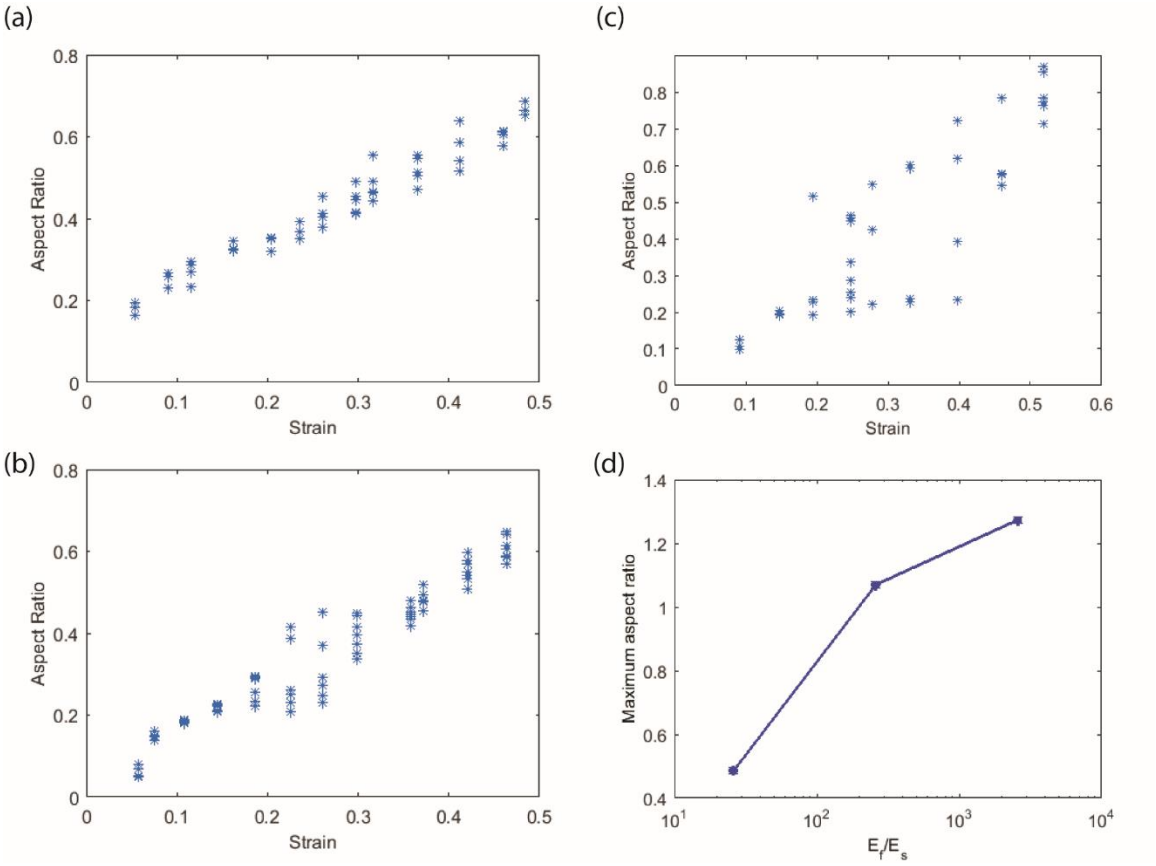

Figure 5-8. Experimental result measuring the aspect ratio versus strain for bi-layers with a thickness contrast 3.0 ±0.5 and a modulus contrast of (a) 250; (b) 500; and (c) 870; (d) FEM simulation of the maximum aspect ratio with respect to modulus contrast

To examine the effect of modulus contrast on the maximum achievable aspect ratio for bi-layers with modest thickness contrast, we plot bifurcation curves of wrinkle amplitude with respect to strain for three samples with different modulus contrast in Figure 5-8. The thickness contrast for each sample in Figure 5-8 (a-c) is 3.0 ± 0.5. The aspect ratio of at least four waves was plotted for each strain; therefore, the more

uniform the wrinkles are, the less scatter is observed in the plots. As we increase the modulus contrast, the scatter in aspect ratio increases. In Figure 5-8 (b), the aspect ratio is uniform until a strain of 0.19 where ridges begin to form, leading to a bifurcation into high- and low-amplitude features. However, further compression causes the sample to evolve back into a state of uniform wrinkles by a strain of 0.35, corresponding to a collapse of the two branches on the bifurcation diagram in Figure 5-8(b) back to a single curve. Increasing the modulus contrast increases the range over which ridges are present, as seen in Figure 5-8(c) (which corresponds to the sample in Figure 5-6). Unfortunately, measuring the maximum aspect ratio is limited by characterization methods and the ability to achieve high strains (> 0.55). Therefore, we use FEM simulations to plot the maximum aspect ratio with respect to modulus contrast (Figure 5-8d). It is expected that with more compression, the highest modulus contrast bi-layer (Figure 5-8c) would be able to achieve an aspect ratio close to 1.2 as predicted by FEM simulations. Overall, as the modulus contrast increases, the maximum aspect ratio also increases.

5.5 Conclusion

Combining the knowledge gained in previous chapters about substrate pre-stretch, modulus contrast and thickness contrast effects on post-wrinkling behaviors, we have proposed two approaches to increase the aspect ratio to values greater than the average aspect ratio reported in many publications. The first is to pre-stretch a thin substrate. Using substrates pre-compressed to λ=0.7, we observed the substrate thickness affects the type of post-wrinkling mode that is present: for thin substrate, only

pure period doubling is seen whereas for thick substrate, chaotic behavior is observed. We can only conclude that the 'chaotic' behavior is delayed if not eliminated by decreasing the substrate thickness in pre-compressed bi-layers at λ=0.7. Moreover, decreasing substrate thickness in pre-stretched bi-layers delays post-wrinkling bifurcations to greater compressive strains. For pre-compressed bi-layers, there is a rapid increase of aspect ratio to 0.45; however, to achieve even higher aspect ratios, reducing the thickness contrast and increasing the modulus contrast is key. The second strategy, increasing the modulus contrast while keeping the thickness contrast at a value of 3, should yield aspect ratios larger than 1.3, as predicted by finite element simulations. Experimentally, we can achieve an aspect ratio of greater than 0.85 with strains less than 0.6. Being able to create uniform high aspect ratio wrinkles at low strains increases the range of materials used in the fabrication of applications such as flexible electronics.

5.6 References

[1] S.F. Ahmed, G.-H. Rho, K.-R. Lee, A. Vaziri, M.-W. Moon, High aspect ratio wrinkles on a soft polymer, Soft Matter. 6 (2010) 5709. doi:10.1039/c0sm00386g.

[2] C. Cao, H.F. Chan, J. Zang, K.W. Leong, X. Zhao, Harnessing Localized Ridges for High-Aspect-Ratio Hierarchical Patterns with Dynamic Tunability and Multifunctionality., Adv. Mater. (2013). doi:10.1002/adma.201304589.

[3] Y.-C. Chen, A.J. Crosby, High Aspect Ratio Wrinkles via Substrate Prestretch, Adv. Mater. (2014) n/a–n/a. doi:10.1002/adma.201401444.

[4] J.G. Gaillard, C. Hendrus, B.D. Vogt, Tunable wrinkle and crease surface morphologies from photoinitiated polymerization of furfuryl alcohol., Langmuir. 29 (2013) 15083–9. doi:10.1021/la4038167.

[5] P.-C. Lin, S. Yang, Mechanically switchable wetting on wrinkled elastomers with dual-scale roughness, Soft Matter. 5 (2009) 1011. doi:10.1039/b814145b.

[6] S.G. Lee, D.Y. Lee, H.S. Lim, D.H. Lee, S. Lee, K. Cho, Switchable transparency and wetting of elastomeric smart windows., Adv. Mater. 22 (2010) 5013–7. doi:10.1002/adma.201002320.

[7] J.Y. Chung, J.P. Youngblood, C.M. Stafford, Anisotropic wetting on tunable micro-wrinkled surfaces, Soft Matter. 3 (2007) 1163. doi:10.1039/b705112c.

[8] E. Lee, M. Zhang, Y. Cho, Y. Cui, J. Van der Spiegel, N. Engheta, et al., Tilted Pillars on Wrinkled Elastomers as a Reversibly Tunable Optical Window., Adv. Mater. (2014) 1–7. doi:10.1002/adma.201400711.

[9] M.S. White, M. Kaltenbrunner, E.D. Głowacki, K. Gutnichenko, G. Kettlgruber, I. Graz, et al., Ultrathin, highly flexible and stretchable PLEDs, Nat. Photonics. 7 (2013) 811–816. doi:10.1038/nphoton.2013.188.

[10] D.-Y. Khang, H. Jiang, Y. Huang, J.A. Rogers, A stretchable form of single-crystal silicon for high-performance electronics on rubber substrates., Science. 311 (2006) 208–12. doi:10.1126/science.1121401.

[11] J.A. Rogers, T. Someya, Y. Huang, Materials and mechanics for stretchable electronics., Science. 327 (2010) 1603–7. doi:10.1126/science.1182383.

[12] D. Qin, Y. Xia, G.M. Whitesides, Soft lithography for micro- and nanoscale patterning., Nat. Protoc. 5 (2010) 491–502. doi:10.1038/nprot.2009.234.

[13] A. Auguste, L. Jin, Z. Suo, R.C. Hayward, The role of substrate pre-stretch in post-wrinkling bifurcations., Soft Matter. 10 (2014) 6520–9. doi:10.1039/c4sm01038h.

[14] A. Takei, L. Jin, J.W. Hutchinson, H. Fujita, Ridge Localizations and Networks in Thin Films Compressed by the Incremental Release of a Large Equi-biaxial Pre-

stretch in the Substrate., Adv. Mater. (2014) 1–7. doi:10.1002/adma.201306162.

CHAPTER 6

CONCLUSION

This thesis described an investigation of the initiation and evolution of various post-wrinkling bifurcations in layered elastic polymers. By systematically varying the geometrical and mechanical parameters, in particular the substrate pre-stretch, and the modulus and thickness contrast between the film and substrate, we demonstrated how to control the onset and evolution of the wrinkle to crease or wrinkle to fold transitions. Understanding these transitions will help not only to advance fundamental understanding of phenomena in biology and flexible electronics, but also to enable fabrication of advanced materials with dynamic surfaces for tunable optical and wetting properties.

Substrate pre-stretch is a common method used to study wrinkling behaviors in bi-layers. We developed a method to study the effect of substrate pre-stretch on post-wrinkling behaviors by using a multi-layer system that consists of a stiff silicon oxide film formed on a soft substrate that has been pre-stretched by a mounting layer. We discovered that adding pre-tension to the substrate leads to a delay in the appearance of post-wrinkling modes. Likewise, adding pre-compression not only causes a decrease in the critical strain for the appearance of post-wrinkling modes but also changes the evolution of the post-wrinkling structures, and incites a new 'chaotic' surface morphology. This new morphology is the result of the system losing preference for a particular post-wrinkling mode, highlighting the importance of substrate elasticity in determining the nature of post-wrinkling bifurcations.

Knowing that pre-stretch affects the onset and evolution of post-wrinkling modes, we studied the next two parameters, modulus and thickness contrast, under conditions with no substrate pre-stretch. We found that the modulus contrast between the film and substrate determines which surface instability mode occurs first as well as shifts the critical strain for the primary and secondary bifurcations. Below a modulus ratio of 1.65, supercritical or subcritical creases form first. Slightly above 1.65, either wrinkles or creases can form first, depending on the presence of surface defects. However, if wrinkles occur first, a subcritical crease forms soon after, prompting us to explore secondary bifurcations. At modest modulus ratios, we examined two types of secondary bifurcations, type 1 and type 2. For a type 1 secondary bifurcation, wrinkles form first, but then subcritical creases channel in and relax the wrinkles. In a type 2 bifurcation, which occurs at a higher modulus contrast than type 1, wrinkles transition to supercritical creases and are preceded by period doubling. Creases form in the deepest troughs of the period doubled state, leading to the patterning of creases without the use of substrate patterns or lithography.

A modest thickness contrast between the substrate and film also affects post-wrinkling behaviors. We found that creases will form below a thickness contrast of 2 due to the presence of the stiff mounting layer. However, in this range, the system is no longer a bi-layer but a tri-layer system; therefore, we focused on systems above a thickness contrast of 3. As the thickness contrast decreases to the limit of 3, the critical strain for post-wrinkling behaviors increases while the onset of wrinkles remains relatively unchanged. The delay in post-wrinkling behavior leads to wrinkles with high aspect ratios

of around 0.6. Wrinkles with high aspect ratios can be used to improve the range of surface properties such as wetting, and stretchability in flexible electronic.

Using the information about substrate pre-stretch, modest modulus contrast, and thickness, we created high aspect ratio wrinkles. When substrate pre-compression is combined with modest thickness contrast, we can eliminate the chaotic behavior observed in Chapter 2. Even though substrate pre-tension with modest thickness contrast delays post-wrinkling behaviors, these behaviors still occur at relatively low strains, 0.24, and therefore do not create wrinkles with very high aspect ratios. However, if the modulus contrast is high and the thickness contrast is low, ridges are formed which then turn into uniform wrinkles with an aspect ratio exceeding 1.3 in simulations. This system allows for the formation of ridges and ultimately high aspect ratio wrinkles without the use of a highly pre-stretched substrate.

The new understanding of post-wrinkling behaviors established here can shed light on patterns formed by biological growth processes, and lead to new methods for patterning high aspect ratio surface features without lithographic processes. However, our studies have been limited to post-wrinkling behaviors that occur below 60% compressive strain. The ability to examine systems under higher compressive strains is expected to allow access to additional post-wrinkling behaviors, such as the wrinkle to crease transition with period quadrupling preceding creases. Another limitation of the experimental set-up has been the manual addition of compression, which restricted our experiments to low strain rates. In the future, the use of a system that can control loading

rates would allow additional questions about post-wrinkling behaviors to be addressed. For example, increasing the loading rate can increase the defect density in the wrinkle pattern, which will also impact the post-wrinkling behavior. Finally, this thesis only considered elastic effects in layered polymers; however, introducing viscoelastic character to the layers could yield additional rate-dependent effects on post-wrinkling behaviors and possibly qualitatively new types of instability modes.

The work presented in this thesis systematically varies the mechanical and geometrical properties of an elastic bi-layer in order to understand of how each variable (substrate pre-stretch, thickness contrast and modulus contrast) affects post-wrinkling behaviors in uni-axially compressed systems. There are still interesting questions which remain for more complex systems where compression occurs in a non-planar layered systems. In biology, for example, several types of biological tissues, such as the brain and esophagus, contain a type of curvature which affects the strain state within the layers as the tissues form, grow or expand. Hence, understanding the effects of modest thickness contrast and modulus contrast in systems with varying degrees of curvature is important.

APPENDIX

MEASURING WRINKLE PROPERTIES

This thesis examined the wrinkle amplitudes, wavelengths, and critical strains as they are affected by substrate pre-stretch, modulus contrast, and thickness contrast. The purpose of this appendix describes the methods used to determine (1) amplitude, (2) wavelength, and (3) critical strain for post-wrinkling behaviors.

To determine the amplitude, optical profilometry and/or confocal microscopy is used. Both techniques generate a cross-sectional profile. For optical profilometry, a measurement is taken at each strain measured. Using the MetroPro Software from Zygo, a surface profile and a line profile is displayed in Fig. S1. Due to the curvature of a wrinkled surface, only the peaks and troughs are displayed.

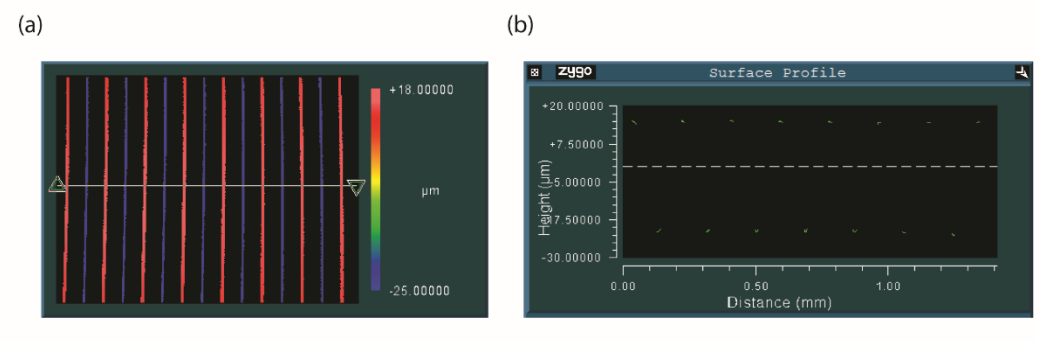

Figure S1. Surface profile (a) and line profile (b) of a wrinkled surface using optical profilometry

Using Fig. S1(b), we are able to determine the amplitude and wrinkle wavelength. Fig. S2 shows how the amplitude and wavelength is defined in each sample. Half the height difference between the peak and the neighboring trough is defined as the amplitude, A. In order to eliminate the effects of a sloped surface, $A = (A_1+A_2)/2$. The

distance between A1 and A2 is the wrinkle wavelength for that specific A. Using this method for Fig.S2, we are able to obtain six amplitudes and their corresponding wavelength.

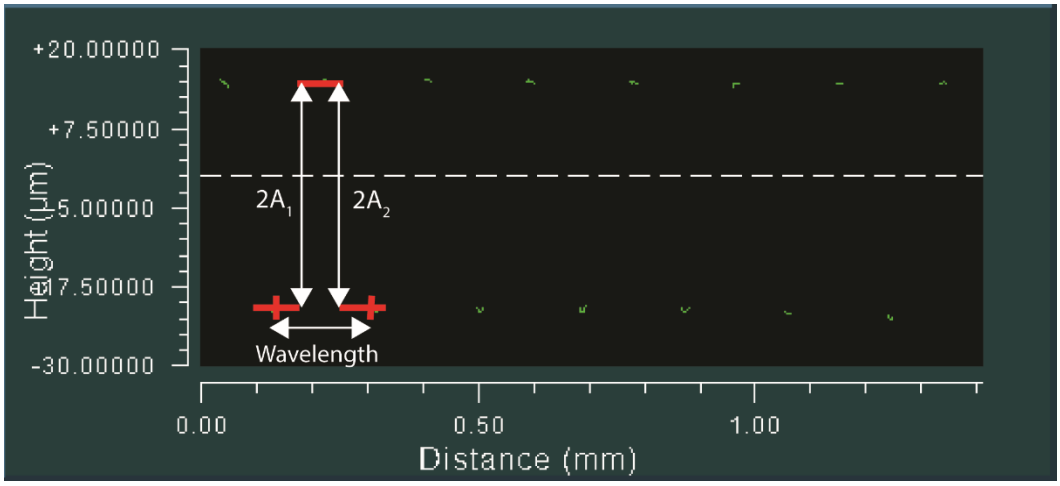

Figure S2. The measurement of amplitude and wavelength using the line profile from the MetroPro software.

The raw data from the line profile is uploaded to MATLAB and a spline is used to fill in the missing segments of the surface profile.

```
l=x(1)
L=x(length(x))
xx = l:.002:L;
yy = spline(x,y,xx);
plot(xx,yy)
```

The MATLAB code above is used to create the graph in Fig. S3 from the data in Fig. S2.

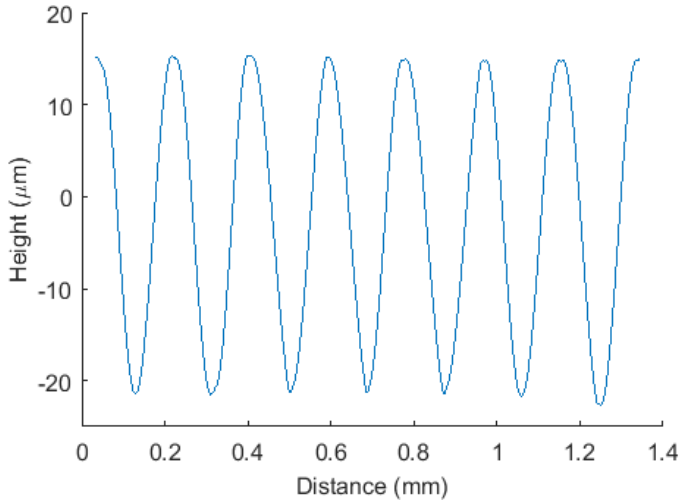

Figure S3. Using the data from Figure S2, a spline plot was created using a MATLAB code

In confocal microscopy, the complete cross-sectional profile is given so there is no need to use the spline MATLAB code. Instead, using the Zeiss LSM Image Browser, the distance between the peaks and troughs of the top surface is measured and the amplitude is half of those values. Figure S4 shows the measured values of 2A and the wavelength using the software. In this example, the amplitude for one wrinkle is A = [(34.84/2)+(32.85/2)]/2. In order to measure more amplitudes, multiple frames are taken.

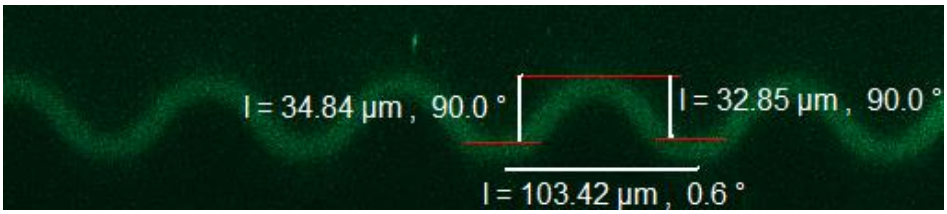

Figure S4. The measurement of amplitude and wavelength using the line profile from the MetroPro software.

The amplitudes and wavelengths are recorded for each strain measured. Then the amplitude is plotted versus strain to determine the critical strain for the post-wrinkling bifurcation.

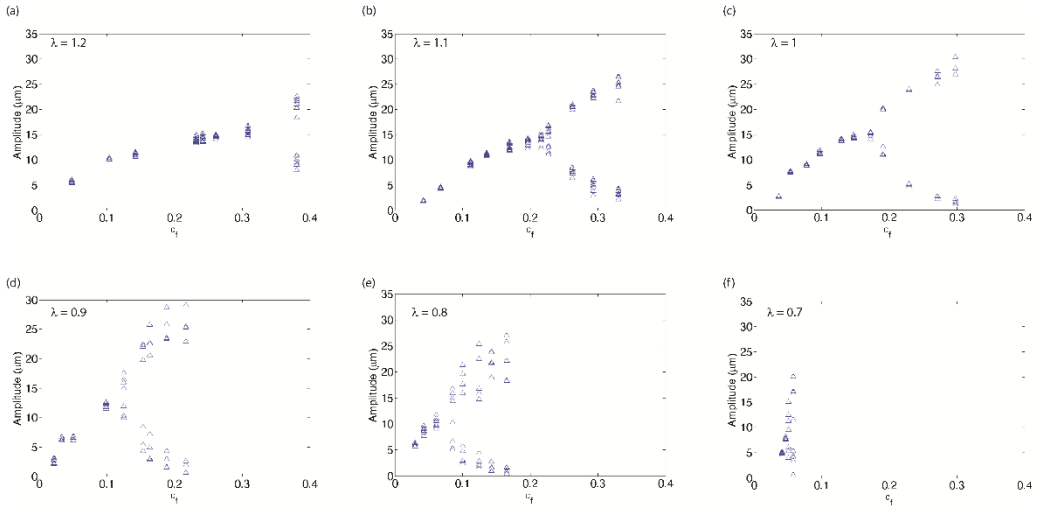

Figure S5. An example of bifurcation curves with the wrinkle amplitude plotted as a function of film strain for a substrate pre-stretched to λ_0 = (a) 1.2, (b) 1.1, (c) 1.0, (d) 0.9, (e) 0.8 and (f) 0.7.

When the amplitudes are uniform, they appear as a single point on the plot. However, if the amplitudes are not uniform, each individual point become visible. Since bifurcations lead to a spread of amplitudes, the standard deviation of the amplitudes at a particular strain is taken to determine the critical strain for post-wrinkling bifurcation.

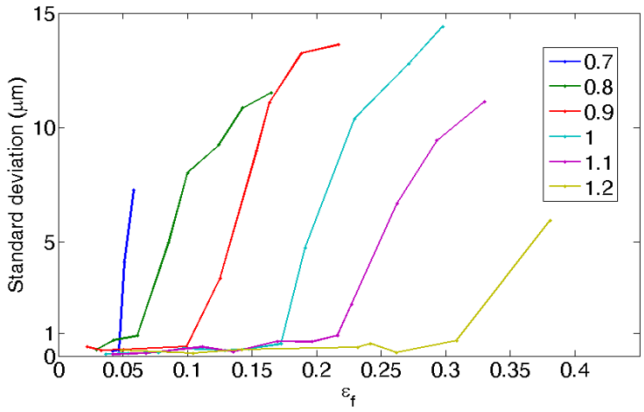

Figure S6. Using the experimental data from Figure S5, the standard deviations of the amplitudes are plotted as a function of film strain.

In the wrinkle regime of the bifurcation curves, the standard deviation is less than 1 μm, but when the amplitudes bifurcate the standard deviation becomes greater than 1 μm. The critical strain for the post-wrinkling bifurcation is reported as the average of two strains: (1) last strain measured with a standard deviation below 1 μm and (2) first strain measured with a standard deviation above 1 μm. The lower bound of the error bar is strain (1) while the upper bound is strain (2).

In the projects where aspect ratio (amplitude/wavelength) is calculated, the same characterizations and methods are used except the amplitudes are multiplied by two. This is done to compare the aspect ratios with literature values since literature concerning high aspect ratio wrinkles define the amplitude as the distance between the peak and the trough.

BIBLIOGRAPHY

[1] S. Yang, K. Khare, P.-C. Lin, Harnessing Surface Wrinkle Patterns in Soft Matter, Adv. Funct. Mater. 20 (2010) 2550–2564. doi:10.1002/adfm.201000034.

[2] J.A. Rogers, T. Someya, Y. Huang, Materials and mechanics for stretchable electronics., Science. 327 (2010) 1603–7. doi:10.1126/science.1182383.

[3] D.-Y. Khang, H. Jiang, Y. Huang, J.A. Rogers, A stretchable form of single-crystal silicon for high-performance electronics on rubber substrates., Science. 311 (2006) 208–12. doi:10.1126/science.1121401.

[4] B. Xu, D. Chen, R.C. Hayward, Mechanically Gated Electrical Switches by Creasing of Patterned Metal/Elastomer Bilayer Films, Adv. Mater. 26 (2014) 4381–4385. doi:10.1002/adma.201400992.

[5] J.B. Kim, P. Kim, N.C. Pegard, S.J. Oh, C.R. Kagan, J.W. Fleischer, et al., Wrinkles and deep folds as photonic structures in photovoltaics, Nat. Photonics. 6 (2012) 327. doi:10.1038/NPHOTON.2012.70.

[6] J. Kim, J. Yoon, R.C. Hayward, Dynamic display of biomolecular patterns through an elastic creasing instability of stimuli-responsive hydrogels., Nat. Mater. 9 (2010) 159–64. doi:10.1038/nmat2606.

[7] M. Arifuzzaman, Z.L. Wu, R. Takahashi, T. Kurokawa, T. Nakajima, J.P. Gong, Geometric and edge effects on swelling-induced ordered structure formation in polyelectrolyte hydrogels, Macromolecules. 46 (2013) 9083–9090. doi:10.1021/ma401773w.

[8] A. Schweikart, A. Fery, Controlled wrinkling as a novel method for the fabrication of patterned surfaces, (2009) 249–263. doi:10.1007/s00604-009-0153-3.

[9] Q. Li, X. Han, J. Hou, J. Yin, S. Jiang, C. Lu, Patterning Poly(dimethylsiloxane) Microspheres via Combination of Oxygen Plasma Exposure and Solvent Treatment, J. Phys. Chem. B. 119 (2015) 13450–13461. doi:10.1021/acs.jpcb.5b07208.

[10] S.G. Lee, D.Y. Lee, H.S. Lim, D.H. Lee, S. Lee, K. Cho, Switchable transparency and wetting of elastomeric smart windows., Adv. Mater. 22 (2010) 5013–7. doi:10.1002/adma.201002320.

[11] P. Görrn, M. Lehnhardt, W. Kowalsky, T. Riedl, S. Wagner, Elastically tunable self-organized organic lasers., Adv. Mater. 23 (2011) 869–72. doi:10.1002/adma.201003108.

[12] C. Harrison, C.M. Stafford, W. Zhang, A. Karim, Sinusoidal phase grating created by a tunably buckled surface, Appl. Phys. Lett. 85 (2004) 4016. doi:10.1063/1.1809281.

[13] E. Lee, M. Zhang, Y. Cho, Y. Cui, J. Van der Spiegel, N. Engheta, et al., Tilted pillars on wrinkled elastomers as a reversibly tunable optical window., Adv. Mater. 26 (2014) 4127–33. doi:10.1002/adma.201400711.

[14] P.-C. Lin, S. Vajpayee, A. Jagota, C.-Y. Hui, S. Yang, Mechanically tunable dry adhesive from wrinkled elastomers, Soft Matter. 4 (2008) 1830. doi:10.1039/b802848f.

[15] E.P. Chan, E.J. Smith, R.C. Hayward, A.J. Crosby, Surface Wrinkles for Smart Adhesion, Adv. Mater. 20 (2008) 711–716. doi:10.1002/adma.200701530.

[16] E.P. Chan, J.M. Karp, R.S. Langer, A “self-pinning” adhesive based on responsive surface wrinkles, J. Polym. Sci. Part B Polym. Phys. 49 (2011) 40–44. doi:10.1002/polb.22165.

[17] J.Y. Chung, J.P. Youngblood, C.M. Stafford, Anisotropic wetting on tunable micro-wrinkled surfaces, Soft Matter. 3 (2007) 1163. doi:10.1039/b705112c.

[18] K. Khare, J. Zhou, S. Yang, Tunable open-channel microfluidics on soft poly(dimethylsiloxane) (PDMS) substrates with sinusoidal grooves., Langmuir. 25 (2009) 12794–9. doi:10.1021/la901736n.

[19] M.A. Biot, Surface instability of rubber in compression, Appl. Sci. Res. 12 (1963) 168–182.

[20] W. Hong, X. Zhao, Z. Suo, Formation of creases on the surfaces of elastomers and gels, Appl. Phys. Lett. 95 (2009) 111901. doi:10.1063/1.3211917.

[21] Y. Cao, J.W. Hutchinson, From wrinkles to creases in elastomers: the instability and imperfection-sensitivity of wrinkling, Proc. R. Soc. A Math. Phys. Eng. Sci. 468 (2011) 94–115. doi:10.1098/rspa.2011.0384.

[22] B. Li, Y.-P. Cao, X.-Q. Feng, H. Gao, Mechanics of morphological instabilities and surface wrinkling in soft materials: a review, Soft Matter. 8 (2012) 5728. doi:10.1039/c2sm00011c.

[23] V. Trujillo, J. Kim, R.C. Hayward, Creasing instability of surface-attached hydrogels, Soft Matter. 4 (2008) 564. doi:10.1039/b713263h.

[24] J. Yoon, J. Kim, R.C. Hayward, Nucleation, growth, and hysteresis of surface creases on swelled polymer gels, Soft Matter. 6 (2010) 5807. doi:10.1039/c0sm00372g.

[25] S. Cai, D. Chen, Z. Suo, R.C. Hayward, Creasing instability of elastomer films, Soft Matter. 8 (2012) 1301. doi:10.1039/c2sm06844c.

[26] D. Chen, L. Jin, Z. Suo, R.C. Hayward, Controlled formation and disappearance of creases, Mater. Horizons. (2014). doi:10.1039/c3mh00107e.

[27] E. Cerda, L. Mahadevan, Geometry and Physics of Wrinkling, Phys. Rev. Lett. 90 (2003) 074302. doi:10.1103/PhysRevLett.90.074302.

[28] J. Genzer, J. Groenewold, Soft matter with hard skin: From skin wrinkles to templating and material characterization, Soft Matter. 2 (2006) 310. doi:10.1039/b516741h.

[29] N. Bowden, W.T.S. Huck, K.E. Paul, G.M. Whitesides, The controlled formation of ordered, sinusoidal structures by plasma oxidation of an elastomeric polymer, Appl. Phys. Lett. 75 (1999) 2557. doi:10.1063/1.125076.

[30] D.-Y. Khang, J.A. Rogers, H.H. Lee, Mechanical Buckling: Mechanics, Metrology, and Stretchable Electronics, Adv. Funct. Mater. 19 (2009) 1526–1536. doi:10.1002/adfm.200801065.

[31] Z.Y. Huang, W. Hong, Z. Suo, Nonlinear analyses of wrinkles in a film bonded to a compliant substrate, J. Mech. Phys. Solids. 53 (2005) 2101–2118. doi:10.1016/j.jmps.2005.03.007.

[32] F. Brau, P. Damman, H. Diamant, T. a. Witten, Wrinkle to fold transition: influence of the substrate response, Soft Matter. 9 (2013) 8177. doi:10.1039/c3sm50655j.

[33] D. Holmes, A.J. Crosby, Draping Films: A Wrinkle to Fold Transition, Phys. Rev. Lett. 105 (2010) 1–4. doi:10.1103/PhysRevLett.105.038303.

[34] K. Srinivasan, G. Subbarayan, T. Siegmund, Wrinkling on irreversibly deforming foundations, Thin Solid Films. 520 (2012) 5671–5682. doi:10.1016/j.tsf.2012.04.071.

[35] Y. Ebata, A.B. Croll, A.J. Crosby, Wrinkling and strain localizations in polymer thin films, Soft Matter. 8 (2012) 9086. doi:10.1039/c2sm25859e.

[36] Q. Wang, X. Zhao, Phase Diagrams of Instabilities in Compressed Film-Substrate Systems, J. Appl. Mech. 81 (2013). doi:10.1115/1.4025828.

[37] Y. Cao, J.W. Hutchinson, Wrinkling Phenomena in Neo-Hookean Film/Substrate Bilayers, J. Appl. Mech. 79 (2012) 031019. doi:10.1115/1.4005960.

[38] F. Brau, H. Vandeparre, A. Sabbah, C. Poulard, A. Boudaoud, P. Damman, Multiple-length-scale elastic instability mimics parametric resonance of nonlinear oscillators, Nat. Phys. 7 (2010) 56–60. doi:10.1038/nphys1806.

[39] J.W. Hutchinson, The role of nonlinear substrate elasticity in the wrinkling of thin films, Philos. Trans. R. Soc. A Math. Phys. Eng. Sci. 371 (2013).

http://rsta.royalsocietypublishing.org/content/371/1993/20120422.short (accessed November 26, 2013).

[40] J. Zang, X. Zhao, Y. Cao, J.W. Hutchinson, Localized ridge wrinkling of stiff films on compliant substrates, J. Mech. Phys. Solids. 60 (2012) 1265–1279. doi:10.1016/j.jmps.2012.03.009.

[41] R. Zhao, T. Zhang, M. Diab, H. Gao, K.-S. Kim, The primary bilayer ruga-phase diagram I: Localizations in ruga evolution, Extrem. Mech. Lett. (2015). doi:10.1016/j.eml.2015.04.006.

[42] Y.-C. Chen, A.J. Crosby, High Aspect Ratio Wrinkles via Substrate Prestretch, Adv. Mater. (2014) n/a–n/a. doi:10.1002/adma.201401444.

[43] C. Cao, H.F. Chan, J. Zang, K.W. Leong, X. Zhao, Harnessing Localized Ridges for High-Aspect-Ratio Hierarchical Patterns with Dynamic Tunability and Multifunctionality., Adv. Mater. (2013). doi:10.1002/adma.201304589.

[44] A. Takei, L. Jin, J.W. Hutchinson, H. Fujita, Ridge Localizations and Networks in Thin Films Compressed by the Incremental Release of a Large Equi-biaxial Pre-stretch in the Substrate., Adv. Mater. (2014) 1–7. doi:10.1002/adma.201306162.

[45] Q. Wang, X. Zhao, A three-dimensional phase diagram of growth-induced surface instabilities, Sci. Rep. 5 (2015) 8887. doi:10.1038/srep08887.

[46] J. Dervaux, M. Ben Amar, Morphogenesis of Growing Soft Tissues, Phys. Rev. Lett. 101 (2008) 068101. doi:10.1103/PhysRevLett.101.068101.

[47] C.T. McKee, J.A. Last, P. Russell, C.J. Murphy, Indentation versus Tensile Mesurements of Young ’s Modulus for Soft Biological Tissues, Tissue Eng. B. 17 (2011). doi:10.1089/ten.teb.2010.0520.

[48] J. Yin, X. Chen, I. Sheinman, Anisotropic buckling patterns in spheroidal film/substrate systems and their implications in some natural and biological systems, J. Mech. Phys. Solids. 57 (2009) 1470–1484. doi:10.1016/j.jmps.2009.06.002.

[49] L. Pocivavsek, R. Dellsy, A. Kern, S. Johnson, B. Lin, K.Y.C. Lee, et al., Stress and fold localization in thin elastic membranes., Science. 320 (2008) 912–6. doi:10.1126/science.1154069.

[50] R. Huang, H. Yin, J. Liang, J. Sturn, K. Hobart, Z. Suo, Mechanics of relaxing SiGe islands of a viscous glass, Acta Mech. Sin. 18 (2002) 441–456.

[51] B. Audoly, Localized buckling of a floating elastica, Phys. Rev. E. 84 (2011) 011605. doi:10.1103/PhysRevE.84.011605.

[52] S. Cai, D. Breid, A.J. Crosby, Z. Suo, J.W. Hutchinson, Periodic patterns and energy states of buckled films on compliant substrates, J. Mech. Phys. Solids. 59 (2011) 1094–1114. doi:10.1016/j.jmps.2011.02.001.

[53] J.-Y. Sun, S. Xia, M.-W. Moon, K.H. Oh, K.-S. Kim, Folding wrinkles of a thin stiff layer on a soft substrate, Proc. R. Soc. A Math. Phys. Eng. Sci. 468 (2011) 932–953. doi:10.1098/rspa.2011.0567.

[54] C.M. Stafford, C. Harrison, K.L. Beers, A. Karim, E.J. Amis, M.R. VanLandingham, et al., A buckling-based metrology for measuring the elastic moduli of polymeric thin films., Nat. Mater. 3 (2004) 545–50. doi:10.1038/nmat1175.

[55] J.Y. Chung, A.J. Nolte, C.M. Stafford, Surface wrinkling: a versatile platform for measuring thin-film properties., Adv. Mater. 23 (2011) 349–68. doi:10.1002/adma.201001759.

[56] C.M. Stafford, C. Harrison, K.L. Beers, A. Karim, E.J. Amis, M.R. VanLandingham, et al., A buckling-based metrology for measuring the elastic moduli of polymeric thin films., Nat. Mater. 3 (2004) 545–50. doi:10.1038/nmat1175.

[57] R.M. May, Simple mathematical models with very complicated dynamics, Nature. 261 (1976) 459–467.

[58] J. Testa, J. Perez, C. Jeffries, Evidence for universal chaotic behavior of a driven nonlinear oscillator, Phys. Rev. Lett. 48 (1982) 714–717.

[59] J. Yin, X. Chen, I. Sheinman, Anisotropic buckling patterns in spheroidal film/substrate systems and their implications in some natural and biological systems, J. Mech. Phys. Solids. 57 (2009) 1470–1484. doi:10.1016/j.jmps.2009.06.002.

[60] T. Tallinen, J.Y. Chung, J.S. Biggins, L. Mahadevan, Gyrification from constrained cortical expansion., Proc. Natl. Acad. Sci. U. S. A. 111 (2014) 12667–72. doi:10.1073/pnas.1406015111.

[61] B.R. Wiggs, C. a Hrousis, J.M. Drazen, R.D. Kamm, On the mechanism of mucosal folding in normal and asthmatic airways., J. Appl. Physiol. 83 (1997) 1814–1821.

[62] W. Yang, T.C. Fung, K.S. Chian, C.K. Chong, Instability of the two-layered thick-walled esophageal model under the external pressure and circular outer boundary condition, J. Biomech. 40 (2007) 481–490. doi:10.1016/j.jbiomech.2006.02.020.

[63] J. Yoon, J. Kim, R.C. Hayward, Nucleation, growth, and hysteresis of surface creases on swelled polymer gels, Soft Matter. 6 (2010) 5807. doi:10.1039/c0sm00372g.

[64] E. Hohlfeld, L. Mahadevan, Unfolding the Sulcus, Phys. Rev. Lett. 106 (2011) 105702. doi:10.1103/PhysRevLett.106.105702.

[65] A. Auguste, L. Jin, Z. Suo, R.C. Hayward, The role of substrate pre-stretch in post-wrinkling bifurcations., Soft Matter. 10 (2014) 6520–9. doi:10.1039/c4sm01038h.

[66] Y.B. Fu, P. Ciarletta, Buckling of a coated elastic half-space when the coating and substrate have similar material properties, (2015).

[67] M. Diab, T. Zhang, R. Zhao, H. Gao, K. Kim, P.R.S. A, Ruga mechanics of creasing : from instantaneous to setback creases Ruga mechanics of creasing : from instantaneous to setback creases, (2013).

[68] G. Miquelard-Garnier, A.B. Croll, C.S. Davis, A.J. Crosby, Contact-line mechanics for pattern control, Soft Matter. 6 (2010) 5789. doi:10.1039/c0sm00165a.

[69] S. Park, Y.S. Huh, H.G. Craighead, D. Erickson, A method for nanofluidic device prototyping using elastomeric collapse., Proc. Natl. Acad. Sci. U. S. A. 106 (2009) 15549–15554. doi:10.1073/pnas.0904004106.

[70] J. Yin, Z. Cao, C. Li, I. Sheinman, X. Chen, Stress-driven buckling patterns in spheroidal core/shell structures., Proc. Natl. Acad. Sci. U. S. A. 105 (2008) 19132–5. doi:10.1073/pnas.0810443105.

[71] Q. Wang, L. Zhang, X. Zhao, Creasing to Cratering Instability in Polymers under Ultrahigh Electric Fields, Phys. Rev. Lett. 106 (2011) 1–4. doi:10.1103/PhysRevLett.106.118301.

[72] A. Schweikart, A. Horn, A. Böker, A. Fery, Controlled Wrinkling as a Novel Method for the Fabrication of Patterned Surfaces, (2010) 75–99. doi:10.1007/12.

[73] C.-C. Lin, F. Yang, S. Lee, Surface wrinkling of an elastic film: effect of residual surface stress., Langmuir. 24 (2008) 13627–31. doi:10.1021/la802517b.

[74] D. Chen, J. Yoon, D. Chandra, A.J. Crosby, R.C. Hayward, Stimuli-responsive buckling mechanics of polymer films, J. Polym. Sci. Part B Polym. Phys. 52 (2014) 1441–1461. doi:10.1002/polb.23590.

[75] L. Pocivavsek, R. Dellsy, A. Kern, S. Johnson, B. Lin, K.Y.C. Lee, et al., Stress and fold localization in thin elastic membranes., Science. 320 (2008) 912–6. doi:10.1126/science.1154069.

[76] M.S. White, M. Kaltenbrunner, E.D. Głowacki, K. Gutnichenko, G. Kettlgruber, I. Graz, et al., Ultrathin, highly flexible and stretchable PLEDs, Nat. Photonics. 7 (2013) 811–816. doi:10.1038/nphoton.2013.188.

[77] E. a. Wilder, S. Guo, S. Lin-Gibson, M.J. Fasolka, C.M. Stafford, Measuring the Modulus of Soft Polymer Networks via a Buckling-Based Metrology. Volume 39, Number

12, June 13, 2006, pp 4138−4143., Macromolecules. 39 (2006) 5956–5956. doi:10.1021/ma0615607.

[78] L. Jin, A. Auguste, R.C. Hayward, Z. Suo, Bifurcation diagrams for the formation of wrinkles or creases in soft bilayers, J. Appl. Mech. 82 (2015) 1–11. doi:10.1115/1.4030384.

[79] E. Hohlfeld, L. Mahadevan, Scale and nature of sulcification patterns, Phys. Rev. Lett. 109 (2012) 1–5. doi:10.1103/PhysRevLett.109.025701.

[80] S.F. Ahmed, G.-H. Rho, K.-R. Lee, A. Vaziri, M.-W. Moon, High aspect ratio wrinkles on a soft polymer, Soft Matter. 6 (2010) 5709. doi:10.1039/c0sm00386g.

[81] J.G. Gaillard, C. Hendrus, B.D. Vogt, Tunable wrinkle and crease surface morphologies from photoinitiated polymerization of furfuryl alcohol., Langmuir. 29 (2013) 15083–9. doi:10.1021/la4038167.

[82] P.-C. Lin, S. Yang, Mechanically switchable wetting on wrinkled elastomers with dual-scale roughness, Soft Matter. 5 (2009) 1011. doi:10.1039/b814145b.

[83] E. Lee, M. Zhang, Y. Cho, Y. Cui, J. Van der Spiegel, N. Engheta, et al., Tilted Pillars on Wrinkled Elastomers as a Reversibly Tunable Optical Window., Adv. Mater. (2014) 1–7. doi:10.1002/adma.201400711.

[84] D. Qin, Y. Xia, G.M. Whitesides, Soft lithography for micro- and nanoscale patterning., Nat. Protoc. 5 (2010) 491–502. doi:10.1038/nprot.2009.234.